CODED TRANSMIT DIVERSITY IN CDMA OVER NAKAGAMI-M FADING CHANNELS

Ariel Sacramento

A thesis
in
The Department
of
Electrical And Computer Engineering

Presented in Partial Fulfillment of the Requirements
For the Degree of Master of Applied Science
Concordia University
Montréal, Québec, Canada

April 2008

Your file Votre référence
ISBN: 978-0-494-40895-7
Our file Notre référence
ISBN: 978-0-494-40895-7

Abstract

Coded Transmit Diversity In CDMA Over Nakagami-m Fading Channels

Ariel Sacramento

With applications such as video conferencing, extensive web browsing and live video streaming, future wireless systems become extremely demanding in terms of high data rates and improved signal quality.

In this thesis the performance of a space-time spreading transmit diversity scheme is examined over a frequency-flat Nakagami-m fading channel. The Nakagami-m channel model is considered as it is well known for modeling signal fading conditions ranging from severe to moderate, to light fading or no fading, through its parameter m.

We also propose in this thesis a coded transmit diversity scheme which is based on a combination of a convolutional code with a space-time transmit diversity scheme that uses direct-sequence code division multiple access (DS-CDMA) for multiuser access.

Our focus will be on the uplink of the communication system. The space-time scheme employs $N = 2$ and N_r antennas at the mobile station (MS) side and at the base station (BS) side respectively. DS-CDMA is used to support many users and a linear decorrelator detector is used to combat the effect of multiuser interference.

We study the performance of both the uncoded and coded transmit diversity schemes over slow fading and fast fading channels. In all cases, the investigations start by determining the probability density function (PDF) of the signal to interference and noise ratio at the output of the space-time combiner at the BS receiver side. Using this PDF we derive a closed-form (or an approximation) expression for the bit error rate (BER) of the system under consideration. The accuracy of the PDF and BER expressions are verified when compared to simulation results for different values of the fading figure m and for different combinations of transmit and receive antennas.

In the case of the coded space-time transmit diversity scheme, the pairwise error probability and the corresponding BER upper bounds are obtained for fast and slow fading channels. The derived error bounds, when compared to system simulations, are shown to be tight at high signal-to-noise ratios.

Furthermore, our analytical results explicitly show the achieved system diversity in terms of the number of transmit and receive antennas and the fading figure m. When the coded space-time scheme is considered, its diversity is shown to be a function of the minimum free distance d_{free} of the convolutional code used. Furthermore we show that the diversity of the different schemes considered is always independent of the system load.

Acknowledgments

I would like to express my deepest appreciation to my thesis supervisor, Dr. Walaa Hamouda for his guidance and encouragement. He is a great teacher that takes at heart the success of his students. His time, patience and extreme selflessness made the making of the research summarized herein possible.

I would also like to thank my parents, my brother, my sister and my girlfriend for their unlimited support and patience. My thoughts go also to all of my friends and anyone who helped me in one way or another toward the completion of this work.

I would like finally to thank everyone at Concordia University who works hard everyday to make Concordia a great place for students to get a better education.

Table of Contents

List of Figures

List of Tables

List of Symbols

m	Nakagami fading figure
f_d	Doppler shift
$f_{d_{max}}$	maximum Doppler shift
μ^2_{Ric}	noncentrality parameter of Rician distribution
s_k	spreading sequence of k^{th} user
N_{seq}	spreading factor or processing gain of spreading sequence
g_k	received amplitude of k^{th} CDMA user
x_k	k^{th} user information sequence
$n(t)$	additive noise
$\mathbf{R}$	spreading sequence autocorrelation matrix
$\mathbf{G}$	CDMA received amplitudes matrix
$\mathbf{H}$	Nakagami-m fading channel coefficients matrix
F	Nakagami-m random variable
h_k	Nakagami-m fading coefficient amplitude affecting k^{th} user
N_t	number of transmit antennas
N_r	number of receive antennas
σ^2_n	noise power
$E[.]$	statistical expectation
$I_o(.)$	bessel function of the first kind and zero order
R_c	convolutional code rate
$\mathbb{M}(.,.,.)$	WhittakerM function

d_{free}	Minimum free distance of convolutional code
${}_pF_q(a_1,\ldots,a_p;$ $b_1,\ldots,b_q;x)$	generalized hypergeometric function

List of Acronyms

MAI	multiaccess interference
TDMA	time division multiple access
FDMA	frequency division multiple access
CDMA	code division multiple access
STC	space-time code
CC	convolutional code
DS-CDMA	direct-sequence code division multiple access
SINR	signal-to-interference-and-noise ratio
SNR	signal-to-noise ratio
BER	bit error rate
PDF	probability density function
CDF	cumulative distribution function
RV	random variable
PN sequence	pseudonoise sequence
AWGN	additive white Gaussian noise
CC	convolutional code
MIMO	multiple-input multiple-output
ML	maximum likelihood
MMSE	minimum mean square error
MSE	mean square error
MUD	multiuser detection
STBCs	space-time block codes

STTCs	space-time trellis codes
RS	Reed-Solomon
SISO	single-input single-output
STS	space-time spreading
FEC	forward-error coding

Chapter 1

Introduction

1.1 Introduction

Wireless transmission over fading channels is subject to multipath fading and multiaccess interference (MAI) among other phenomenon that cause degradation of the overall quality of the communication system.

Reflection, diffraction, and scattering are the main causes of multipath propagation which in turn causes fading effect in the radio channel. Because of the multiplicity of factors involved in propagation in a wireless mobile environment, it is convenient to apply statistical methods in order to describe signal variations. Statistical models for the wireless fading channel have been studied widely along with wireless communication techniques. Several statistical models for fading channels are well investigated. The Rayleigh distribution is broadly used to model multipath fading channels [4]. The Nakagami-m distribution, proposed by Nakagami [5], has also gained widespread application in the modeling of physical channels. There are many theoretical and analytical results of the performance of diverse communication systems operating in a Nakagami-m fading channel in the literature, but there has not been an extensive work on the simulation of the Nakagami-m fading channel coefficients. A simulation method for Nakagami-m fading channels based on a "direct inverse method" is proposed by the authors in [1, 6] and was shown to be very efficient.

Bandwidth is a valuable resource and the most efficient use of this resource has to be engineered. In order to make an optimal use of the available bandwidth and

to provide maximal flexibility, many wireless systems operate as multiple-access systems, in which channel bandwidth is shared among many users on a random access basis. Among various techniques used to allow many users to share a common communication channel we have time division multiple access (TDMA) where users are multiplexed by orthogonal time slots, frequency division multiple access (FDMA) where users are multiplexed by orthogonal frequency bands and code division multiple access (CDMA) where users are multiplexed by distinct codes. CDMA is of special interest in this thesis as it is the multiaccess scheme that is used. CDMA allows different users to transmit at the same time and over the entire available frequency spectrum. The performance of a CDMA system can be impaired by three major factors, MAI, the near-far effect and multipath fading. MAI is due to the fact that non-orthogonal sequences are used to multiplex the different users' signals. Also space-time codes (STCs) that employ multiple antennas at the transmit and/or receive sides of the communication system will be studied in this thesis in order to combat the effects of multipath fading.

Wireless systems rarely use only an STC, but instead utilize a convolutional code (CC), a turbo code, or a low-parity density-check (LDPC) code as a channel outer code used in combination with space-time coding. The use of this additional coding improves the performance.

1.2 Thesis Contribution

The major contributions of this thesis can be summarized as follows:

- The study of the uncoded space-time spreading system over a Nakagami-m slow and fast fading channel. In this we derive the closed-form expression of the BER for N_t=2, and N_r antenna systems.

- The derivation of the full diversity of the system, and the proof that, under certain conditions full diversity order can be achieved. We show that the diversity of the system under consideration is not a function of the system load, but instead it is only a function of the number of transmit and receive antennas, as well as of the fading figure.

- We study the performance of a coded space-time spreading system. We consider

a unique combination of CDMA, MIMO transmit diversity and channel coding. We consider the improvement in diversity over the uncoded scheme.

- The derivation of performance error bounds for the coded space-time spreading scheme. We can obtain the order of diversity of the scheme from the derived performance bounds and show that the promised diversity can be fully achieved under certain conditions. We also show that the achieved diversity is not a function of the system load, but instead of the number of transmit and receive antennas, and the fading figure, and the free Hamming distance d_{free} of the CC under consideration.

The contributions of this thesis have resulted so far in two published conference papers [7, 8].

1.3 Thesis Outline

The content of this thesis is organized as follows. Chapter 2 gives a brief overview of some background principles needed to get a better overall understanding of the content of the thesis. Chapter 2 covers topics such as multipath fading, multiaccess communications, CDMA communications and different multiuser detectors, and diversity and space-time coding. An efficient Nakagami-m fading channel simulator introduced in [1, 6] will be presented along with simulation results.

In chapter 3, we present a space-time transmission scheme for DS-CDMA systems over both fast and slow fading channels along with the appropriate combining scheme. The performance of the scheme is analyzed for multiuser scenario over a Nakagami-m fading channel. The performance is studied for the particular case when a decorrelator detector is used. We derive a closed-form expression of the probability of bit error. After presenting the multiuser system model, we derive the probability density function (PDF) of the signal to interference and noise ration (SINR) as well as the bit-error-rate (BER) of the space-time system under investigation. Then we present simulation results to assess the accuracy of our theoretical results. We also assess the diversity order.

Chapter 4 presents a concatenation of the space-time transmit diversity scheme presented in chapter 3 with an outer CC operating over a Nakagami-m fading channel. Here again we consider both fast fading and slow fading scenarios. Particularly, we

consider improvements in terms of diversity gains over the uncoded scheme presented in chapter 3. We obtain BER upper bounds for fast fading Nakagami channels. These error bounds are shown to be tight at high signal-to-noise ratios (SNRs), indicating the achieved system diversity. Both analytical and Monte-Carlo simulation results are presented.

Chapter 5 is a conclusion of the thesis. Some suggestions for future works are also made to extend the research presented in this thesis.

Chapter 2

Background

2.1 Multipath Fading

In a mobile radio network, radio waves are subject to reflection and refraction on surrounding objects, such as buildings, hills, trees. Multiple copies of the originally transmitted radio wave, that have attenuated amplitudes and phases are picked up by the receiving antenna from different directions and with different propagation delays. When the different copies are picked up by a receiver antenna, they can combine either constructively or destructively depending on their random phases. This is called multipath fading and is shown schematically on Fig. 2.1.

The *coherence bandwidth* of a channel is defined as the frequency range over which all spectral components of the transmitted signal are subject to the same fading attenuation. In a narrowband system, the transmitted signals bandwidth is usually smaller than the channel's *coherence bandwidth* and this type of fading is referred to as *frequency nonselective* or *frequency flat* fading. On the other hand, when the transmitted signal's bandwidth is greater than the channel coherence bandwidth, the received signal spectrum becomes distorted. This phenomenon is known as *frequency selective fading* and occurs in wideband systems.

Each multipath wave is subject to a shift in frequency due to the relative motion between the transmitter and the receiver where this shift in frequency of the received signal is called *Doppler shift* and is proportional to the speed of the mobile. If we consider a single tone signal transmitted at frequency f_c and picked up by the receiver at an incident angle θ with respect to the direction of the vehicle motion in

a 2-dimensional system, then the Doppler shift f_d is given by

$$f_d = \frac{v f_c}{c} \cdot \cos\theta \tag{2.1}$$

where c is the speed of light and v is the speed of the mobile. This phenomenon will induce a spread of the bandwidth within the range of $f_c \pm f_{d_{max}}$ where $f_{d_{max}}$ is the maximum Doppler shift and is defined as

$$f_{d_{max}} = \frac{v f_c}{c}. \tag{2.2}$$

The direct consequence of the Doppler shift is that the single transmitted tone will give rise to a received signal with a spectrum of nonzero width and this phenomenon is called *frequency dispersion.*

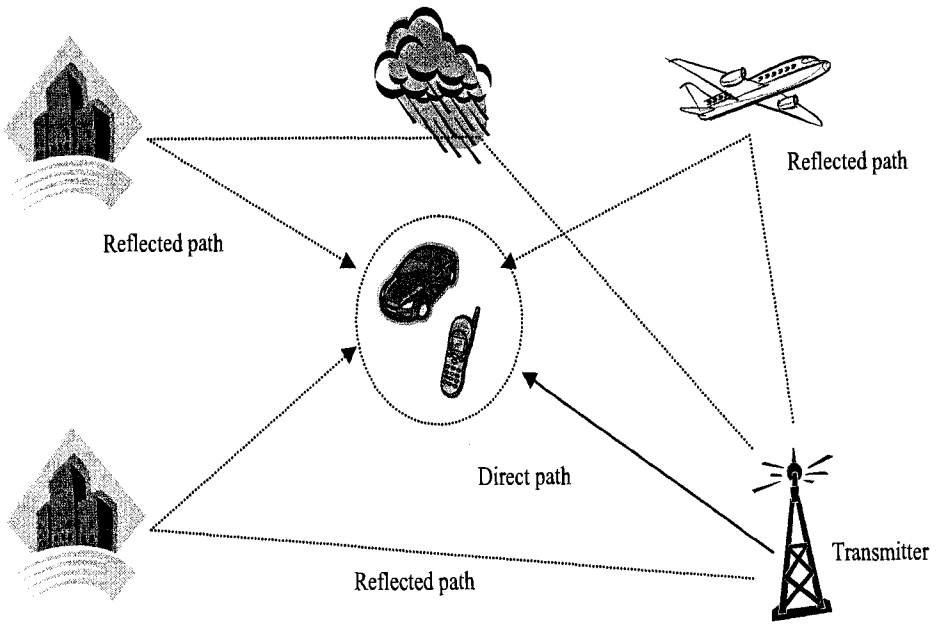

Figure 2.1: Multipath fading.

2.1.1 Fading Channel Models

Because of the multiplicity of factors involved in propagation in a wireless mobile environment, it is convenient to apply statistical techniques to describe signal variations.

Different probability distributions are considered in order to model fading including the Rayleigh fading channel model, the Rician model, the Nakagami-m model, the Nakagami-q model, and the lognormal fading model. In the following subsections, we will briefly present a few of those statistical fading models.

Rayleigh Fading

When there is a large number of scatterers in the channel that contribute to the signal at the receiver, as is the case in ionospheric or tropospheric signal propagation, an application of the central limit theorem leads to a Gaussian process model for the channel impulse response [4]. When the process is zero-mean, the envelope of the channel response at anytime has a Rayleigh distribution with PDF defined as

$$p_{Ray}(r) = \begin{cases} \frac{2r}{\Omega} \cdot e^{-\frac{r^2}{\Omega}}, & r \geq 0 \\ 0, & r < 0 \end{cases} \tag{2.3}$$

where

$$\Omega = E[R^2].$$

The phase of the channel response has a uniform distribution in the interval $(0, 2\pi)$. The Rayleigh fading channel is characterized by the single parameter Ω.

The Rayleigh distribution with PDF (2.3) is closely related to the central chi-square distribution [4, pp. 41-44]. If we let $Y = Y_1^2 + Y_2^2$ where Y_1 and Y_2 are zero-mean statistically independent Gaussian random variables (RVs), each having variance σ_y^2, then Y is chi-square distributed with two degrees of freedom [4]. If we define a new RV R as

$$R = \sqrt{Y_1^2 + Y_2^2} = \sqrt{Y}$$

then R follows a Rayleigh distribution with PDF given in (2.3) and parameter $\Omega = E[R^2] = \sigma_y^2$. The PDF of the Rayleigh distribution is shown in Fig. 2.2 for $\Omega = 2$.

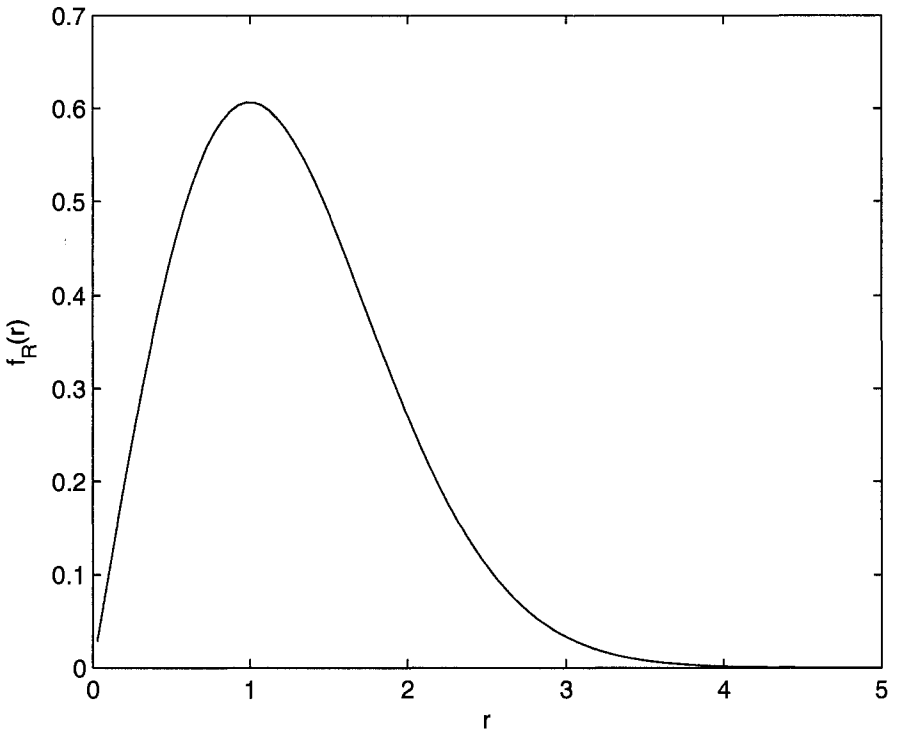

Figure 2.2: PDF of Rayleigh distribution, $\Omega = 2$.

Rician Fading

In some propagation scenarios such as satellite or microcellular mobile radio channels, there is a strong line-of-sight (LOS) path between the transmitter and the receiver on top of the different reflected paths. The sum of the many scattered components can still be modeled as having a Rayleigh probability distribution. The sum of the constant amplitude direct signal (LOS) and the Rayleigh distributed scattered signal results in a signal with a Rician envelope distribution.

The Rice distribution is closely related to the noncentral chi-square distribution. That is if we let $Y = Y_1^2 + Y_2^2$ where Y_1 and Y_2 are statistically independent Gaussian RVs with means $\mu_i, i = 1, 2$, and common variance σ_y^2, then Y follows a noncentral chi-square distribution with noncentrality parameter $\mu_{Ric}^2 = \mu_1^2 + \mu_2^2$. In this case the

RV $R = \sqrt{Y}$ has a Rician distribution with PDF given by

$$p_{Ric}(r) = \begin{cases} \frac{r}{\sigma_y^2} \cdot e^{-\frac{r^2+\mu_{Ric}^2}{2\sigma_y^2}} \cdot I_0\left(\frac{r\mu_{Ric}}{\sigma_y^2}\right), & r \geq 0 \\ 0, & r < 0 \end{cases} \tag{2.4}$$

where μ_{Ric}^2 is the power of the direct signal and $I_0(.)$ is the modified Bessel function of the first kind and zero order [9]. If we assume that the total average signal power is normalized to unity, the PDF of (2.4) becomes

$$p_{Ric}(r) = \begin{cases} 2r(1+K)e^{-K-(1-K)r^2} I_o(2r\sqrt{K(K+1)}), & r \geq 0 \\ 0, & r < 0 \end{cases} \tag{2.5}$$

where K is the Rician factor, denoting the power ratio of the direct and the scattered signal components, and is given by

$$K = \frac{\mu_{Ric}^2}{2\sigma_y^2}, \tag{2.6}$$

where small values of K indicate a severely faded channel. For $K = 0$ there is no direct signal component and the Rician PDF is equivalent to a Rayleigh PDF. Large values of K indicates slightly faded channels and as K approaches infinity, the channel behaves as an additive white Gaussian noise (AWGN) channel.The Rician distribution with various K is shown in Fig. 2.3.

Finally another widely used fading channel model is the Nakagami-m model.

2.1.2 Nakagami-m Fading

Nakagami has reported in [5] that signal fading in radio wave propagation can be well modeled by the PDF

$$p_{Naka}(r) = \begin{cases} \frac{2m^m r^{2m-1}}{\Gamma(m)\Omega^m} e^{-(m/\Omega)r^2}, & r \geq 0 \\ 0, & r < 0 \end{cases} \tag{2.7}$$

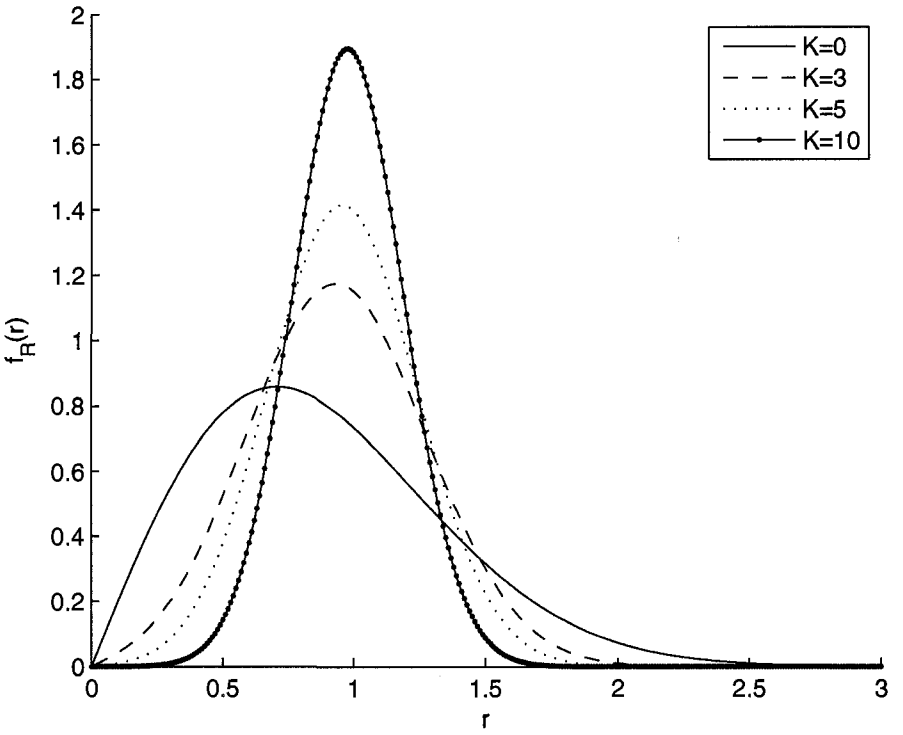

Figure 2.3: PDF of normalized Rician distribution for different values of K.

where

$$\Omega = E[R^2], \tag{2.8}$$

with E[·] being the expectation operator and

$$m = \frac{\overline{R^2}}{(R^2 - \overline{R^2})^2} \geq \frac{1}{2}. \tag{2.9}$$

The m parameter controls the severity, or depth, of the fading which can range from severe to moderate, to light or no fading. The value $m = 1$ results in the widespread Rayleigh-fading model, while values of m less than one correspond to fading more severe than Rayleigh fading and values of m greater than one correspond to fading less severe than Rayleigh fading. The PDF of the Nakagami-m distribution is shown in Fig. 2.4 for $\Omega = 2$ and for different values of the fading figure m.

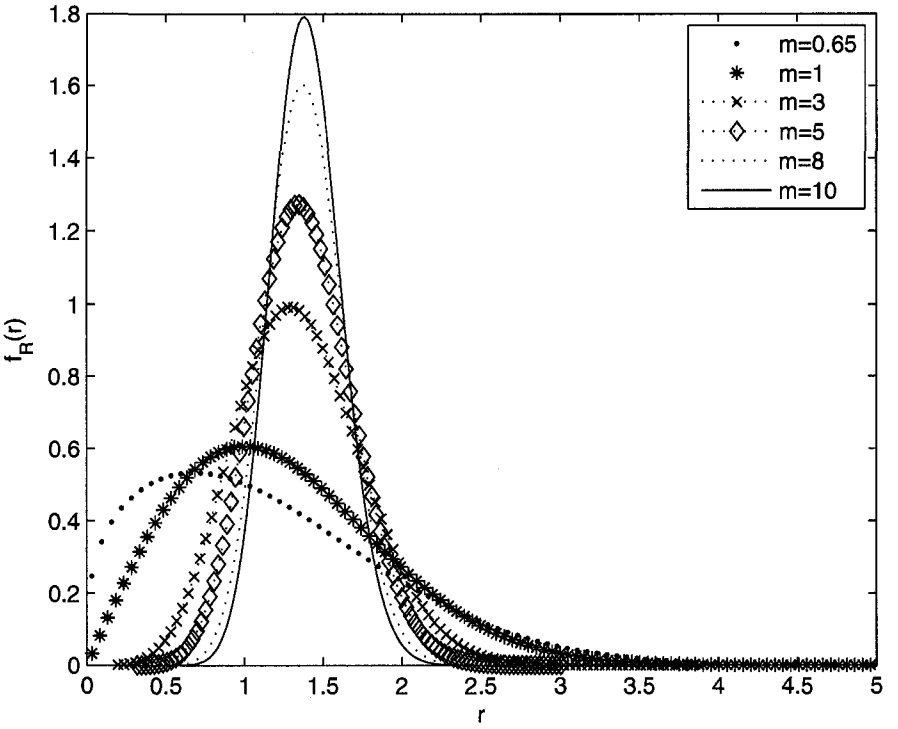

Figure 2.4: PDF of Nakagami-m distribution for different values of fading figure m.

2.1.3 Nakagami-m Channel Simulation

The Nakagami-m distribution is widely used to model multipath fading in radio channels. The use of a Nakagami-m model for fading is stimulated by the fact that it fits into empirical data. The author of [10] proceeded to a field test in order to better understand the digital mobile radio channel and he was able to fit his empirical data closely to a Nakagami-m distribution. Other empirical studies of the pertinence of the Nakagami-m channel model can be found in [11] and [12].

In order to simulate the performance of communication systems in a Nakagami-m fading environment, we must come up with a reliable and effective way of generating channel fading coefficients. A "brute force method" for integer and half-integer values of m was developed by noticing that the square root of a sum of squares of n zero-mean identically distributed Gaussian random variables has a Nakagami-m distribution with $m=n/2$ [4]. This method is used in [13] but becomes quickly computationally

inefficient as the fading figure m increases. Yip and Ng in [14] proposed a Nakagami-m fading channel simulator based on implementing the product of a square-root beta process and a complex Gaussian process but this method is restricted to values of $0.5 \leq m \leq 1$. The authors of [15] developed a semi-empirical method, partially simulation based using a theoretical model proposed in [16]. The method requires determining the values of certain coefficients from measured data. Furthermore, the generation of 100 dissimilarly distributed Gaussian RVs is required to obtain one random envelope/phase sample pair. Finally Cheng [6] and Beaulieu *et.al* [1] proposed an efficient method for generating correlated Nakagami-m fading envelop samples for arbitrary values of m. They derived a new useful approximation of the inverse cumulative distribution function (CDF) of the Nakagami-m distribution. The authors also discuss longstanding uncertainties regarding the autocorrelation of the Nakagami-m fading amplitude model appropriate to Nakagami-m amplitude fading.

2.2 Nakagami-m Fading Simulator [1]

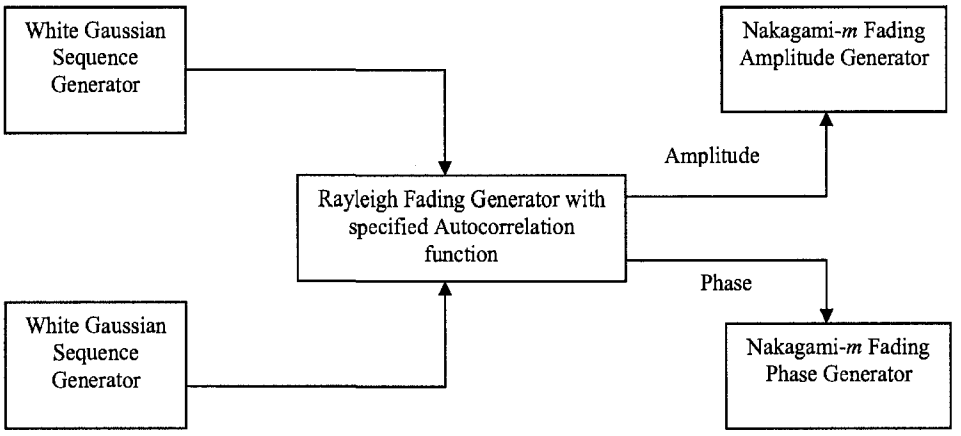

Figure 2.5: Schematic of the Nakagami-m fading channel simulator in [1].

In [1], an inverse transformation method is used to obtain a Nakagami-m phasor. The method proposed in [1] is schematically shown in Fig. 2.5. First an existing Rayleigh-fading simulator generates a Rayleigh-faded envelope sample sequence having the specified autocorrelation and phase properties. Let the RV R_{ray} denote a

Rayleigh envelope sample and the let the RV Θ denote the phase corresponding to R_{ray}. The authors of [1] then proceed to the transformation

$$u = F_{ray}(r) = 1 - e^{-r^2/2\sigma_{ray}^2} \tag{2.10}$$

where σ_{ray}^2 is the second moment of the RV R_{ray}. This transforms R_{ray} into a uniform RV on [0,1). The proof of that lies within the fact that $F_{ray}(r)$ is the CDF of a Rayleigh RV [4, p. 45]

The inverse function $F_{naka}^{-1}(u)$ of the Nakagami-m CDF is then applied to the uniformly distributed outcome u of (2.10). It is well known that transforming a uniformly distributed u over an interval [0,1) by an inverse CDF function $F^{-1}(u)$ results in a RV having CDF given by $F(u)$ [4, pp. 101-102]. The RV A_{naka} thus defined as

$$A_{naka} = F_{naka}^{-1}(u) \tag{2.11}$$

has a Nakagami-m distribution with PDF given by (2.7) and shown in Fig. 2.4. One method for approximating the function $F_{naka}^{-1}(u)$ that was proposed in [1] will be presented shortly.

Note that the generator presented here generates a uniform random variable from a Rayleigh variable using the transformation (2.10), rather than starting directly from a uniform random variable. This design builds in appropriate correlation properties and appropriate higher order statistical properties into both the generated uniform RV at the intermediate stage and into the generated Nakagami-m RV at the final stage.

2.2.1 Inverse CDF Approximation

The CDF of the Nakagami-m is explicitly defined as [5]

$$F_{naka}(x) = \int_0^x \frac{2m^m t^{2m-1}}{\Gamma(m)\Omega^m} \cdot e^{-(m/\Omega)t^2} dt. \tag{2.12}$$

There is no closed-form expression for $F_{naka}^{-1}(u)$ except for the special case of $m = 1$. A useful and accurate approximation to the Nakagami-m inverse CDF function is

proposed in [1]. The derivation in [1] follows the approach of Hastings [17] who had derived approximations to the inverse complementary CDF of Gaussian distribution that are widely used [9, pp. 937-933]. Following the approach of Hastings thus, Cheng [6] obtained the following approximation for the inverse function of the Nakagami-m distribution

$$F_{naka}^{-1}(u) \approx G(\eta_{naka}(u)), \tag{2.13}$$

where

$$G(\eta_{naka}) = \eta_{naka} + \frac{a_1\eta_{naka} + a_2\eta_{naka}^2 + a_3\eta_{naka}^3}{1 + b_1\eta_{naka} + b_2\eta_{naka}^2}, \tag{2.14}$$

and η_{naka} is an ancillary variable defined as

$$\eta_{naka}(u) = \left(\sqrt{ln\frac{1}{1-u}}\right)^{\frac{1}{m}}. \tag{2.15}$$

In (2.14), a_1,a_2,a_3,b_1 and b_2 are coefficients chosen to minimize the approximation error. There is no proposed solution to finding a set of coefficients that will result in an accurate approximation for all values of the fading parameter m. Cheng proceeded to a minimum-maximum error criterion implementation by numerical search in [6]. Using this method, the sets of coefficients for fading figures m = 0.65, 0.75, 0.85, 1.5, 2.0, 3.0, 4.0, 5.0, 6.0, 7.0, 8.0 and 10 were derived and are shown in Table 2.1.

Table 2.1: Inverse Nakagami CDF approximation coefficients [1].

m	a_1	a_2	a_3	b_1	b_2
0.65	-0.828	-4.5634	-15.8819	63.1955	23.2981
0.75	-0.0547	-0.3679	-1.0336	6.2107	1.8533
0.85	-0.0336	-0.1543	-0.4733	4.9250	1.2082
1.50	0.0993	0.0560	0.2565	0.5276	0.0770
2.00	0.1890	-0.0128	0.2808	0.0809	0.0638
3.00	0.3472	-0.2145	0.2626	-0.6779	0.1690
4.00	0.4846	-0.4231	0.2642	-0.9729	0.2727
5.00	0.6023	-0.6238	0.2789	-1.1798	0.3732
6.00	0.7139	-0.8305	0.3223	-1.3232	0.4558
7.00	0.8167	-1.0244	0.3761	-1.4233	0.5192
8.00	0.9260	-1.2350	0.4557	-1.4872	0.5628
10.00	1.1088	-1.6095	0.6015	-1.6046	0.6488

2.2.2 Phase Generator

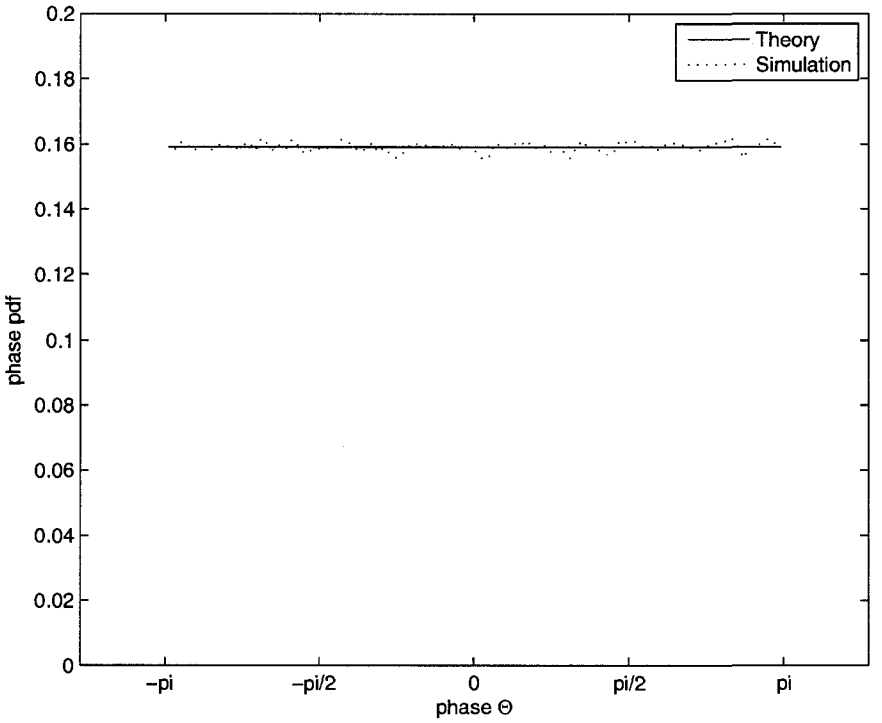

Figure 2.6: Phase PDF for Nakagami-m distribution with fading figure m=10.

Having determined the amplitude of the Nakagami-m phasor as described in the previous section, we are left with assigning a phase to the Nakagami fading in order to have a phasor Nakagami simulator. The authors in [1] have proposed to assign a uniform phase to the faded Nakagami signal and that decision is motivated (but not justified) by the fact that the Rayleigh-faded signal has a uniformly distributed phase. Therefore the phase of our Nakagami fading phasor is uniformly distributed as shown on Fig. 2.6.

2.2.3 Simulation Results

Due to the accuracy of the simulator proposed in [1] we will use it throughout this thesis for simulation purposes. Fig. 2.7 shows a perfect match between the PDF of the Nakagami-m distribution obtained both theoretically and by simulation. The

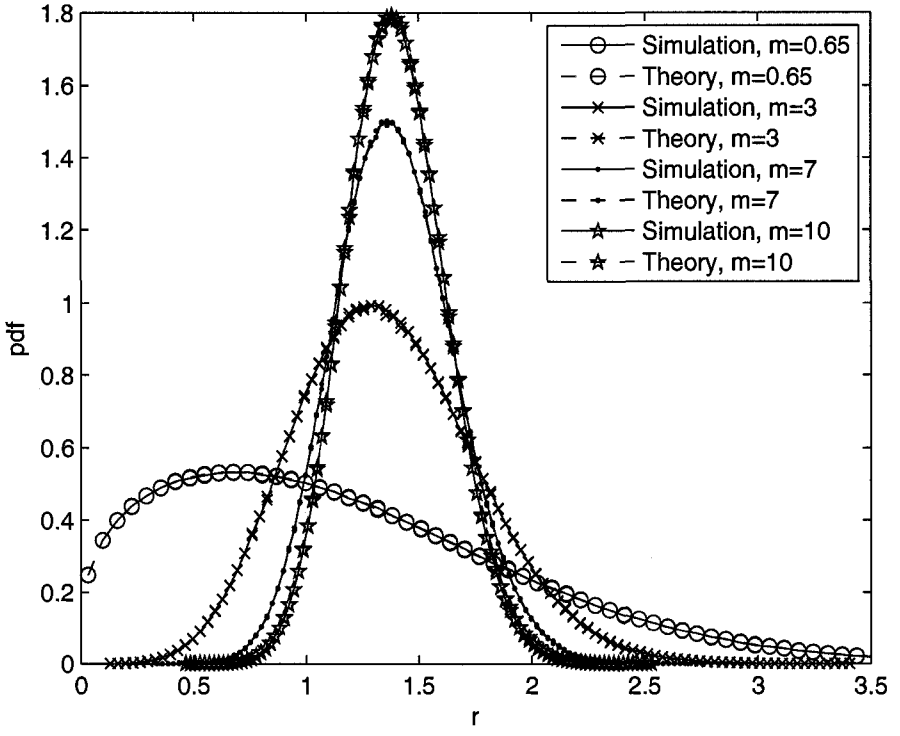

Figure 2.7: PDF of Nakagami-m distribution, theoretical V.S. simulation results.

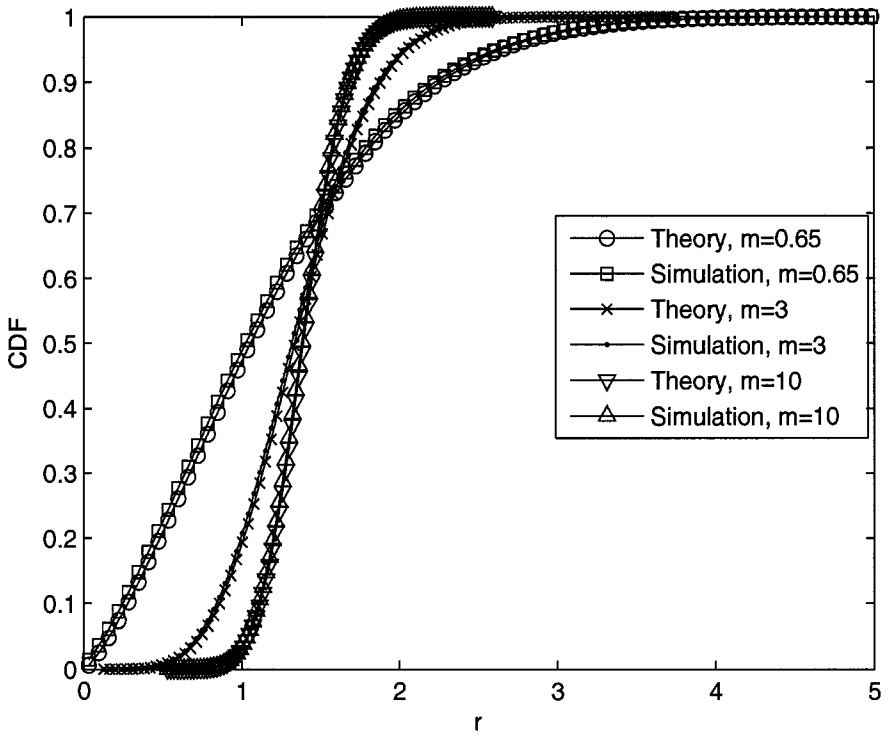

Figure 2.8: CDF of Nakagami-m distribution, theoretical V.S. simulation results.

Table 2.2: Expected values V.S. empirical values of m.

m	$\hat{m}$
0.65	0.6487
0.75	0.7511
0.85	0.8483
1.50	1.5013
2.00	2.0002
3.00	3.0012
4.00	4.0082
5.00	5.0084
6.00	6.0001
7.00	6.9998
8.00	8.0010
10	9.9907

simulated PDF is obtained by generating 10^6 Nakagami phasors. The accuracy of the Nakagami-m phasor generator is also shown by comparing the theoretical and empirical PDF of the phase and also comparing the theoretical and empirical CDF of the amplitude in Fig. 2.6 and Fig. 2.8 respectively.

As a check, we computed the empirical values of the parameter m from the Nakagami-m phasor samples that we generated and these results were compared to the expected values of m as shown in Table 2.2. We see that the empirical values and the expected values of the fading figure m are in perfect match.

2.3 Multiaccess Communication

Multiaccess techniques are designed to allow several users to share common communication channels and/or resources, at the same time, without interfering with each other.

In wireless communication, with the ever-increasing demand in bandwidth, it has become a necessity to design multiaccess techniques that can allow for the most efficient share of the channel bandwidth among users. Among multiaccess communication techniques designed for wireless communication systems we have TDMA, FDMA, and CDMA. CDMA will be used throughout this thesis in order to allow for multiaccess to our Nakagami-m fading wireless channel. This is motivated by the fact that CDMA is a promising technology for multiuser transmission in a wireless

environement. CDMA can support many users transmitting at the same time with each of them using the entire available frequency spectrum. Other features of CDMA such as robustness to frequency selective fading, and multipath combining motivate the use of CDMA for multiuser access throughout this thesis.

2.3.1 CDMA

CDMA is a widely used multiple access technique in wireless cellular systems. In DS-CDMA many different users share a common frequency band and a common time slot but they are assigned different signature waveforms.

CDMA does not assign a specific frequency to each user. Instead, every channel can use the full available spectrum. Signals are encoded with a pseudo-random digital sequence also called signature. Another benefit of CDMA is that it facilitates frequency reuse.

Two major drawbacks of CDMA systems are the "near-far" effect and MAI. In short, the near-far effect is one of detecting and receiving a weaker signal amongst stronger signals [18]. This problem constrains CDMA systems to very strict power control schemes so that the transmitted signals arrive at the receivers with equal power levels.

One of the most important properties used in CDMA is orthogonality. Theoretically speaking, the pseudo-random spreading codes are chosen to be orthogonal to each other, so that the receiver can easily identify transmitted signals. Practically speaking, users do not use completely orthogonal spreading codes. This leads to the creation of residual MAI. MAI adds some additional noise to the received signal, which in turn can degrade the overall system performance.

2.4 DS-CDMA

2.4.1 Spread-Spectrum Techniques

CDMA uses spread spectrum modulation which provides resistance to jamming. This is why spread spectrum techniques were initially adopted in military applications. Spread-spectrum signals are distributed over a wide range of frequencies resulting in a noise like signal difficult to detect or to interfere with.

2.4.2 Direct-Sequence

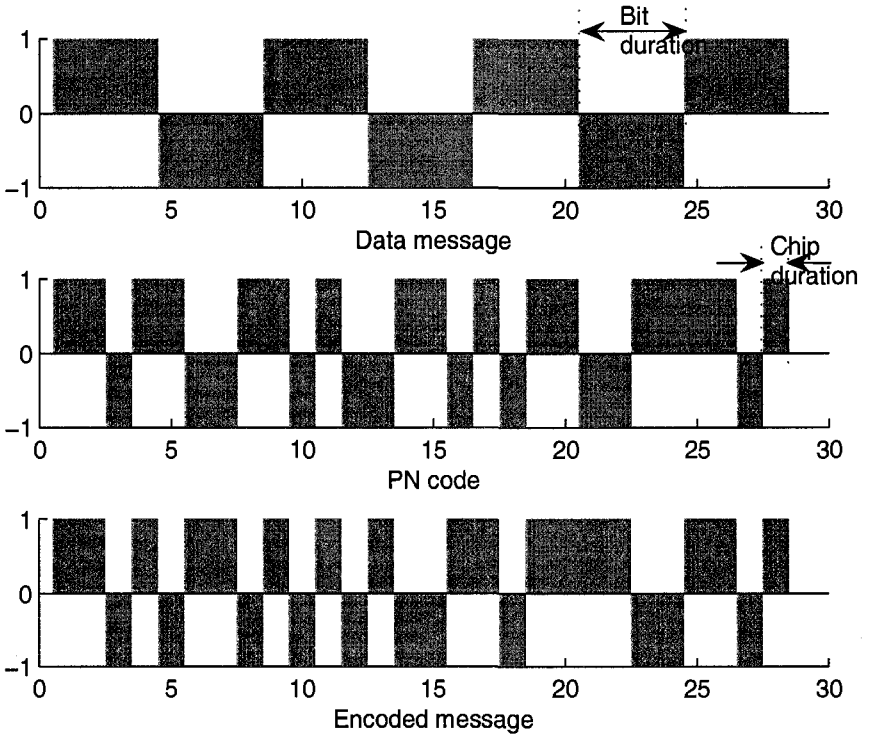

Figure 2.9: Example of a direct spreading with a processing gain of $T_b/T_c = 4$.

DS-CDMA is the most popular and the most frequently used spread spectrum technique. Its key concept is the simplest to understand: the transmitter spreads the original data by multiplying this data with a unique pseudonoise sequence (PN sequence) as is illustrated in Fig. 2.9. The original data is then recovered at the receiver by remultiplying the spreaded received information sequence with the same PN sequence. A PN sequence is a succession of chips (time periods of the PN sequence) which are valued -1 to 1 in polar systems or 0 and 1 in non-polar systems. The period of a chip T_c is always shorter than the period of a bit T_b (bit duration in the original signal). The quality and efficiency of the spreading are measured by the spreading factor (or processing gain) which is equal to $N_{seq} = T_b/T_c$ (the spreading factor in Fig. 2.9 is then equal to 4). However, the power contents stay the same: as the bandwidth increases, the spectral power density decreases.

2.4.3 Generation of DS Signals

The most important characteristic of PN sequences is orthogonality: in fact, two orthogonal signals can be transmitted at the same time and without interfering with each other. The cross-correlation between two spreading sequences s_n and s_k is given by:

$$\int_0^{T_b} s_n(t)s_k(t)dt. \tag{2.16}$$

One of the most popular family of PN sequences are maximum length sequences, also sometimes called n-sequences or m-sequences [19]. They are generated using maximal linear feedback shift registers [19]. However in DS-CDMA the cross-correlation values of the m-sequences are not optimal. The use of Gold sequences (or Gold codes) is more appropriate. A Gold sequence is constructed by the XOR (binary operation) of two m-sequences with the same clocking. Gold codes permit the transmission to be asynchronous and allow the energy to be spread uniformly over the whole bandwidth. Their main drawback is that they are not perfectly orthogonal due to the fact that the cross-correlation values are low yet not exactly equal to zero.

2.4.4 Basic DS-CDMA System Model

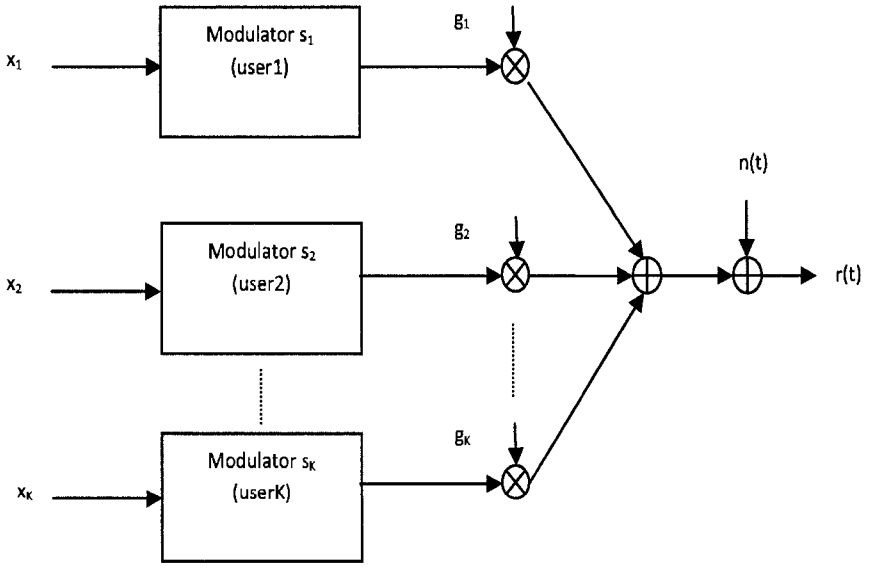

Figure 2.10: Basic K-user DS-CDMA system.

The basic DS-CDMA system model is shown in Fig. 2.10. If all the bits from

every user are aligned in time at the receiver, the channel is synchronous. In this case, the received signal is given for K users by:

$$r(t) = \sum_{k=1}^{K} g_k x_k(t) s_k(t) + n(t), \quad 0 \leq t \leq T_b \tag{2.17}$$

where g_k, $x_k(t)$, $s_k(t)$ are respectively the received amplitude, the data signal and the signature waveform of the k^{th} user, and $n(t)$ is the AWGN process with power spectral density $N_o/2$. However, the channel can be asynchronous if random delays are introduced between different users' signals at the receiver. In this case the received signal is given by:

$$r(t) = \sum_{k=1}^{K} g_k x_k(t - \tau_k) s_k(t - \tau_k) + n(t), \quad 0 \leq t \leq T_b \tag{2.18}$$

where τ_k is the delay corresponding to the k_{th} user's signal.

For simplicity we will assume that the transmission is synchronous in this thesis. Many times it will be very handy to use matrix representation for the different equations while studying CDMA systems. Vectors and matrices in equations presented in this thesis will be in bold fonts, for example g_k will represent a scalar, while $\mathbf{G}$ will represent a matrix. The matrix form of the received signal (2.17) is given by:

$$\mathbf{r} = \mathbf{SGx} + \mathbf{n} \tag{2.19}$$

where $\mathbf{S} = [s_1, .., s_K]$ is the $N_{seq} \times K$ spreading code matrix, $\mathbf{G} = diag[g_1, .., g_K]$ is the $K \times K$ diagonal matrix of the received amplitudes, (g_k is the received amplitude of the k^{th} user), $\mathbf{x} = [x_1, .., x_k]^T$ is the $K \times 1$ information vector from all K users, $\mathbf{n}$ is the $N_t \times 1$ vector of AWGN samples. Here also $(.)^T$ represents the transpose operation.

In what follows, we will give an overview of different receiver structures.

2.5 Single and Multiuser Detectors

2.5.1 Single-User Detection

The conventional detector for the received signal $r(t)$ described in (2.17) consists of a bank of K correlators as shown in Fig. 2.11.

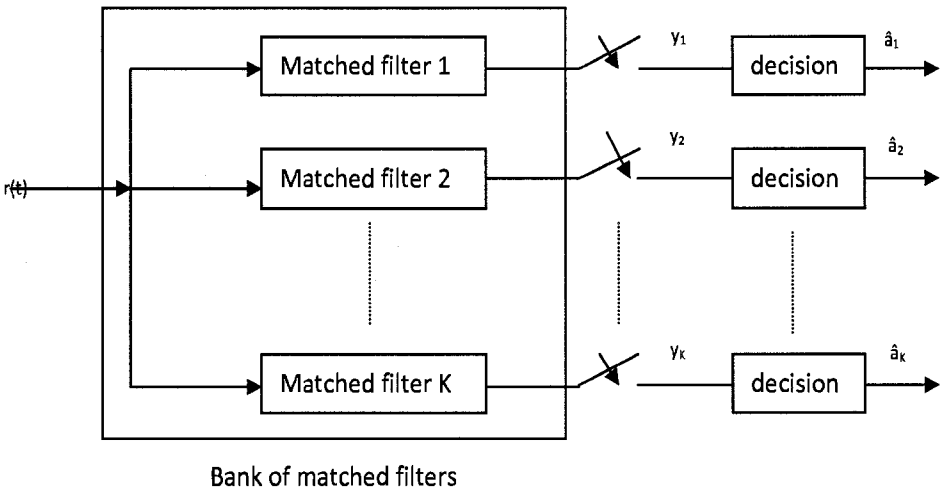

Figure 2.11: Conventional detector.

The conventional detector, also called matched filter, correlates the received signal $r(t)$ with a code waveform which is specific to each user. After sampling at the bit times, the output of the matched filter of the k^{th} user is given by:

$$y_k(t) = \int_0^{T_b} r(t)s_k(t)dt \tag{2.20}$$

where $s_k(t)$ is the signature waveform specific to the k^{th} user. Substituting (2.17) into (2.20) and expanding (2.20) we obtain

$$\begin{aligned} y_k(t) &= \int_0^{T_b} s_k(t) \left[\sum_{j=1}^{K} g_j x_j s_j(t) + n(t) \right] dt \\ &= g_k x_k + \sum_{j \neq k}^{K} g_j x_j \rho_{kj} + \int_0^{T_b} s_k(t) n(t) dt \end{aligned} \tag{2.21}$$

where ρ_{kj} is the cross-correlation between the spreading sequences of the k^{th} and j^{th} users. The soft estimate of user k has three terms, $g_k x_k$ which is the desired data of the k^{th} user with received amplitude g_k, $\sum_{j \neq k}^{K} g_j x_j \rho_{kj}$ is the total MAI caused by the other $K-1$ users interefering. Finally $\int_0^T s_k(t)n(t)dt$ is an AWGN. The performance of the detector thus depends on the correlation between different users. In matrix

form, soft estimates can be expressed as

$$\mathbf{y} = \mathbf{S}^H\mathbf{r} = \mathbf{S}^H(\mathbf{SGx} + \mathbf{n}) = \mathbf{RGx} + \mathbf{S}^H\mathbf{n} \tag{2.22}$$

where $(\mathbf{S})^H$ represents the Hermitian of matrix $\mathbf{S}$ which means the transpose and component-wise complex conjugate of $\mathbf{S}$. We define $\mathbf{R} = \mathbf{S}^H\mathbf{S}$ as the cross correlation matrix with diagonal elements equal to 1 for $k = j$ and $0 < \rho_{kj} < 1$ for $k = j$. $\mathbf{G} = diag[g_1, ..., g_k]$, $\mathbf{y} = [y_1, ..., y_k]^T$, $\mathbf{x} = [x_1, ..., x_k]^T$ and $\mathbf{S}^H\mathbf{n}$ is a random Gaussian vector with zero mean. The final hard decisions are given by

$$\hat{\mathbf{x}} = sgn(\mathbf{y}), \tag{2.23}$$

where $\hat{\mathbf{x}}$ is a vector containing the estimates of the information bits in $\mathbf{x}$.

The conventional detector is a single-user detector, where each branch detects a specific user regardless of the other users. Hence, a specific user views other users as background noise. In fact, as the number of users increases, the amount of MAI increases as well, and this results in degradation in the system performance. In addition, the presence of stronger users exacerbates the MAI of the weaker users. This situation arises when signals arrive at the receiver at different powers. As a consequence, weaker users will be "dominated" by stronger users. In order to illustrate the impact of MAI on the performance of the system, it is interesting to compare the probability of error of a perfectly orthogonal system (MAI=0) and a non-orthogonal system. For orthogonal codes, the probability of error for user k is given by [18]

$$P_e^k = Q\left(\frac{g_k}{\sigma}\right) \tag{2.24}$$

where g_k represents the power or the received signal of user k and σ is the AWGN standard variation.

In the non-orthogonal case, we can approximate the interference of a large number of users by a Gaussian RV, where we get [18]

$$P_e^k = Q\left(\frac{g_k}{\sqrt{\sigma^2 + \sum_{j \neq k} g_{kj}^2 \rho_{jk}^2}}\right). \tag{2.25}$$

We see form (2.24) and (2.25) that the probability of error is expressed as a function of the total MAI, and thus by combatting MAI, the overall performance of the system can be much improved. We will now review multiuser detectors in the following section. In multiuser detection, the receiver jointly detects all users' signal.

2.5.2 Multiuser Detection

Fig. 2.12 schematically shows the major categories of multiuser detectors. They as divided into two fundamentally different groups, optimal detectors and suboptimal detectors. The optimal detector offers the best performance but it is computationally complex. On the other hand, suboptimal detectors can achieve performance close to optimal performance but with affordable complexity.

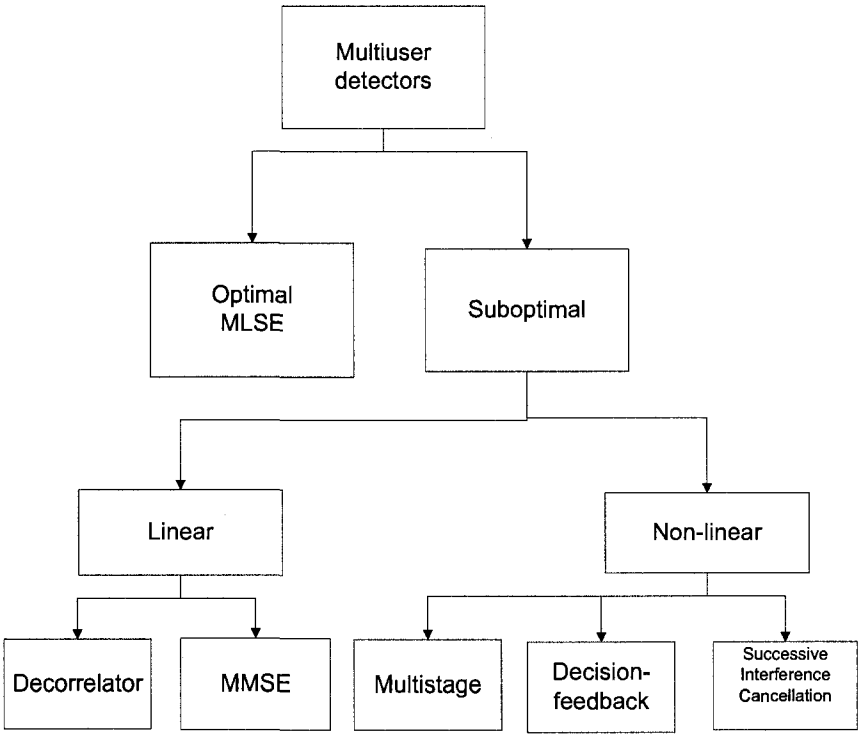

Figure 2.12: Multiuser detectors.

Maximum Likelihood Sequence Detector

An optimum multiuser detector was proposed by Verdu in [20]. This optimum detector is based on maximum likelihood (ML) detection. The ML detector selects through

all possible transmitted signal sets the set that is closest to the received signal set at the output of the matched filters.

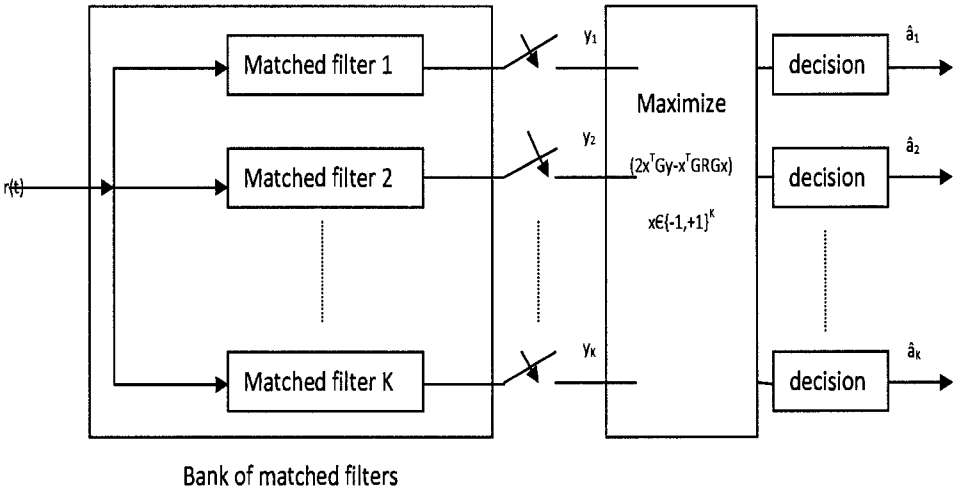

Figure 2.13: Maximum-likelihood (optimum) detector.

The ML detector will select a set $\mathbf{x}$ such that the probability of $\mathbf{x}$ being transmitted given that $\mathbf{r}$ is received is maximized. The probability $P(\mathbf{x}|\mathbf{r})$ is referred as joint a-posteriori probability. From [20], the ML detector can be mathematically expressed as

$$\hat{x} = \arg\left(\max_{x\epsilon\{-1,+1\}^K}\left\|r(t) - \sum_{j=1}^{K} g_j x_j s_j(t)\right\|\right). \tag{2.26}$$

$$\begin{aligned}\hat{x} &= \arg\max_{x\epsilon\{-1,+1\}^K}\int_0^{T_b}\left[r(t) - \sum_{j=1}^{K} g_j x_j s_j(t)\right]^2 dt \\ &= \arg\min_{x\epsilon\{-1,+1\}^K}\int_0^{T_b} r^2(t)dt - 2\sum_{j=1}^{K} g_j x_j \int_0^{T_b} r(t)s_j(t)dt \\ &+ \sum_{u=1}^{K}\sum_{j=1}^{K} g_u x_u g_j x_j \int_0^{T_b} s_u(t)s_j(t)dt. \end{aligned} \tag{2.27}$$

Eq. (2.27) can be expressed in matrix form as

$$\hat{\mathbf{x}} = \arg\max_{\mathbf{x}\epsilon\{-1,+1\}^K}\left(2\mathbf{x}^T\mathbf{G}\mathbf{y} - \mathbf{x}^T\mathbf{G}\mathbf{R}\mathbf{G}\mathbf{x}\right). \tag{2.28}$$

Here $\mathbf{y}$ is a vector containing the outputs of the bank of matched filters. This

detector offers optimum performance but at the cost of computational complexity. As we can see from (2.27), in a synchronous transmission scheme, the ML detector requires an exhaustive search over 2^K possible combinations of the vector $\mathbf{x}$. This in turn implies that, as the number of active users increases, the ML detector becomes almost impossible to implement. Many suboptimum multiuser detectors, that have the advantage of easier implementation have been proposed and we will now present a few of them.

Decorrelator Detector

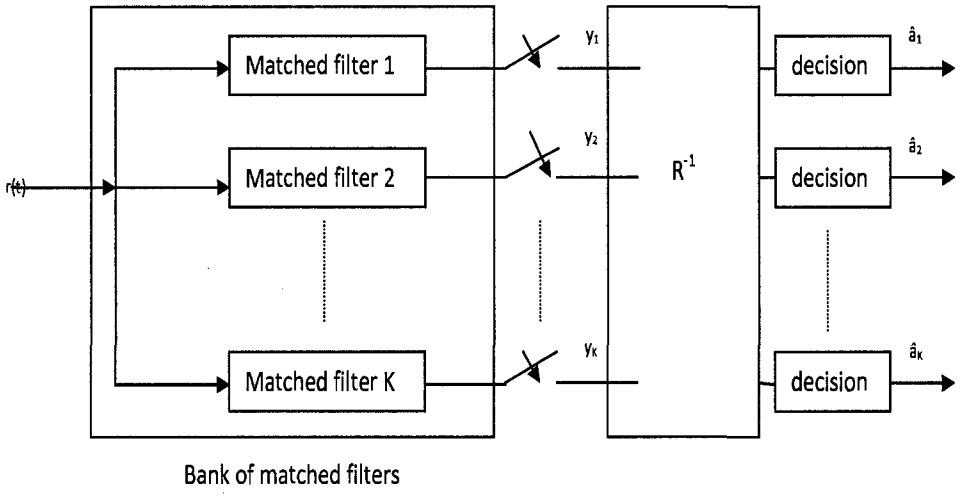

Figure 2.14: Decorrelator detector.

As we can observe from Fig. 2.14, the deccorelator detector applies the linear transformation $\mathbf{R}^{-1}$ to the output of the conventional detector. Hence, the soft estimates of the decorrelator detector are given by

$$\mathbf{y}_{dec} = \mathbf{R}^{-1}\mathbf{y}. \tag{2.29}$$

If we expand the expression in (2.29) we obtain

$$\mathbf{y}_{dec} = \mathbf{R}^{-1}(\mathbf{RGx} + \mathbf{n}) = \mathbf{Gx} + \mathbf{R}^{-1}\mathbf{n}. \tag{2.30}$$

We can see from (2.30) that the output of the system is just the decoupled data plus a noise term. In other words, MAI is completely eliminated and in the absence of

background noise, we would have an error free transmission. The decorrelator detector provides substantial improvement over the conventional detector. The probability of error when detecting the information of user k using the decorrelator detector is given by [18]

$$P_k(\sigma) = Q\left(\frac{g_k}{\sqrt{\sigma^2 \mathbf{R}_{kk}^{-1}}}\right). \tag{2.31}$$

Minimum Mean-Squared Error (MMSE) Detector

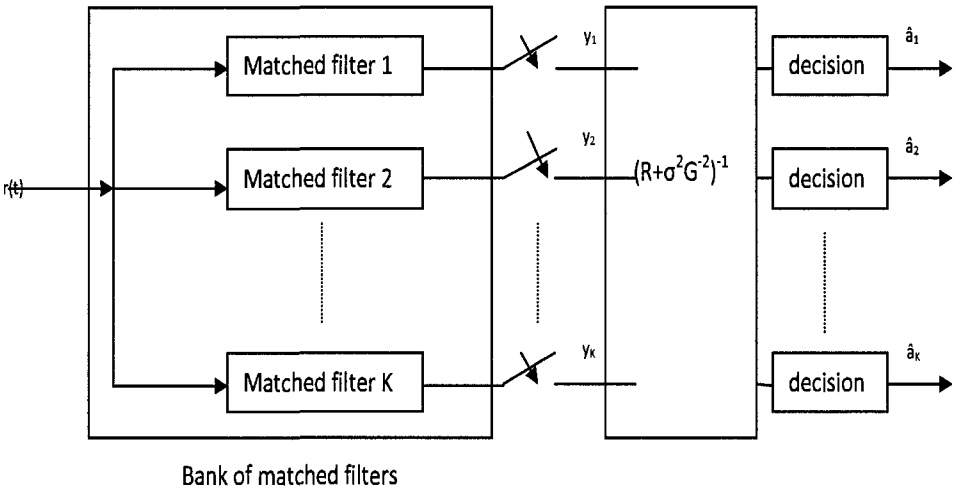

Figure 2.15: MMSE detector.

Unlike the decorrelator , the MMSE detector compensates for the background noise and the MAI. Its linear transform $\mathbf{T}$ is chosen such that the minimum mean-squared error between the actual data sent $\mathbf{x}$ and the soft estimates of the system $\hat{\mathbf{x}}$ is minimized. Mathematically

$$\mathbf{T} = \arg\min_{\mathbf{T}} E\left[|\mathbf{x} - \hat{\mathbf{x}}|^2\right] \tag{2.32}$$

It is easily shown that the linear transformation satisfying (2.32) is the following [18]

$$\mathbf{T} = \left(\mathbf{R} + \sigma^2 \mathbf{G}^{-2}\right)^{-1}. \tag{2.33}$$

We note from (2.33) that the linear transformation $\mathbf{T}$ is expressed as a function of the cross-correlation matrix $\mathbf{R}$, the background noise and the received amplitudes.

Other techniques are used in wireless communications to combat the effect of fading. We will review in the following section diversity techniques which are efficient in combatting multipath fading.

2.6 Diversity

Diversity techniques are widely used in wireless communication systems in order to combat multipath fading. They offer significant improvement in performance without increasing the transmitted power or sacrificing the bandwidth [21, 22]. The key idea behind the diversity techniques is that multiple replicas of the same signal are combined to recover the original transmitted signal. The different replicas will undergo independent fading through the channel. The probability that all signals will be faded below a certain threshold value at the same time will thus be smaller. By properly combining those independently faded replicas, a significant reduction in the effect of multipath fading can be achieved. Diversity can be introduced in time, frequency and space domain.

2.6.1 Time Diversity

In order to achieve time diversity, identical symbols or messages are transmitted at different time slots. The required time separation is at least equal to the coherence time of the channel, or the reciprocal of the fading rate $1/f_d = c/vf_c$. The coherence time is a statistical measure of the period of time over which the channel fading process is correlated. This technique is effective in fast fading environments since the coherence time of the channel is small. In mobile communication systems, error control coding can be combined with interleaving in order to achieve time diversity. In that case, the different replicas of the originally transmitted signal are provided to the receiver in the form of redundancy in time domain [23]. A disadvantage of this technique is the loss in bandwidth efficiency caused by the redundancy introduced in the time domain.

2.6.2 Frequency Diversity

In frequency diversity techniques, many different frequencies are used to transmit replicas of the original message. In order to avoid correlation in fading, the frequency separation between replicas should be greater than the coherence bandwidth of the channel. The transmitter is usually provided with many replicas of the original signal in the form of redundancy in the frequency domain introduced by spread spectrum techniques, multicarrier modulation and frequency hopping. Like time diversity, frequency diversity induces a loss in bandwidth efficiency due to the redundancy introduced in the frequency domain.

2.6.3 Space Diversity

Antenna or space diversity is achieved using multiple antennas that are separated physically by a proper distance so that the individual signals are uncorrelated. The separation requirements depend on the antenna height, the propagation environments and frequency. In this case, redundancy is provided to the receiver in the spatial domain and this does not induce any loss in bandwidth efficiency. In a receive diversity scheme, multiple receive antennas pick up independent copies of the transmitted signals to reduce the effect of multipath fading. In transmit diversity techniques, messages are processed at the transmitter and then transmitted across multiple antennas.

2.6.4 Diversity Combining Techniques

Diversity techniques can also be classified according to the type of combining methods employed at the receiver. We can have in this case four main types of diversity combining techniques as follows:

- *Selection combining*: among all the different uncorrelated replicas, the signal with the largest instantaneous SNR at every symbol interval is chosen in such a way that the output SNR is equal to that of the best incoming signal. In practice the signal with the highest sum of the signal and noise power is used, since it is difficult to measure the SNR.

- *Switched combining*: in this scheme, the receiver scans all the diversity branches and selects a particular branch with the SNR above a certain predetermined

threshold. The output is then set to that branch until its SNR drops below the threshold. This is also referred to as *scanning diversity* and can be used to achieve transmit diversity. Since this technique does not systematically pick the best branch, its performance can be lower than that of a selection combining scheme, although switched combining is much easier to implement. Both selection combining and switched combining do not require any knowledge of the channel state information.

- *Maximum ratio combining*: It is used in the Alamouti scheme [24] as a linear combining method. In this method, various signal inputs are individually weighted and added together to get an output signal. The weighting factors can be chosen in several ways. This method is called optimum combining since it can maximize the output SNR and it requires the knowledge of channel fading amplitude and signal phases.

- *Equal gain combining*: this is a suboptimal linear technique that does not require estimation of the fading amplitude for individual branches. Instead, the receiver sets the amplitudes of the weighting factors to unity so that all received signals are co-phased and then added together with equal gain. Equal gain combining has a performance marginally inferior to maximum ratio combining.

2.7 Multiple-Input Multiple-Output (MIMO) Systems and Space-Time Coding

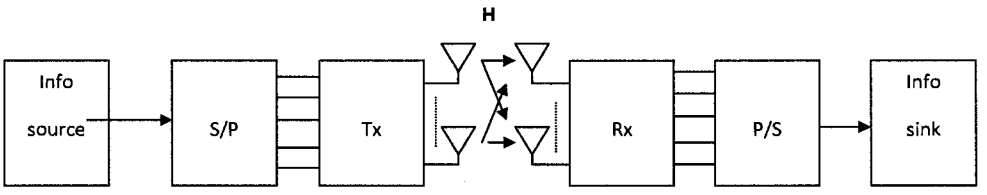

Figure 2.16: Schematic representation of a MIMO system.

Wireless communication systems with multi antennas have been a field of intensive research over the last decade. MIMO systems achieve higher data rates and reliability through the presence of various antennas at both the transmitter and the receiver

sides of a communication channel [25]. The authors of the [26] provide an overview of the state-of-the-art in MIMO communications, ranging from its roots in antenna array processing to advanced cellular systems. MIMO schemes are being used in many wireless communication systems such as Wireless Local Area Networks (WLAN) Wireless Wide Area Network (WWAN), and third generation (3G) [27] and fourth generation (4G) cellular networks [28, 29]. A MIMO system consisting of N_t and N_r transmit and receive antennas respectively is shown schematically on Fig. 2.16. The transmitted information in every symbol is represented by a column vector $\mathbf{x} = \{x_j\}, j = 1 \dots N_t$ where x_j represent the information transmitted by the j^{th} transmit antenna at a particular symbol period.

The channel is described by an $N_t \times N_r$ complex matrix $\mathbf{H}$, defined as follows

$$\mathbf{H} = \begin{bmatrix} h_{1,1} & h_{1,2} & \cdots & h_{1,N_t} \\ h_{2,1} & h_{2,2} & \cdots & h_{2,N_t} \\ \vdots & \vdots & \ddots & \vdots \\ h_{N_r,1} & h_{N_r,2} & \cdots & h_{N_r,N_t} \end{bmatrix}. \tag{2.34}$$

The ij^{th} component h_{ij} of the channel matrix, $\mathbf{H}$, represents the complex channel coefficient that affects the information sent from transmit antenna i to receive antenna j. We normalize the power of the signal picked up by every receive antenna to be equal to the number of transmit antennas i.e.

$$\sum_{j=1}^{N_t} |h_{ij}|^2 = N_t, \quad i = 1 \dots N_r. \tag{2.35}$$

The transmitted data are encoded by a space-time encoder which maps a block of $N_{t,o}$ binary input data into N_t modulation symbols from a signal set of $M = 2^{N_{t,o}}$ points. The N_t modulated symbols are applied to serial to parallel converters which assign them to each of the N_t transmit antennas.

At the receiver, the signal picked up by each of the N_r receive antennas is given by

$$r_j = \sum_{j=1}^{N_t} h_{ij} x_j + n_i \tag{2.36}$$

where n_i is the noise component at the i^{th} receive antenna, and is modeled as an

independent sample of a zero-mean complex Gaussian RV with one-sided power spectral density of N_0. If we represent the received signals from the N_r antennas at a particular time instant t by an $N_r \times 1$ column vector $\mathbf{r}_t$, and the noise by an $N_r \times 1$ column vector $\mathbf{n}_t$, then

$$\mathbf{r}_t = (r_1, r_2, \ldots, r_{N_r})^T \tag{2.37a}$$

$$\mathbf{n}_t = (n_1, n_2, \ldots, n_{N_r})^T \tag{2.37b}$$

where the operator $(.)^T$ represents transpose operation. Then one can write the received vector at time instant t as follows:

$$\mathbf{r}_t = \mathbf{H}_t \mathbf{x}_t + \mathbf{n}_t. \tag{2.38}$$

If we assume that the receiver uses a maximum likelihood algorithm to estimate the transmitted information sequence, then the decision metric at the receiver is computed based on the squared Euclidian distance between the hypothesized received sequence and the actual received sequence as

$$\sum_t \sum_{i=1}^{N_r} \left| r_t^i - \sum_{j=1}^{N_t} h_{ij} x_j \right|^2. \tag{2.39}$$

The channel coefficients can be either deterministic or random. Most of the time they are chosen to be of a given RV family such as the Rayleigh RVs or the Nakagami-m RVs in order to model a certain type of behavior of the channel. In this thesis we will model our channel to have a Nakagami-m amplitude distribution and a uniform phase distribution.

2.7.1 Space-Time Block Codes

The implementation of a transmit diversity scheme can be motivated in the downlink (base station to mobile station) of a cellular system where the cost of implementing receive diversity on the mobile units will be too high in terms of embedded electronics. It will thus be easier to exploit transmit diversity in that case by using multiple antennas at the base station.

The first STBC scheme that exploits the full transmit diversity using two transmit antennas is the Alamouti scheme [24]. The transmitter and receiver in the Alamouti scheme are illustrated in Fig. 2.17.

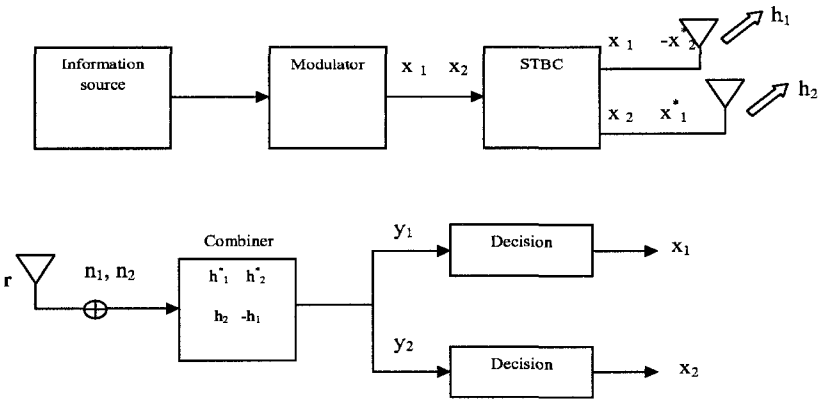

Figure 2.17: 2×1 Alamouti transmit diversity scheme.

As can be seen from Fig. 2.17, the incoming information stream is first modulated. The encoder then maps a block of two encoded symbols x_1 and x_2 to the transmit antennas according to a code matrix given by

$$\mathbf{X} = \begin{bmatrix} x_1 & -x_2^* \\ x_2 & x_1^* \end{bmatrix}. \tag{2.40}$$

The outputs of the encoder are transmitted over two consecutive transmission periods from two antennas. During the first transmission period, two signals x_1 and x_2 are transmitted simultaneously from antenna one and antenna two, respectively. In the second time period, signals $-x_2^*$ and x_1^* are transmitted from antenna one and two respectively. The operator $(^*)$ denotes complex conjugate. The encoding process is clearly done in time and space (thus the name space-time coding). Notice also that two symbols are sent over two symbol periods. This makes the Alamouti scheme full rate. Let the transmit sequence from antenna one and two, $\mathbf{x}^1$ and $\mathbf{x}^2$, respectively be

$$\begin{aligned} \mathbf{x}^1 &= [x_1, -x_2^*] \\ \mathbf{x}^2 &= [x_2, x_1^*]. \end{aligned} \tag{2.41}$$

The key feature of the Alamouti scheme is that the transmit sequence from the two transmit antennas are orthogonal, as their inner product is zero, i.e.

$$\mathbf{x}^1 \cdot \mathbf{x}^2 = x_1 x_2^* - x_2^* x_1 = 0.$$

Assuming a single receiver and setting h_1 and h_2 to be the channel coefficients for transmit antenna one and two respectively. The received signal is given by

$$y_1 = h_1 x_1 + h_2 x_2 + n_1 \tag{2.42a}$$

$$y_2 = -h_1 x_2 + h_2 x_1 + n_2. \tag{2.42b}$$

If we assume that the decoder has full knowledge of the channel state information (CSI), then the Alamouti block code can be decoded using a maximum-likelihood detector as follows

$$\hat{x}_1 = h_1^* y_1 + h_2 y_2^* = (|h_1|^2 + |h_2|^2) x_1 + n_1 \tag{2.43a}$$

$$\hat{x}_2 = h_2^* y_1 - h_1 y_2^* = (|h_1|^2 + |h_2|^2) x_2 + n_2. \tag{2.43b}$$

The Alamouti scheme discussed above achieves full diversity with a very simple maximum-likelihood decoding algorithm.

Tarokh *et al.* [30, 2] extended the Alamouti's 2-transmit diversity scheme to more than two antennas and introduced a more general definition of STBCs. A key characteristic of STBCs is that the transmitted symbols are organized in a matrix (block) fashion that is then transmitted over the different antennas over one or more symbol periods. The STBCs can achieve the full transmit diversity specified by the number of the transmit antennas N_t, while allowing a simple maximum-likelihood decoding algorithm, based on a linear processing of the received signal [2]. Generally a STBC is defined by an $N_t \times p$ transmission matrix $\mathbf{x}$ where N_t represents the number of transmit antennas and p is the number of time periods for transmission of one block of coded symbols.

In order to achieve the full transmit diversity of N_t, the transmission vector $\mathbf{x} = [x_1, x_1, \ldots, x_k]$ is constructed based on orthogonal design such that

$$\mathbf{x} \cdot \mathbf{x}^H = c(|x_1|^2 + |x_1|^2 + \cdots + |x_k|^2)\mathbf{I}_{N_t} \tag{2.44}$$

where c is a constant, $\mathbf{x}^H$ is the Hermitian of $\mathbf{x}$ and $\mathbf{I}_{N_t}$ is and $N_t \times N_t$ identity matrix.

At the receiver, the N_r receive antennas use maximum-likelihood (ML) decoding. In orthogonal STBC, the ML decoding is equivalent to maximum ratio combining

(MRC). Assuming perfect channel state-information, the decoder at antenna j maximizes

$$\sum_{t}\sum_{i=1}^{N_r}\left|r_t^i - \sum_{j=1}^{N_t} h_{ij}x_j\right|^2 . \tag{2.45}$$

Since the block coding requires only linear processing at the receiver, the decoding can be done efficiently. Space-time block codes can be constructed for any type of signal constellation and provide full diversity. However, only real constellations such as pulse amplitude modulation (PAM) can give full rate for any number of antennas. For complex constellations such as phase shift keying (PSK), full rate STBCs exist only for two transmit antennas.

2.7.2 Space-Time Trellis Codes

STBCs can achieve a maximum possible diversity with a simple decoding algorithm. Their simplicity is very attractive but they do not achieve any coding gain, while non-full rate space-time block codes can introduce bandwidth expansion. Space-time trellis codes (STTCs), originally proposed by Tarokh *et al.* [2], incorporate joint channel coding, modulation, transmit diversity and optional receive diversity. As the name suggests, the structure of space-time trellis code is given by a trellis. A trellis for 4-state quartenary phase shift keying (QPSK) STTC with two transmit antennas is shown on Fig. 2.18.

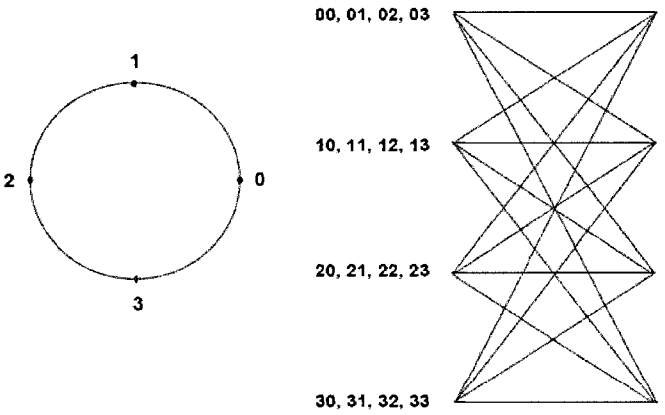

Figure 2.18: Tarokh's 4-state QPSK space-time trellis code. [2]

Here the first QPSK symbol is transmitted from the first antenna and the second

QPSK symbol is transmitted from the second antenna, at time t. Thus, at each time instance, one information symbol is transmitted, and the rate is one. The $N_r \times 1$ received signal is given by

$$\mathbf{y}_t = \mathbf{H}_t \mathbf{s}_t + \mathbf{n}_t \tag{2.46}$$

where $\mathbf{H}_t = \{h_{ij}\}, i = 1, \ldots, N_t; \quad j = 1, \ldots, N_r$ is the channel coefficients matrix, and $\mathbf{x} = [x_1, \ldots, x_{N_t}]^T$ is the transmitted data vector at time instance t. A codeword $\mathbf{c}$ is defined as

$$\mathbf{c} = \begin{bmatrix} c_1(1) & c_1(2) & \cdots & c_1(a) \\ c_2(1) & c_2(2) & \cdots & c_2(a) \\ \vdots & \vdots & \ddots & \vdots \\ c_{N_t}(1) & c_{N_t}(2) & \cdots & c_{N_t}(a) \end{bmatrix} \tag{2.47}$$

where an error event is given by $\mathbf{B}(\mathbf{c}, \mathbf{e}) = \mathbf{c} - \mathbf{e}$. The probability of erroneously decoding $\mathbf{e}$ when $\mathbf{c}$ was transmitted, called pairwise error probability (PEP), is given by [2]

$$P(c, e) \leq \left(\prod_{i=1}^{r} \lambda_i \right)^{-N_r} \left(\frac{E_s}{4N_o} \right)^{-rN_r} \tag{2.48}$$

where r is the rank of $\mathbf{A}(\mathbf{c}, \mathbf{e}) = \mathbf{B}(\mathbf{c}, \mathbf{e})\mathbf{B}^H(\mathbf{c}, \mathbf{e})$ and λ are the nonzero eigenvalues of $\mathbf{A}(\mathbf{c}, \mathbf{e})$. From [2], the design criteria can be given as

- Rank criterion: To achieve maximum possible diversity, $N_t \times N_r$, the matrix $\mathbf{A}(\mathbf{c}, \mathbf{e})$ should be full rank for all the codewords.
- Determinant criterion: To maximize the coding gain, the minimum determinant of $\mathbf{A}(\mathbf{c}, \mathbf{e})$ should be maximized over all codewords.

2.8 Conclusion

We have reviewed in this chapter some background notions that will help us understand better the content of this thesis. We have reviewed the notion of multipath fading, along with statistical representation of fading channels. We have also reviewed multiaccess communication, along with single and multiuser detectors used to detect signals in a multiuser environment. Finally we covered the principle of diversity, MIMO communication and STC schemes.

In the following chapter we shall proceed to the performance analysis of space-time spreading scheme that combines CDMA technology for multiuser access and MIMO technology used to improve the performance of the system over a Nakagami-m fading channels

Chapter 3

Space-Time CDMA Systems over Nakagami-m Fading Channels

3.1 Introduction

MAI is a major limiting factor of the performance of DS-CDMA systems. To overcome the effect of MAI, in the literature, several multiuser based detectors have been introduced [18]. Another major factor affecting the performance of communication systems is signal fading. Recently, much research has been conducted in order to assess different methods that can improve the signal quality reception and increase data rates [30, 31]. One solution to these problems resides in the use of multiple antennas at the transmitter and receiver sides (referred as MIMO systems).

STC techniques that are based on MIMO were introduced [2] and can provide spatial diversity and/or coding gain. By exploiting the independent fading between the channels of different transmit and receive antennas, spatial diversity can be achieved. Examples of STCs are STTCs which were first introduced by Tarokh *et. al.* [2] as a generalization of trellis-coded modulation (TCM) to multiple transmit antennas and STBCs [24, 2]. STTCs, although offering tremendous performance improvement over fading channels present complexity issues that make them hard to implement in practice. In order to go around the complexity of STTCs, a simple space-time transmit diversity scheme using two transmit antennas at the base-station and a single receive antenna at the mobile user was introduced by Alamouti [24]. The signal detection in this case is based on a ML receiver which can be implemented using linear processing. Alamouti's scheme was then generalized by Tarokh *et. al.* [30] to multiple transmit

antennas resulting in the so-called STBC.

STCs were initially introduced for quasi-static fading channels where time variation of the channel is assumed to be constant over a frame and varies independently from one frame to another. Interest then grew in exploiting the time diversity of the channel and STCs for fast fading channels were proposed. Firmanto *et. al.* [32] have proposed a STTC for fast fading channels where the fading coefficients change independently from one symbol to the other. Motivated by the work of Firmanto *et. al.* [32], the authors of [33] proposed a scheme suitable for DS-CDMA system over fast fading channels that employs a space-time block coding scheme satisfying the orthogonality condition by using two codes per user. The proposed scheme is simple to implement, and adds minimal complexity to the transmit diversity schemes introduced in [24] and [3].

Since the initial proposal of STCs, significant research efforts have aimed at their integration with DS-CDMA systems [3, 34]. For instance, the authors in [3] have proposed a novel spreading scheme that is inspired by STCs referred to as space-time spreading (STS).

In this chapter we investigate the space-time spreading scheme introduced in [35, 36], that combines CDMA for multiuser access and MIMO used to improve the performance of the system over a Nakagami-m fading channels. We will study the performance of our system over both slow fading and fast fading channels. We will first derive the probability of error of the system. To do so, we obtain an expression for the PDF of the SINR at the output of the STS combiner.

The remainder of this chapter is organized as follows. In section 3.2 we proceed to the performance analysis of the space-time spreading scheme operating in a slow fading Nakagami-m fading channel. After presenting the multiuser system model, we derive the PDF of the SINR as well as the BER of the space-time system under investigation. Then we present simulation results to assess the accuracy of our theoretical results. The same paradigm is used to assess the performance of space-time scheme operating in a fast fading Nakagami-m channel. For the fast fading scenario, a characteristic function based approach is used to obtain the PDF of the SINR. A conclusion will then come to end this chapter.

3.2 Slow Fading Channel

3.2.1 System Model

The use of a Nakagami-m model for fading is motivated by the fact that it fits into empirical data (see section 2.1.2). The fading signal amplitude in this case is well modeled by the PDF

$$f_R(r) = \frac{2m^m r^{2m-1}}{\Gamma(m)\Omega^m} e^{-(m/\Omega)r^2} \tag{3.1}$$

where $\Omega = E[R^2] = \overline{R^2}$ with E[$\cdot$] represents statistical expectation and $m = \frac{\overline{R^2}}{(R^2 - \overline{R^2}^2)} \geq \frac{1}{2}$. Given the practical importance of the Nakagami fading, in what follows, we study the performance of the STS scheme presented in [3] over such a channel model.

Now let us consider a CDMA system with K users where the k^{th} user transmits a data stream of real symbols x_k. The data stream is first split into two independent data streams, namely odd and even substreams x_{k1} (odd) and x_{k2} (even). A single spreading sequence s_k is used per user. We assume for now that we are referring to user k and we will keep the k subscript in order to be consistent with the remaining part of the section. We also assume for now that each receiver is equipped with one receive antenna.

The two substreams, x_{k1} and x_{k2}, is spread using two orthogonal codes s_{k1} and s_{k2} defined as follows [3]:

$$s_{k1} = \begin{bmatrix} s_k & 0_{P\times 1} \end{bmatrix}^T, s_{k2} = \begin{bmatrix} 0_{P\times 1} & s_k \end{bmatrix}^T \tag{3.2}$$

where T and P represent matrix transpose and processing gain of s_k, respectively. $0_{P\times 1}$ is a zero-vector of length P.

In this fashion the signals transmitted from the first and second antennas of user k are given respectively by:

$$\begin{aligned} t_{k1} &= (1/\sqrt{2})(x_{k1}s_{k1} + x_{k2}s_{k2}) \\ t_{k2} &= (1/\sqrt{2})(x_{k2}s_{k1} - x_{k1}s_{k2}) \end{aligned} \tag{3.3}$$

where, s_{k1} and s_{k1} are orthogonal $2P\times 1$ unit-norm spreading sequences i.e. $s_{k1}^* s_{k2} = 0$

with $*$ denotes conjugate transpose. Note that two spreading codes of length $2P$ are employed for both data streams. The STS scheme that was just described is shown schematically in Fig. 3.1. The transmitted signals then go through the fading channel and at the receiver end they are despread using s_{k1} and s_{k2}. The received signals after despreading are then given by:

$$\begin{aligned} y_{k1} &= (1/\sqrt{2})(h_{k1}x_{k1} + h_{k2}x_{k2}) + s_{k1}^{*}n_{k1} \\ y_{k2} &= (1/\sqrt{2})(-h_{k2}x_{k1} + h_{k1}x_{k2}) + s_{k2}^{*}n_{k2} \end{aligned} \tag{3.4}$$

where h_{kn} models the Nakagami-m fading between the n^{th} (out of N_t) transmit and the receive antenna for user k^{th} channel, and n_{k1}, n_{k2} are Gaussian noise samples of zero mean and variance $N_o/2$. If we define

$$\mathbf{y}_k = (1/\sqrt{2})[y_{k1}\ y_{k2}]^T,$$

we have in matrix formulation

$$\mathbf{y}_k = (1/\sqrt{2})\mathbf{H}_k\mathbf{x}_k + \boldsymbol{\nu}_k. \tag{3.5}$$

Here the channel matrix

$$\mathbf{H}_k = \begin{bmatrix} h_{k1} & h_{k2} \\ -h_{k2} & h_{k1} \end{bmatrix}$$

consists of Nakagami-m coefficients as defined above, $\mathbf{x}_k = [x_{k1}\ x_{k2}]^T$ represents the odd and even information bits, and $\boldsymbol{\nu}_k = [s_{k1}^{*}n_k\ s_{k2}^{*}n_k]^T$ is a Gaussian noise vector.

Assuming that CSI is perfectly known at the receiver and multiplying (3.5) by $\mathbf{H}_k^H$ gives,

$$\mathbf{H}_k^H\mathbf{y}_k = (1/\sqrt{2}) \begin{bmatrix} |h_{k1}|^2 + |h_{k2}|^2 & h_{k1}^{*}h_{k2} - h_{k2}^{*}h_{k1} \\ h_{k2}^{*}h_{k1} - h_{k1}^{*}h_{k2} & |h_{k1}|^2 + |h_{k2}|^2 \end{bmatrix} \mathbf{x}_k + \mathbf{H}_k^H\boldsymbol{\nu}_k. \tag{3.6}$$

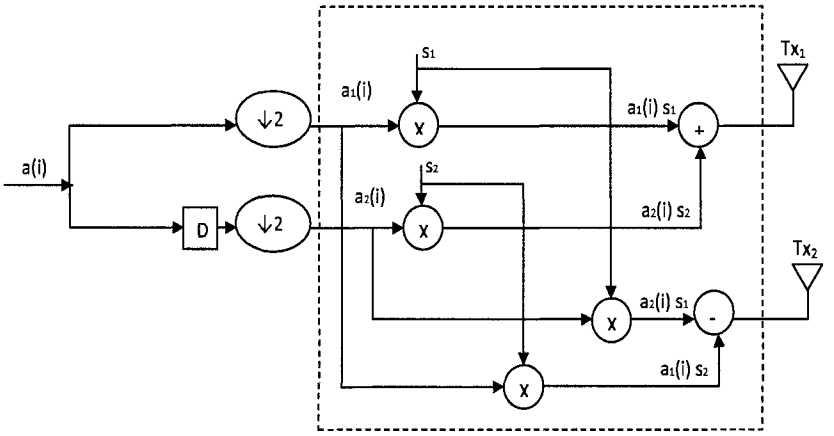

Figure 3.1: A (2,1) STS scheme [3].

The real part of (3.6) is

$$\mathrm{Re}\{\mathbf{H}_k^H \mathbf{y}_k\} = (1/\sqrt{2}) \begin{bmatrix} |h_{k1}|^2 + |h_{k2}|^2 & 0 \\ 0 & |h_{k1}|^2 + |h_{k2}|^2 \end{bmatrix} \mathbf{x}_k + \mathrm{Re}\{\mathbf{H}_k^H \boldsymbol{\nu}_k\}. \quad (3.7)$$

The soft data estimates are obtained from (3.7) as

$$\begin{aligned} \hat{\mathbf{x}}_k &= \mathrm{Re}\{\mathbf{H}_k^H \mathbf{y}_k\} = \frac{1}{\sqrt{2}} \left[|h_{k1}|^2 + |h_{k2}|^2\right] \mathbf{x}_k \\ &\quad + \mathrm{Re}\left\{\mathbf{H}_k^H \boldsymbol{\nu}_k\right\}. \end{aligned} \quad (3.8)$$

We see from (3.8) that the space-time system delivers a diversity order of two when the fading coefficients are Rayleigh distributed.

Considering a synchronous DS-CDMA system [18], and using vector notation, the single-user system model can be generalized to a multiuser system with K users. From now on we also consider a general scenario where the receiver is equipped with N_r receive antennas at the BS and $N_t = 2$ antennas at the user side. The output of the $2K$ matched filters at the l^{th} receive antenna of the BS can be expressed as:

$$\mathbf{y}_l = \mathbf{R}\mathbf{H}_l\mathbf{x} + \mathbf{n}_l \quad (3.9)$$

where

$$\mathbf{y}_l = [y_{11,l}\ y_{12,l} \cdots y_{k1,l}\ y_{k2,l} \cdots y_{K1,l}\ y_{K2,l}]^T,$$

$$\mathbf{x} = [x_{11,l}x_{12,l} \ldots x_{k1,l}\ x_{k2,l} \ldots x_{k1,l}x_{k2,l}]^T$$

is the $(2K \times 1)$ odd and even data vector, and $\mathbf{n}_l$ consists of AWGN elements with variance $\sigma_k^2 = N_0/2$ per dimension. The $(2K \times 2K)$ cross-correlation matrix $\mathbf{R}$ consists of elements ρ_{ij} representing the cross-correlation between the ith and jth spreading codes. Finally $\mathbf{H}_l$ is defined as

$$\mathbf{H}_l = \begin{bmatrix} \mathbf{H}_{l1} & 0 & \ldots & 0 & 0 \\ 0 & \ldots & \ldots & 0 & 0 \\ \ldots & \ldots & \mathbf{H}_{lk} & \ldots & \ldots \\ 0 & \ldots & \ldots & \ldots & 0 \\ 0 & 0 & \ldots & 0 & \mathbf{H}_{lK} \end{bmatrix},$$

with

$$\mathbf{H}_{lk} = \begin{bmatrix} h_{k1,l} & h_{k2,l} \\ -h_{k2,l} & h_{k1,l} \end{bmatrix}$$

where $h_{kn,l}$, represents the fading coefficient corresponding to the channel between transmit antenna n=1,2, and receive antenna l for user k.

3.2.2 Performance Analysis

Without loss of generality, we consider user k as the desired user. From (3.9), the vector of user data estimates at the output of the conventional detector of the l^{th} antenna is given by:

$$\hat{\mathbf{x}}_{conv}^l = \frac{1}{\sqrt{2}} \mathrm{Re}\{\mathbf{H}_l^H \mathbf{y}_l\}. \tag{3.10}$$

Employing the decorrelator detector widely used in the literature, the vector of user data estimate at the output of the l^{th} decorrelator detector is given by:

$$\begin{aligned} \hat{\mathbf{x}}_{dec}^l &= \frac{1}{\sqrt{2}} \mathrm{Re}\{\mathbf{H}_l^H \mathbf{R}^{-1} \mathbf{y}_l\} \\ &= \frac{1}{\sqrt{2}} \mathrm{Re}\{\mathbf{H}_l^H \mathbf{H}_l\}\mathbf{x} + \mathrm{Re}\{\mathbf{H}_l^H \mathbf{R}^{-1} \mathbf{n}_l\}. \end{aligned} \tag{3.11}$$

Hence, the SNR for user k at the l^{th} decorrelator output is given by:

$$SNR_{k,l,dec} = \frac{|h_{k1,l}|^2 + |h_{k2,l}|^2}{2\sigma_k^2(R^{-1}_{2k-1,2k-1} + R^{-1}_{2k,2k})} \tag{3.12}$$

where $R^{-1}_{2k-1,2k-1}, R^{-1}_{2k,2k}$ are the $2k-1^{th}$ and $2k^{th}$ diagonal elements of the inverse of the cross-correlation matrix, $\mathbf{R}^{-1}$.

The receiver will now need to combine the output of all of its antennas. Since we are considering BPSK transmission, the conditional probability of error (i.e., conditioned on the channel realization) is given by

$$\begin{aligned} P_{x|\mathbf{h}} &= Q\left(\sqrt{2\sum_{l=1}^{N_r} SNR_{k,l,dec}}\right) \\ &= Q\left(\sqrt{\frac{\sum_{l=1}^{N_r}(|h_{k1,l}|^2 + |h_{k2,l}|^2)}{\sigma_k^2(R^{-1}_{2k-1,2k-1} + R^{-1}_{2k,2k})}}\right) \end{aligned} \tag{3.13}$$

where $Q(x) = \int_x^\infty \frac{1}{\sqrt{2\pi}} \exp(-\frac{v^2}{2})dv$. To find the exact BER expression, one needs to average (3.13) over the PDF of $\sum_{l=1}^{N_r} |h_{k1,l}|^2 + |h_{k2,l}|^2$. To do this let us define an instantaneous SNR as:

$$\gamma_{il} = |h_{ki,l}|^2 \left(\frac{2E_{xi}}{N_0 C}\right), \quad i = 1, 2 \tag{3.14}$$

where $C = R^{-1}_{2k-1,2k-1} + R^{-1}_{2k,2k}$, E_{xi} is the transmitted symbol energy from each antenna and $E_{xi} = \left(1/\sqrt{N_t}\right)^2$ since we wish to balance out the power of one symbol normally sent using one antenna over N_t transmit antennas, N_0 is the one-sided power spectral density of the AWGN. The average of γ_{il} is then given by

$$\overline{\gamma}_{il} = E[|h_{ki,l}|^2] \left(\frac{1}{N_0 C}\right), \; i = 1, 2.$$

If $|h_{ki,l}|$, $i = 1, 2$, is characterized by Nakagami-m distribution, then γ_{il} has a gamma

distribution [4]. Hence the PDF of γ_{il} is given by:

$$f_{\gamma_{il}}(\gamma_{il}) = \frac{1}{\Gamma(m)} \left(\frac{m}{\overline{\gamma}_{il}}\right)^m \gamma_{il}^{m-1} e^{-\frac{m\gamma_{il}}{\overline{\gamma}_{il}}}, \qquad m \geq 0.5. \tag{3.15}$$

The SNR after signal combining is then given by

$$\begin{aligned} SNR_{k,dec} &= \sum_{l=1}^{N_r} SNR_{k,l,dec} \\ &= \sum_{l=1}^{N_r} \frac{|h_{k1,l}|^2 + |h_{k2,l}|^2}{2\sigma_k^2 (R^{-1}_{2k-1,2k-1} + R^{-1}_{2k,2k})}. \end{aligned}$$

Finally we have

$$\gamma = SNR_{k,dec} = \sum_{\substack{l=1 \\ i=1,2}}^{N_r} \gamma_{il} = \sum_{l=1}^{2N_r} \gamma_{il}. \tag{3.16}$$

Since we assume the paths from the two transmit antennas to the N_r receive antennas to be mutually independent, then the characteristic function of the sum γ is given for integer values of the fading figure m by [37]:

$$\phi_\gamma(\varsigma) = \left(1 + \frac{\varsigma \overline{\gamma}_{il}}{m}\right)^{2mN_r}. \tag{3.17}$$

Therefore γ is also gamma distributed with the following PDF:

$$f_\gamma(\gamma) = \frac{1}{\frac{\overline{\gamma}_{il}}{m}\Gamma(2mN_r)} \left(\frac{\gamma}{\frac{\overline{\gamma}_{il}}{m}}\right)^{2mN_r - 1} e^{-\frac{m\gamma}{\overline{\gamma}_{il}}}, m \geq 0.5 \tag{3.18}$$

which is a function of $N_t = 2$, and N_r as well as the fading figure m. Now the probability of bit error can be easily found from

$$P_x = \int_0^\infty Q\left(\sqrt{2\gamma}\right) f_\gamma(\gamma) d\gamma. \tag{3.19}$$

A closed form expression for (3.19), for integer values of the fading parameter m, is

given by [4]:

$$P_x = \left(\frac{1-\mu}{\mu}\right)^{2mN_r} \cdot \sum_{k=0}^{2mN_r-1} \binom{2mN_r-1+k}{2mN_r} \left(\frac{1+\mu}{mu}\right)^k \tag{3.20}$$

where

$$\mu = \sqrt{\frac{\overline{\gamma}_{il}/m}{1+\overline{\gamma}_{il}/m}}.$$

When $\overline{\gamma}_{il}/m \gg 1$, $(1+\mu)/2 \approx 1$ and $(1-\mu)/2 \approx 1/4\overline{\gamma}_{il}$; furthermore $\sum_{k=0}^{2mN_r-1} \binom{2mN_r-1+k}{2mN_r} = \binom{2*2mN_r-1}{2mN_r}$. Therefore when $\overline{\gamma}_{il}/m$ is sufficiently large, the probability of error in (3.20) can be approximated by:

$$P_x \approx \left(\frac{1}{4\overline{\gamma}_{il}}\right)^{2mN_r} \binom{4mN_r-1}{2m} \tag{3.21}$$

which clearly shows that the achieved diversity is of order $2mN_r$.

3.2.3 Simulation Results

Here we present simulation results to examine the performance of the space-time transmit diversity system operating in a Nakagami-m fading channel. In order to generate the Nakagami-m fading channel coefficients, we used the method described in section 2.2.

In what follows, each user signal is encoded using spreading codes taken from a family of Gold codes of length 11 chips. BPSK modulation is used, with the assumption of perfect channel state information at the receiver side. The channel is modeled as slowly fading where the channel coefficients are fixed for a block length of 100 symbols and change from one frame to another. We also consider $N_t = 2$ transmit antennas, and simulate for different configurations of receive antennas N_r, system loads and fading figures m. We set as benchmark the performance results of the single-user system and the MRC with $2mN_r$ diversity branches. We consider in our simulations that the CDMA transmission is totally synchronous and that a decorrelator detector is used at the receiver in order to combat MAI. All the transmission channels are assumed to be mutually independent.

In Fig. 3.2 we examine the performance of the STS scheme for different antenna configurations and a fading figure m=3. Note that the 3dB difference between the single-user STS scheme and the MRC is due to the fixed power constraint set at the transmitter side where two antennas are used. Examining the results in this figure, one can see that the theoretical BER results are quite accurate when compared to simulation results. Also note that the systems with the same parameters $N_t = 2$, m, N_r, achieve the same diversity order of $2mN_r$.

In the following section, we will consider the same space-time scheme presented in the current section. We will study the performance of that system in a fast fading channel.

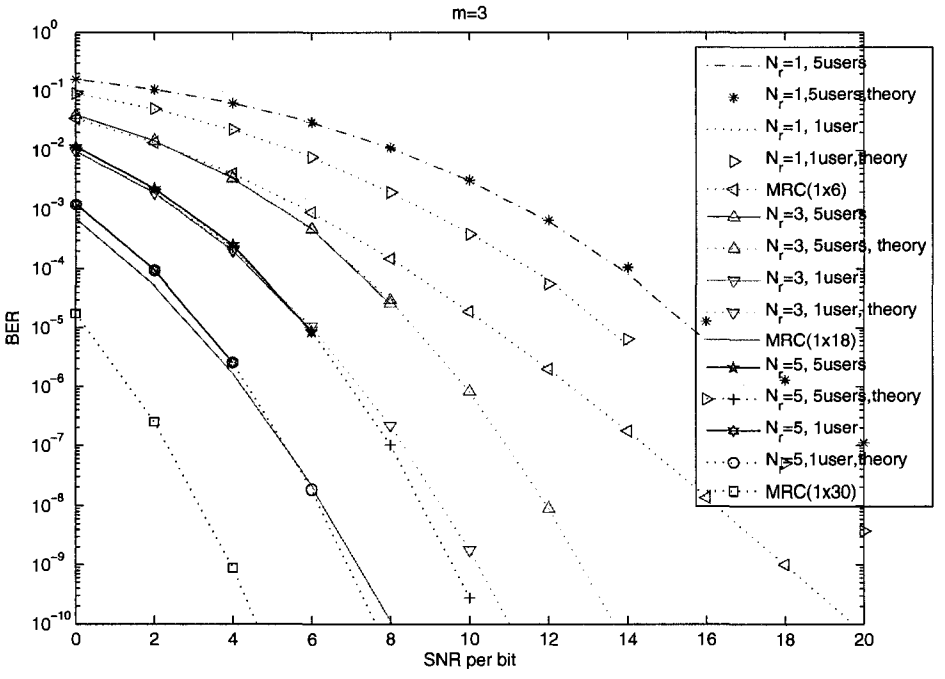

Figure 3.2: Simulation vs. theoretical results in Nakagami-m fading, N_t=2, and N_r=1,3,5.

3.3 Fast Fading Channel

3.3.1 System Model

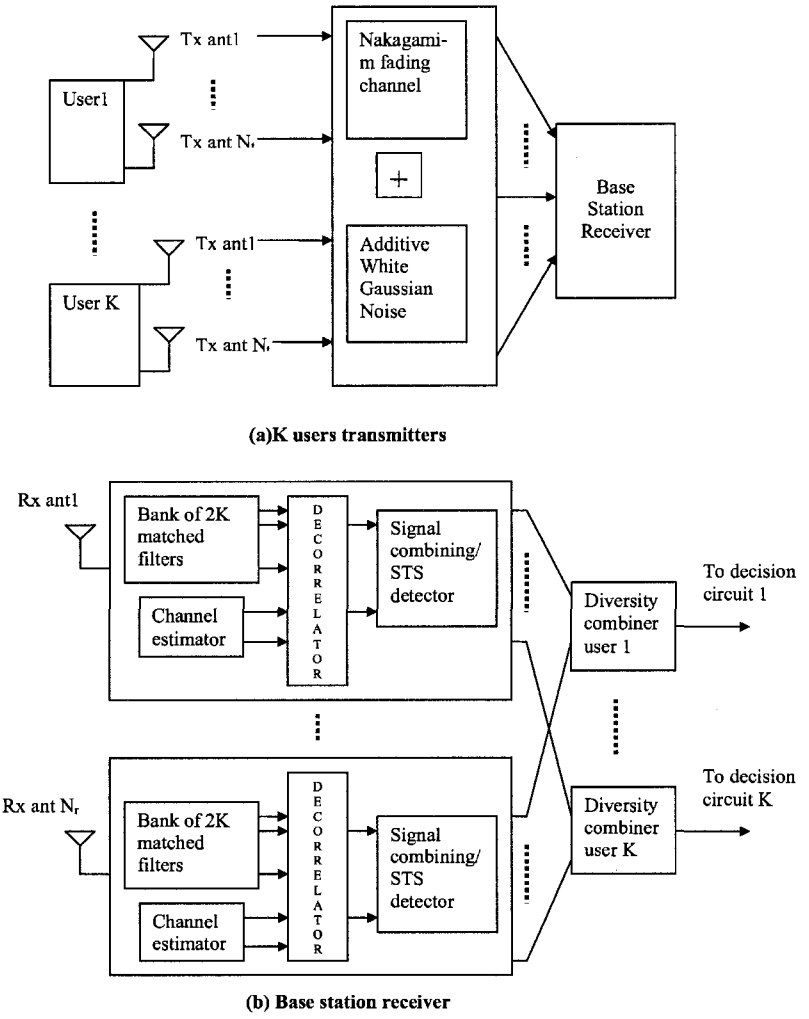

Figure 3.3: Multi-user STS DS-CDMA system operating in a Nakagami-m fading environment (a)K users transmitters (b) Base Station Receiver.

We are interested in a multiuser DS-CDMA wireless communication system. The system model is shown schematically on Fig. 3.3. Without loss of generality we start by considering the simple case of a single user wireless communication system that employs two antennas at the transmitter side and a single antenna at the receiver side. If we let x_1 and x_2 be the input symbols of our user to the STS encoder (x_1

and x_2 can be considered as the odd and even part of the user data stream), then each data symbol is modulated and then spread using two unique spreading codes known only to the desired user, $s_i, i = 1, 2$. We try here to be consistent with the notation used by the authors of [38]. After the information bits have been modulated and spread a space-time code matrix is formed as follows [38]

$$\begin{array}{lcc} & \text{Tx Antenna 1} & \text{Tx Antenna 2} \\ time\ \ t, & x_1^* s_1 + x_2^* s_2 & x_1 s_2 - x_2 s_1 \\ time\ \ t+T, & x_1 s_2 - x_2 s_1 & x_1^* s_1 + x_2^* s_2. \end{array} \tag{3.22}$$

Here $(^*)$ denotes a complex conjugate operation. The encoder produced two codewords $x_1^* s_1 + x_2^* s_2$ and $x_1 s_2 - x_2 s_1$ which are transmitted by antenna 1 and 2 respectively at time t, and switched with respect to the transmit antennas at time $t + T$.

We consider here a synchronous multiuser DS-CDMA system. Using vector notation, the single user model can be generalized to the multiuser DS-CDMA case with K users. The output of the $2K$ matched filters at the l^{th} receive antenna can be expressed as

$$\mathbf{Y}_0^l = \mathbf{R}\mathbf{H}_0^l\mathbf{x} + \mathbf{N}_0^l \tag{3.23}$$

$$\mathbf{Y}_1^l = \mathbf{R}\mathbf{H}_1^l\mathbf{x} + \mathbf{N}_1^l \tag{3.24}$$

at times t and $t + T$ respectively. Here $\mathbf{Y}_j^m$, $j = 0, 1$, is defined as

$$\mathbf{Y}_j^l = \left[y_{j,11}^l, y_{j,12}^l, ..., y_{j,k1}^l, y_{j,k2}^l, ..., y_{j,K1}^l, y_{j,K2}^l\right]^{\mathrm{T}} \tag{3.25}$$

where $y_{j,ki}^l$, $i = 1, 2$, $j = 0, 1$, represents the i^{th} matched filter output of user k at times t and $t + T$. The cross-correlation matrix $\mathbf{R}$ is given by

$$\mathbf{R} = \begin{bmatrix} \rho_{1,1} & .... & \rho_{1,k} & .... & \rho_{1,2K} \\ \rho_{2,1} & .... & \rho_{2,k} & .... & \rho_{2,2K} \\ .... & .... & .... & .... & .... \\ .... & .... & .... & .... & .... \\ \rho_{2K,1} & .... & \rho_{2K,k} & .... & \rho_{2K,2K} \end{bmatrix} \tag{3.26}$$

where $\rho_{i,j}$ represents the cross-correlation between any two spreading codes s_i and s_j. The $(2K \times 2K)$ channel coefficients matrix $\mathbf{H}_j^l$, $j = 0, 1$ at time t and $t + T$ respectively in (3.23) and (3.24), is defined as

$$\mathbf{H}_j^l = \begin{bmatrix} \mathbf{h}_{j,1}^l & 0 & .... & 0 & 0 \\ 0 & \mathbf{h}_{j,2}^l & .... & 0 & 0 \\ .... & .... & .... & .... & .... \\ .... & .... & .... & ..\mathbf{h}_{j,K-1}^l.. & .... \\ 0 & 0 & .... & 0 & \mathbf{h}_{j,K}^l \end{bmatrix} \tag{3.27}$$

where the 2×2 channel coefficients submatrices $\mathbf{h}_{0,k}^l$ and $\mathbf{h}_{1,k}^l$ containing the fading coefficients $h_{il,j,k}$, $j = 0, 1$ and $i = 1, 2$, between the i^{th} transmit antenna of user k and the l^{th} receive antenna at the base station at times t and $t + T$ respectively are defined as

$$\mathbf{h}_{0,k}^l = \begin{bmatrix} h_{1l,0,k} & -h_{2l,0,k} \\ h_{2l,0,k} & h_{1l,0,k} \end{bmatrix}, \tag{3.28}$$

$$\mathbf{h}_{1,k}^l = \begin{bmatrix} h_{2l,1,k} & -h_{1l,1,k} \\ h_{1l,1,k} & h_{2l,1,k} \end{bmatrix}. \tag{3.29}$$

The transmitted data vector $(2K \times 1)$ for the K-user system is given by

$$\mathbf{x} = [x_{1,1}, x_{1,2}, ..., x_{k,1}, x_{k,2}, ..., x_{K,1}, x_{K,2}]^T \tag{3.30}$$

where $x_{k,i}$, $i = 1, 2$, represents the even and odd data symbols for user k. The $(2K \times 1)$ noise vector $\mathbf{N}_j^l$, $j = 0, 1$, consists of N_{kj}^l, $k = 1, ..., K$, $j = 0, 1$, complex Gaussian RVs, each with variance $N_o/2$ per dimension. Given the matched filter outputs of (3.23) and (3.24), the signals at times t and $t + T$ are combined as in [38] in order to give the two transmitted symbols of user k, $\hat{x}_{k,1}$ and $\hat{x}_{k,2}$ in the following way

$$\hat{x}_{k,1} = \sum_{l=1}^{N_r} h_{1l,0,k} y_{0,k1}^{l*} + h_{2l,0,k}^* y_{0,k2}^l + h_{1l,1,k}^* y_{1,k2}^l + h_{2l,1,k} y_{1,k1}^{l*} \tag{3.31a}$$

$$\hat{x}_{k,2} = \sum_{l=1}^{N_r} h_{1l,0,k} y_{0,k2}^{l*} - h_{2l,0,k}^{*} y_{0,k1}^{l} - h_{1l,1,k}^{*} y_{1,k1}^{l} + h_{2l,1,k} y_{1,k2}^{l*}. \tag{3.31b}$$

3.3.2 Performance Analysis

The performance analysis is similar to the one presented in [35, 36]. The major contribution is that we generalize the Rayleigh fading case studied in [35, 36] to a more general Nakagami-m fading case. Without loss of generality we will consider user 1 as the desired user and drop its corresponding subscript k. From [38] we get that using the combining scheme in (3.31a) and (3.31b) to find an estimate $\hat{x}_1$ of the first bit x_1 of user 1 we have

$$\begin{aligned}
\hat{x}_1 &= 2(|h_{11,0}|^2 + |h_{21,0}|^2 + ... + |h_{1N_r,1}|^2 + |h_{2N_r,1}|^2)x_1 \\
&+ h_{11,0}(\mathbf{R}^{-1}\mathbf{N}_0^1)_{11}^{*} + h_{21,0}^{*}(\mathbf{R}^{-1}\mathbf{N}_0^1)_{21} + ... \\
&+ h_{1N_r,0}(\mathbf{R}^{-1}\mathbf{N}_0^{N_r})_{1N_r}^{*} + h_{2N_r,0}^{*}(\mathbf{R}^{-1}\mathbf{N}_0^{N_r})_{2N_r} \\
&+ h_{21,1}(\mathbf{R}^{-1}\mathbf{N}_1^1)_{11}^{*} + h_{11,1}^{*}(\mathbf{R}^{-1}\mathbf{N}_1^1)_{21} + ... \\
&+ h_{2N_r,1}(\mathbf{R}^{-1}\mathbf{N}_1^{N_r})_{1N_r}^{*} + h_{1N_r,1}^{*}(\mathbf{R}^{-1}\mathbf{N}_1^{N_r})_{2N_r}.
\end{aligned} \tag{3.32}$$

We assume here a BPSK modulation scheme and thus we can generally express the probability of making an error in estimating x_1 by $\hat{x}_1$ conditioned on the channel coefficients from (3.32) as

$$P_b(\hat{x}_1 = 1 \mid \mathbf{h}_0, \mathbf{h}_1) = Q\left(\frac{\sum_{l=1}^{N_r} |h_{1l,0}|^2 + |h_{2l,0}|^2 + |h_{1l,1}|^2 + |h_{2l,1}|^2}{\sqrt{\sigma_{\hat{x}_1}^2}}\right) \tag{3.33}$$

where the Gaussian Q-function is defined by

$$Q(x) = \int_x^{\infty} \frac{1}{\sqrt{2\pi}} \exp(-\frac{v^2}{2}) dv.$$

From (3.32), one can show that

$$\sigma_{\hat{x}_1}^2 = \sigma_n^2 \left[R_{11}^{-1} \left(\sum_{l=1}^{N_r} |h_{1l,0}|^2 + |h_{2l,1}|^2 \right) + R_{22}^{-1} \left(\sum_{l=1}^{N_r} |h_{2l,0}|^2 + |h_{1l,1}|^2 \right) \right] \tag{3.34}$$

where R_{11}^{-1}, R_{22}^{-1} are the first and second elements of the diagonal of the inverse of the cross-correlation matrix respectively, and σ_n^2 is the variance of independent complex AWGN samples.

$$P_b(\hat{x}_1 = 1 \mid \mathbf{h}_0, \mathbf{h}_1) = Q \left(\frac{\sum_{l=1}^{N_r} |h_{1l,0}|^2 + |h_{2l,0}|^2 + |h_{1l,1}|^2 + |h_{2l,1}|^2}{\sigma_n \sqrt{\left(\begin{array}{c} R_{11}^{-1} \left(\sum_{l=1}^{N_r} |h_{1l,0}|^2 + |h_{2l,1}|^2 \right) + \\ R_{22}^{-1} \left(\sum_{l=1}^{N_r} |h_{2l,0}|^2 + |h_{1l,1}|^2 \right) \end{array} \right)}} \right). \tag{3.35}$$

PDF of Conditional SINR

Our main constraint here is that the channel is modeled as a Nakagami-m fading channel so that each of the fading coefficients $h_{il,j}$ is a realization of a Nakagami-m RV F. In this case F^2 is a Gamma RV with PDF and characteristic function respectively given by:

$$f_{F^2}(r) = \frac{1}{\Gamma(m)} \frac{r^{m-1}}{\beta^m} \exp^{-\frac{r}{\beta}}, \quad r \geq 0 \tag{3.36}$$

$$\phi_{F^2}(\omega) = (1 - j\omega\beta)^{-m}, \quad j = \sqrt{-1} \tag{3.37}$$

where the parameter β is defined as $\beta = \frac{\Omega}{m}$ and $\Omega = E\left[|h_{jl,l}^2|\right]$ is the power of the Nakagami-m fading coefficients. Let us define $C_1 = R_{11}^{-1}$ and $C_2 = R_{22}^{-1}$, then the argument inside the Q-function in (3.35) renamed in terms of another RV τ, can be written as:

$$\tau = \frac{\alpha_1}{\sqrt{\alpha_2}}. \tag{3.38}$$

The RVs α_1 and α_2 in (3.38) are defined as follows:

$$\alpha_1 = \sum_{l=1}^{N_r} |h_{1l,0}|^2 + |h_{2l,0}|^2 + |h_{1l,1}|^2 + |h_{2l,1}|^2 \tag{3.39}$$

$$\alpha_2 = C_1 \left(\sum_{l=1}^{N_r} |h_{1l,0}|^2 + |h_{2l,1}|^2 \right) + C_2 \left(\sum_{l=1}^{N_r} |h_{2l,0}|^2 + |h_{1l,1}|^2 \right). \tag{3.40}$$

We will also define a new RV as $\lambda = \alpha_2$. We will focus now on the PDF of the RV τ. The joint PDF $f_{\tau,\lambda}$ of τ and λ can be obtained from the joint PDF f_{α_1,α_2} through variable transformation as follows:

$$f_{\tau,\lambda} = f_{\alpha_1,\alpha_2} |J(\tau,\lambda)| \tag{3.41}$$

where $|J(\tau,\lambda)| = \sqrt{\alpha_2}$ is the jacobian of the transformation. Finally the marginal PDF of interest f_τ can be obtained by integrating $f_{\tau,\lambda}$ over all possible values of λ [39].

Joint PDF of α_1 and α_2

We will now proceed to obtain a closed form expression for f_{α_1,α_2} using the joint characteristic function of α_2 and α_2 which is given by:

$$\begin{aligned}
\phi_{\alpha_1,\alpha_2}(\omega_1,\omega_2) &= E\left[e^{j(\omega_1\alpha_1+\omega_2\alpha_2)}\right] \\
&= E\Bigg[\exp\Bigg(j\Big(\omega_1 \sum_{l=1}^{N_r} (|h_{1l,0}|^2 + |h_{2l,0}|^2 + |h_{1l,1}|^2 + |h_{2l,1}|^2) \\
&\quad + \omega_2 C1 \sum_{l=1}^{N_r} |h_{1l,0}|^2 + |h_{2l,1}|^2 + C2 \sum_{l=1}^{N_r} |h_{2l,0}|^2 + |h_{1l,1}|^2 \Big) \Bigg) \Bigg] \\
&= E\left[e^{j\left((\omega_1+\omega_2 C1)\sum_{l=1}^{N_r}|h_{1l,0}|^2\right)} \right] E\left[e^{j\left((\omega_1+\omega_2 C1)\sum_{l=1}^{N_r}|h_{2l,1}|^2\right)} \right] \cdot \\
&\quad E\left[e^{j\left((\omega_1+\omega_2 C2)\sum_{l=1}^{N_r}|h_{2l,0}|^2\right)} \right] E\left[e^{j\left((\omega_1+\omega_2 C2)\sum_{l=1}^{N_r}|h_{1l,1}|^2\right)} \right].
\end{aligned} \tag{3.42}$$

Eq. (3.42) can be expressed in terms of the characteristic function (3.37) as follows:

$$\begin{aligned}\phi_{\alpha_1,\alpha_2}(\omega_1,\omega_2) &= \left[\phi_{F^2}(\omega_1+\omega_2 C1)\right]^{2mN_r}\left[\phi_{F^2}(\omega_1+\omega_2 C1)\right]^{2mN_r} \\ &= \left[1-j(\omega_1+\omega_2 C1)\beta\right]^{-2mN_r}\left[1-j(\omega_1+\omega_2 C2)\beta\right]^{-2mN_r} \\ &= \frac{\beta^{-4mN_r}}{\left[\beta^{-1}-j(\omega_1+\omega_2 C1)\right]^{2mN_r}\cdot\left[\beta^{-1}-j(\omega_1+\omega_2 C2)\right]^{2mN_r}} \\ &= \frac{\beta^{-4mN_r}}{\left[\omega_3-j\omega_2 C_1\right]^{2mN_r}\cdot\left[\omega_3-j\omega_2 C_2\right]^{2mN_r}} \end{aligned} \tag{3.43}$$

where $\omega_3 = (\beta^{-1} - j\omega_1)$. Using the partial fraction expansion, (3.43) can be rewritten as:

$$\phi_{\alpha_1,\alpha_2}(\omega_1,\omega_2) = \sum_{t=1}^{2mN_r} \frac{\beta^{-4mN_r}\cdot b_{2t-1}}{(\omega_3-j\omega_2 C_1)^t\,\omega_3^{4mN_r-t}} + \frac{\beta^{-4mN_r}\cdot b_{2t}}{(\omega_3-j\omega_2 C_2)^t\,\omega_3^{4mN_r-t}} \tag{3.44}$$

where b_{2t-1} and b_{2t} are coefficients obtained from the partial fraction expansion. Using (3.44) the joint PDF, f_{α_1,α_2} is given by:

$$\begin{aligned} f_{\alpha_1,\alpha_2} &= \frac{1}{4\pi^2}\int_{-\infty}^{\infty}\int_{-\infty}^{\infty}\phi_{\alpha_1,\alpha_2}(\omega_1,\omega_2)e^{-j(\omega_1\alpha_1+\omega_2\alpha_2)}d\omega_1 d\omega_2 \\ &= \frac{1}{4\pi^2\beta^{4mN_r}}\sum_{t=1}^{2mN_r} A_{2t-1}+A_{2t}. \end{aligned} \tag{3.45}$$

In (3.45) we define A_d as:

$$A_d = \int_{-\infty}^{\infty}\frac{b_d e^{-j\omega_1\alpha_1}}{\omega_3^{4mN_r-t}}d\omega_1\int_{-\infty}^{\infty}\frac{e^{-j\omega_2\alpha_2}}{(\omega_3-j\omega_2 C_d)^t}d\omega_2 \tag{3.46}$$

where $C_d = C_1$ when $d = 2t-1$ and $C_d = C_2$ when $d = 2t$. We shall now get a closed-form expression for A_d. Using [[40], Eq. (3.382.7)], the integral in terms of ω_2

in (3.46) is given by

$$\int_{-\infty}^{\infty} \frac{e^{-j\omega_2\alpha_2}}{(\omega_3 - j\omega_2 C_d)^t} d\omega_2 = \frac{1}{C_d^t} \int_{-\infty}^{\infty} e^{-j\omega_2\alpha_2} \left(\frac{\omega_3}{C_d} - j\omega_2\right)^{-t} d\omega_2$$
$$= \frac{1}{C_d^t} \frac{2\pi\alpha_2^{t-1} e^{-\frac{\alpha_2\omega_3}{C_d}}}{\Gamma(t)}. \tag{3.47}$$

Substituting (3.47) in (3.46) gives:

$$A_d = \int_{-\infty}^{\infty} \frac{b_d e^{-j\omega_1\alpha_1}}{(\beta^{-1} - j\omega_1)^{4mN_r - t}} \frac{1}{C_d^t} \frac{2\pi\alpha_2^{t-1} e^{-\frac{\alpha_2(\beta^{-1} - j\omega_1)}{C_d}}}{\Gamma(t)} d\omega_1$$
$$= \frac{b_d \cdot 2\pi\alpha_2^{t-1} \cdot e^{-\frac{\alpha_2}{C_d\beta}}}{C_d^t \cdot \Gamma(t)} \int_{-\infty}^{\infty} \frac{e^{-j\omega_1\left(\alpha_1 - \frac{\alpha_2}{C_d}\right)}}{(\beta^{-1} - j\omega_1)^{4mN_r - t}} d\omega_1, \ \alpha_1 - \frac{\alpha_2}{C_d} \geq 0 \tag{3.48}$$
$$= \frac{b_d \cdot 4\pi^2\alpha_2^{t-1} \cdot e^{-\frac{\alpha_2}{C_d\beta}}}{C_d^t \cdot \Gamma(t)\Gamma(4mN_r - t)} \cdot \left(\alpha_1 - \frac{\alpha_2}{C_d}\right)^{4mN_r - t - 1} \cdot$$
$$e^{-\left(\alpha_1 - \frac{\alpha_2}{C_d}\right)\beta^{-1}}, \ \alpha_1 - \frac{\alpha_2}{C_d} \geq 0 \tag{3.49}$$
$$= \frac{4\pi^2 b_d \alpha_2^{t-1}}{C_d^t \Gamma(t)\Gamma(4mN_r - t)} \left(\alpha_1 - \frac{\alpha_2}{C_d}\right)^{4mN_r - t - 1} e^{-\frac{\alpha_1}{\beta}}. \tag{3.50}$$

The transition from (3.48) to (3.49) is due to the fact that the integral in terms of ω_1 in (3.48) can be interpreted as the inverse of the characteristic function (3.37) with the constraint that $\alpha_1 - \frac{\alpha_2}{C_d} \geq 0$. Finally we have the joint PDF of α_1 and α_2 which is given by:

$$f_{\alpha_1,\alpha_2} = \frac{1}{\beta^{4mN_r}} \sum_{t=1}^{2mN_r} \frac{\alpha_2^{t-1} e^{-\frac{\alpha_1}{\beta}}}{\Gamma(t)\Gamma(4mN_r - t)} \left[\frac{b_{2t-1}}{C_1^t} \left(\alpha_1 - \frac{\alpha_2}{C_1}\right)^{4mN_r - t - 1}\right.$$
$$\left. + \frac{b_{2t}}{C_2^t} \left(\alpha_1 - \frac{\alpha_2}{C_2}\right)^{4mN_r - t - 1}\right]. \tag{3.51}$$

PDF of τ

Substituting (3.51) in (3.41) and recalling that $\alpha_1 = \tau\sqrt{\lambda}$ and $\alpha_2 = \lambda$, we can rewrite (3.41) as follows

$$f_{\tau,\lambda} = \frac{\sqrt{\lambda}}{\beta^{4mN_r}} \sum_{t=1}^{2mN_r} \frac{\lambda^{t-1} e^{-\frac{\tau\sqrt{\lambda}}{\beta}}}{\Gamma(t)\Gamma(4mN_r - t)} \cdot \left[\frac{b_{2t-1}}{C_1^t} \left(\tau\sqrt{\lambda} - \frac{\lambda}{C_1} \right)^{4mN_r - t - 1} + \frac{b_{2t}}{C_2^t} \left(\tau\sqrt{\lambda} - \frac{\lambda}{C_2} \right)^{4mN_r - t - 1} \right]. \tag{3.52}$$

In order to obtain the PDF of interest f_τ, we would need to integrate (3.52) over all possible values of λ. We should recall here the constraint from (3.49)

$$\begin{aligned} \alpha_1 - \frac{\alpha_2}{C_d} \geq 0 \quad &\Rightarrow \quad \tau\sqrt{\lambda} - \frac{\lambda}{C_d} \geq 0 \\ &\Rightarrow \quad 0 \leq \lambda \leq C_d^2 \tau^2 \end{aligned} \tag{3.53}$$

which defines the bound for the integration over λ. Thus

$$f_\tau = \frac{1}{\beta^{4mN_r}} \sum_{t=1}^{2mN_r} \frac{b_{2t-1} A'_{2t-1}}{C_1^t \Gamma(t)\Gamma(4mN_r - t)} + \frac{b_{2t} A'_{2t}}{C_2^t \Gamma(t)\Gamma(4mN_r - t)} \tag{3.54}$$

where

$$A'_d = \int_0^{C_d^2 \tau^2} (\sqrt{\lambda})^{2t-1} \left(\tau\sqrt{\lambda} - \frac{\lambda}{C_d} \right)^{4mN_r - t - 1} e^{-\frac{\tau\sqrt{\lambda}}{\beta}} d\lambda. \tag{3.55}$$

Let us here introduce the following formula [9]

$$\begin{aligned} \int_{c_1}^{c_2} x^n e^{-ax} dx = \frac{1}{a(n+1)} \Big[&c_2^n (ac_2)^{-\frac{n}{2}} e^{-\frac{ac_2}{2}} \mathbb{M}(\frac{n}{2}, \frac{n+1}{2}, ac_2) \\ &- c_1^n (ac_1)^{-\frac{n}{2}} e^{-\frac{ac_1}{2}} \mathbb{M}(\frac{n}{2}, \frac{n+1}{2}, ac_1) \Big] \end{aligned} \tag{3.56}$$

where $\mathbb{M}(k, m, z)$ represents the WhittakerM function [40]. If we proceed to a change of variable $\eta = \sqrt{\lambda}$ in (3.55) and we use Newton's binomial theorem and also using

(3.56) we can rewrite (3.55) as follows

$$
\begin{aligned}
A_d^{'} &= \int_0^{C_d^2\tau^2} (\sqrt{\lambda})^{2t-1} \left(\tau\sqrt{\lambda} - \frac{\lambda}{C_d}\right)^{4mN_r-t-1} e^{-\frac{\tau\sqrt{\lambda}}{\beta}} d\lambda \\
&= \sum_{k=0}^{4mN_r-t-1} \binom{4mN_r-t-1}{k} \tau^k \cdot \\
&\qquad \int_0^{C_d^2\tau^2} (\sqrt{\lambda})^{8mN_r-k-3} \left(\frac{-1}{C_d}\right)^{4mN_r-t-k-1} e^{-\frac{\tau\sqrt{\lambda}}{\beta}} d\lambda \\
&= \sum_{k=0}^{4mN_r-t-1} \binom{4mN_r-t-1}{k} \cdot \\
&\qquad 2\tau^k \frac{(-1)^{4mN_r-t-k-1}}{C_d^{4mN_r-t-k-1}} \int_0^{C_d\tau} \eta^{8mN_r-k-2} e^{-\frac{\tau\eta}{\beta}} d\eta \\
&= \sum_{k=0}^{4mN_r-t-1} 2\binom{4mN_r-t-1}{k} \frac{(-1)^{4mN_r-t-k-1}\tau^{k-1}\beta^{4mN_r-\frac{k}{2}} C_d^{t+\frac{k}{2}}}{8mN_r-k-1} \cdot \\
&\qquad \mathbb{M}\left(4ml - \frac{k}{2} - 1; 4ml - \frac{k}{2} - \frac{1}{2}; \frac{\tau^2 C_d}{\beta}\right) e^{-\frac{\tau^2 C_d}{2\beta}}. \qquad (3.57)
\end{aligned}
$$

We can rewrite (3.57) in terms of the confluent hypergeometric function (eq.(13.1.32),[40]) as follows

$$
\begin{aligned}
A_d^{'} = 2 \cdot & \sum_{k=0}^{4mN_r-t-1} \binom{4mN_r-t-1}{k} \frac{(-1)^{4mN_r-t-k-1} C_d^{4mN_r+t}}{8mN_r-k-1} \cdot \\
& \tau^{8mN_r-1} {}_1F_1\left(1; 8ml-k; \frac{\tau^2 C_d}{\beta}\right) e^{-\frac{\tau^2 C_d}{\beta}}. \qquad (3.58)
\end{aligned}
$$

Finally we have the desired PDF as follows

$$f_\tau = \frac{2}{\beta^{4mN_r}} \sum_{t=1}^{2mN_r} \sum_{k=0}^{4mN_r-t-1} \binom{4mN_r-t-1}{k} \cdot \frac{(-1)^{4mN_r-t-k-1}}{(8mN_r-k-1)\Gamma(t)\Gamma(4mN_r-t)} \cdot \tau^{8mN_r-1} \left[b_{2t-1} C_1^{4mN_r} {}_1F_1\left(1; 8ml-k; \frac{\tau^2 C_1}{\beta}\right) e^{-\frac{\tau^2 C_1}{\beta}} + b_{2t} C_2^{4mN_r} {}_1F_1\left(1; 8ml-k; \frac{\tau^2 C_2}{\beta}\right) e^{-\frac{\tau^2 C_2}{\beta}} \right]. \quad (3.59)$$

Probability of Error

Given the PDF in (3.59), the probability of error can be obtained as

$$P_b = \int_0^\infty Q\left(\sqrt{\frac{2\tau^2}{N_o}}\right) f_\tau d\tau \quad (3.60)$$

where $\frac{N_o}{2} = \sigma^2$ is the variance of the Gaussian noise induced in the channel. We will use the *preferred form* of the Gaussian Q-function [21]

$$Q(x) = \frac{1}{\pi} \int_0^{\frac{\pi}{2}} e^{-\frac{x^2}{2\sin^2\theta}} d\theta. \quad (3.61)$$

Using (3.59) - (3.61) we can rewrite P_b as follows

$$\begin{aligned} P_b &= \frac{1}{\pi} \int_0^{\frac{\pi}{2}} \int_0^\infty e^{-\frac{\tau^2}{N_o \sin^2\theta}} f_\tau d\tau d\theta \\ &= \frac{2}{\pi\beta^{4mN_r}} \sum_{t=1}^{2mN_r} \sum_{k=0}^{4mN_r-t-1} \binom{4mN_r-t-1}{k} \cdot \frac{(-1)^{4mN_r-t-k-1}}{(8mN_r-k-1)\Gamma(t)\Gamma(4mN_r-t)} \left[b_{2t-1} C_1^{4mN_r} A''_{2t-1} + b_{2t} C_2^{4mN_r} A''_{2t} \right] \end{aligned} \quad (3.62)$$

where

$$A_d'' = \int_0^{\frac{\pi}{2}} \int_0^{\infty} \tau^{8mN_r-1} {}_1F_1\left(1; 8ml-k; \frac{\tau^2 C_d}{\beta}\right) e^{-\tau^2\left(\frac{C_d}{\beta}+\frac{1}{N_o \sin^2\theta}\right)} d\tau d\theta. \quad (3.63)$$

Let us introduce the following formulas [[40], Eq. (7.621.4)]

$$\int_0^{\infty} e^{-st} t^{b-1} {}_1F_1(a; c; kt) dt = \Gamma(b)(s-k)^{-b} {}_2F_1(c-a, b; c; \frac{k}{k-s}) \quad (3.64)$$

and [[40], Eq. (7.512.12)]

$$\int_0^1 x^{v-1}(1-x)^{\mu-1} {}_pF_q(a_1, \ldots, a_p; b_1, \ldots, b_q; ax) dx$$
$$= \frac{\Gamma(\mu)\Gamma(v)}{\Gamma(\mu+v)} {}_{p+1}F_{q+1}(v, a_1, \ldots, a_p; \mu+v, b_1, \ldots, b_q; a). \quad (3.65)$$

Using (3.64) and (3.65), and appropriate change of variables, we can obtain a closed-form expression for the double integration (3.63) as follow:

$$A_d'' = \frac{\Gamma(1/2)\,\Gamma(4mN_r+1/2)\,N_o^{4mN_r}}{4 \cdot 4mN_r} \cdot$$
$${}_3F_2\left(\frac{8mN_r+1}{2}, 8mN_r-k-1, 4mN_r; 4mN_r+1, 8mN_r-k; -\frac{C_d N_o}{\beta}\right). \quad (3.66)$$

If we define the SNR per channel as $\bar{\gamma} = \dfrac{\beta}{N_o} = \dfrac{E\left[|h_{jl,l}^2|\right]}{mN_o}$, then we have

$$P_b(\bar{\gamma}) = \sum_{t=1}^{2mN_r} \sum_{k=0}^{4mN_r-t-1} \binom{4mN_r - t - 1}{k} \left(\frac{1}{\bar{\gamma}}\right)^{4mN_r} \cdot$$

$$\frac{(-1)^{4mN_r-t-k-1}}{\pi \cdot 8mN_r \cdot (8mN_r - k - 1)} \cdot \frac{\Gamma\left(\frac{1}{2}\right)\Gamma\left(\frac{8mN_r+1}{2}\right)}{\Gamma(t)\Gamma(4mN_r - t)} \cdot$$

$$\Bigg[b_{2t-1} C_1^{4mN_r} \cdot$$

$${}_3F_2\left(\frac{8mN_r+1}{2}, 8mN_r - k - 1, 4mN_r; 4mN_r + 1, 8mN_r - k; -\frac{C_1}{\bar{\gamma}}\right)$$

$$+ b_{2t} C_2^{4mN_r} \cdot$$

$${}_3F_2\left(\frac{8mN_r+1}{2}, 8mN_r - k - 1, 4mN_r; 4mN_r + 1, 8mN_r - k; -\frac{C_2}{\bar{\gamma}}\right) \Bigg]. \quad (3.67)$$

By taking the limit of (3.67) as the SNR becomes high, we can get the asymptotic performance. As $\bar{\gamma}_c$ increases the hypergeometric functions ${}_3F_2(\cdot,\cdot,\cdot)$ tend to one which permits us to write:

$$P_b(\bar{\gamma}_c \to \infty) \equiv K\left(\frac{1}{\bar{\gamma}_c}\right)^{4mN_r}, \quad K \in \mathbb{R}. \quad (3.68)$$

We conclude directly from (3.68) that our system has a diversity of order $4mN_r$.

3.3.3 Numerical Results

Simulations are performed using Gold codes of length 31 chips. We assume that the information bits are BPSK modulated and that different channels from the N_t transmit antennas to the N_r receive antennas are statistically independents. The Nakagami-m channel is assumed to be fast fading and the fading coefficients are fixed for the duration of one symbol. We also assume a synchronous DS-CDMA transmission and a decorrelator detector is used at the receiver in order to combat MAI. CSI is assumed to be perfectly known at the receiver and simulations are run for different system loads and fading figures. We also consider that some AWGN is

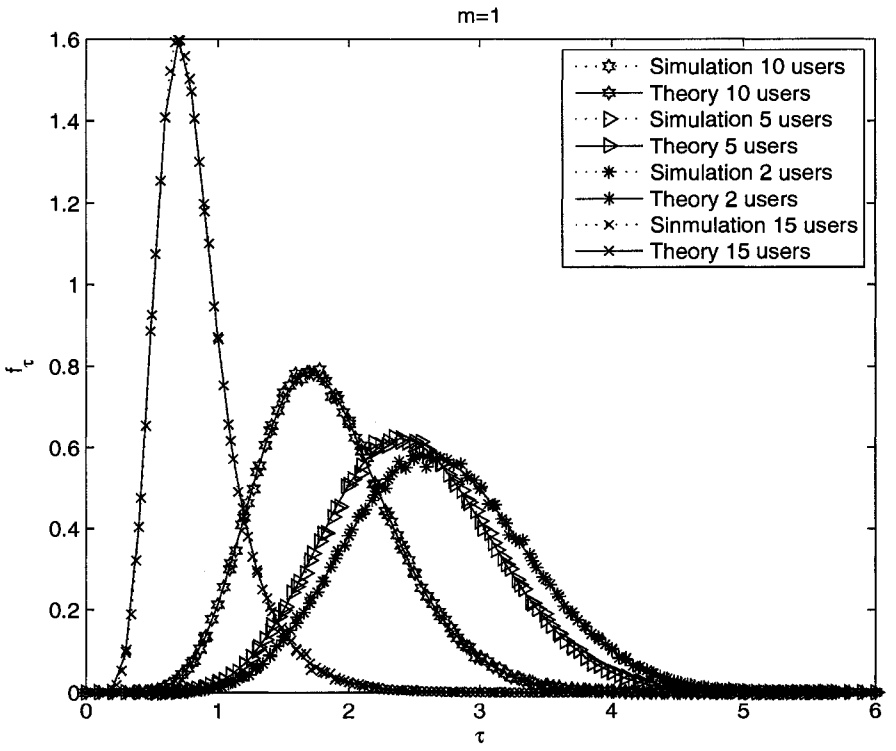

Figure 3.4: The PDF of the SINR for uncoded STS scheme in fast fading channel compared to simulation results with the system parameters: m=1, 2, 5, 10 and 15 users.

added to signals transmitted through the fading channel.

The accuracy of the PDF derived in (3.59) is shown in Fig. 3.4 and Fig. 3.5 where the simulation and theoretical PDFs match perfectly.

Fig. 3.6 shows performance of systems with different configurations of fading figure m and number of receive antennas N_r obtained using the probability of error in (3.67). The accuracy of the probability of error derived in (3.67) is shown in Fig. 3.7 and Fig. 3.8 where there is a perfect match between simulation and analytical results of BER for different configurations of fading figures and number of receive antennas.

Finally Fig. 3.8 shows that no matter what the system load is, the diversity of the system is maintained for a fixed values of the fading figure m and of the number of receive antennas N_r. The only loss incurred by the increase of the number of users in the system is a SNR loss.

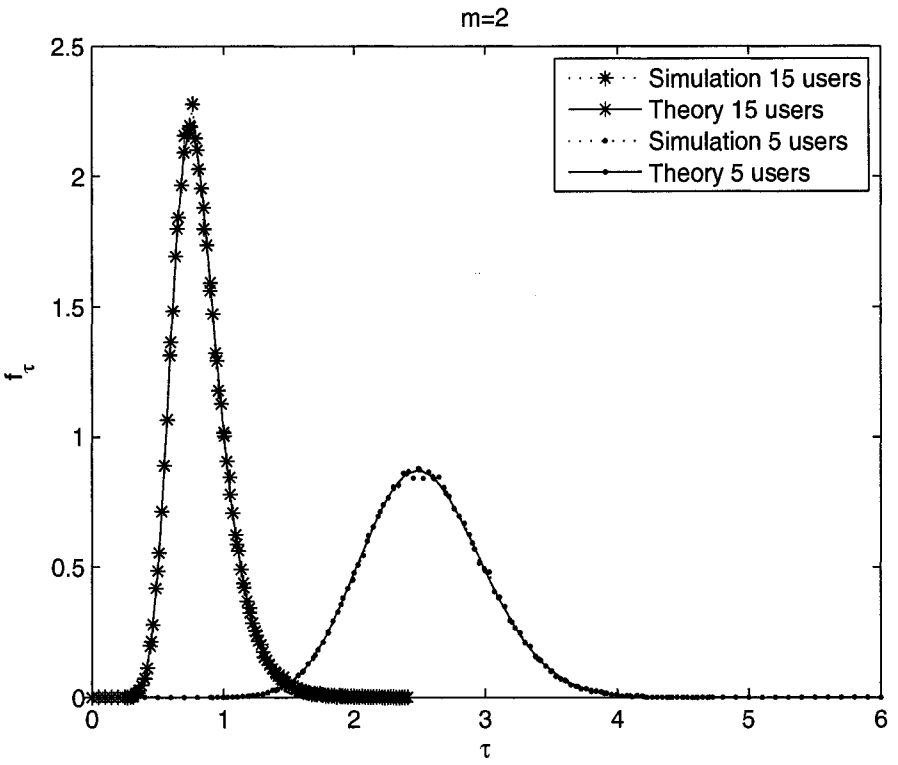

Figure 3.5: The PDF of the SINR for uncoded STS scheme in fast fading channel compared to simulation results with the system parameters: m=2, 5 and 15 users.

3.4 Conclusion

The performance of space-time spreading schemes operating in a Nakagami-m frequency-flat fading channel has been examined for both slow and fast fading conditions. DS-CDMA was used to allow for multiuser access. We assumed a transmitter with two antennas and a receiver with N_r antennas. We derived a closed form expression for the probability of bit error of our space-time scheme when a decorrelator detector is used. The derived bit-error rate was shown to be very accurate when compared to simulation results. Given a perfect channel state information at the receiver side, we have also proved that the diversity order of the underlying space-time system is a function of the number of transmit and receive antennas as well as the Nakagami fading figure m and not a function of the system load; this is the case in both a fast fading and in a slow fading channels. The expression derived for the probability of errors are valid only for integer values of the fading coefficients m and the probability

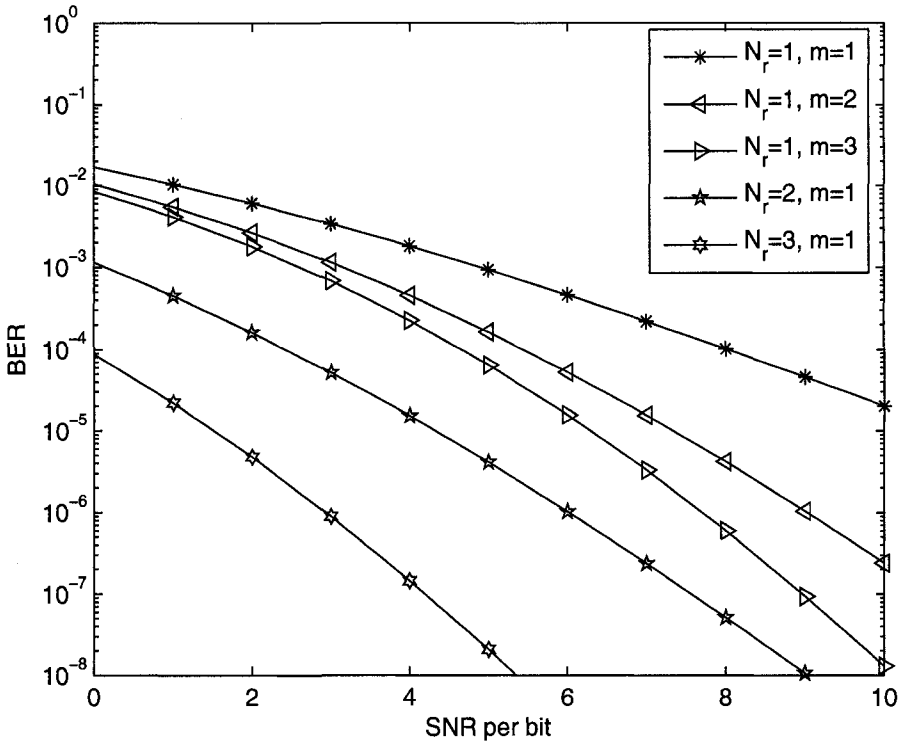

Figure 3.6: Theoretical probability of error for a 5-user STS scheme in a frequency-flat and fast Nakagami-m fading channel for different values of fading figures m and number of receive antennas N_r.

of error for non-integer values of m can be obtained numerically.

In the next chapter we will consider the integration of our space-time scheme with convolutional codes in Nakagami fading channels. We shall derive analytically the upper bound on the performance of the system.

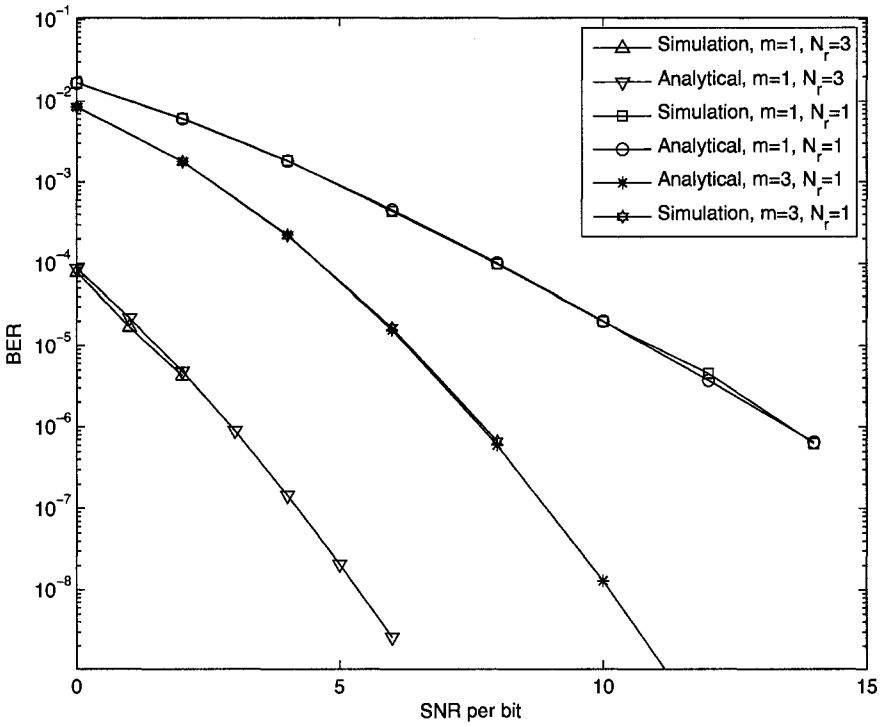

Figure 3.7: Simulation v.s. theoretical results for the probability of error of a 5-user STS scheme in a frequency-flat and fast Nakagami-m fading channel for different values of fading figures m and number of receive antennas N_r.

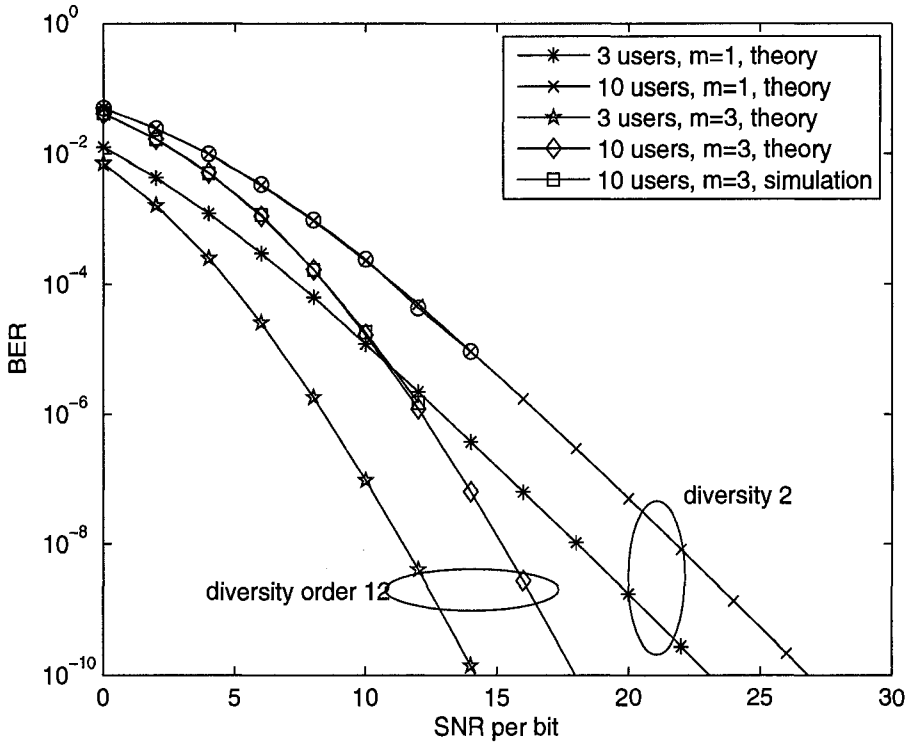

Figure 3.8: Theoretical probability of error for a 5-user STS scheme in a frequency-flat and fast Nakagami-m fading channel showing that diversity is maintained for fixed fading figure m=1,3, fixed N_r=1 number of receive antennas and different system loads.

Chapter 4

Coded Multiuser CDMA System with Transmit Diversity over Nakagami-m Fading Channels

It is evident from the previous chapter that wireless communication systems using MIMO improve the performance relative to single antenna systems. Also, a major phenomenon limiting the performance of wireless systems is multipath fading and a well know solution to multipath fading is through diversity. The performance of a wireless communication channel can also be improved by channel coding.

4.1 Introduction

Transmit diversity techniques are widely proposed as a way of improving the performance of a system with a limited number of receive antennas. DS-CDMA is a typical multiple access scheme used in third (3G) and fourth generation (4G) of wireless systems. [41] presents an overview of different open-loop and closed-loop transmit diversity techniques used in 3G CDMA systems while [42] proposes a novel way of combining phase-sweep transmit diversity and space-time spreading in order to obtain full advantage of those two techniques. A new architecture using space-time multiple access (SDMA) and CDMA that offers transmit diversity is proposed by Wei *et al.* in [43]. Other works on the integration of DS-CDMA with transmit diversity include [44] where Sherwin *et al.* focused on increasing the reverse link capacity of 3G CDMA systems using transmit diversity.

Space-time coding techniques based on MIMO are known to provide spatial diversity as well as coding gains [2]. The integration of STCs with DS-CDMA referred to as space-time spreading was proposed by Hochwald *et al.* [3] and shown to offer substantial diversity gain in a multiuser fading environment. Yang *et al.* [45] studied the performance of STS in a broadband multicarrier system, while Abou-Khousa *et al.* [46] proposed a multipath detection scheme for CDMA STS systems based on estimating the interference power in the individual resolved multipath components. Aljerjawi *et al.* [38, 35] focused on their hand on the performance of multiuser STS in a fast fading channel. STS is an open-loop technique that requires the channel state information (CSI) to be known at the receiver side. Although CSI estimation techniques are available in the literature [47, 48] we will assume that the CSI is perfectly known at the receiver.

Given that channel coding is an integral part of any communication system, we investigate in this chapter the performance of a multiuser STS scheme operating in a fast fading environment and combined with forward error control coding (FEC). The performance of a combination of W-CDMA MIMO transmit diversity with FEC in a correlated Nakagami-m fading channel was studied in [49]. Transmit diversity is introduced in [49] using the Alamouti scheme [24] and a Rake receiver is considered. The authors in [49] consider a single user system. The authors of [50] studied the performance of different transmit diversity schemes used in conjunction with CDMA in a Nakamagi-m fading channel. They consider the effect of imperfect channel state information on diversity but do not take channel coding into consideration. Other related works on space-time coded systems focus on concatenated coding in MIMO systems [51, 52] in a single user scenario. We consider in this chapter STS as a transmit diversity MIMO scheme. We assess the performance of a space-time multiuser system that combines STS with convolutional coding in Nakagami-m channels. An uplink DS-CDMA system is considered where the receiver base-station adopts a decorrelator detector for MAI suppression. We first determine the PDF of the SINR at the output of the multiuser detector and after signal combining. This PDF is used to obtain a closed form expression for the average pairwise error probability, and the corresponding BER upper bound for the Nakagami channel. This error bound is shown to be tight at all SNRs, indicating the overall system diversity. Both analytical and Monte-Carlo simulation results show that the overall system diversity is only a

function of the transmit and receive antennas, the fading figure, and the minimum free distance of the code.

The rest of the chapter is organized as follows. In section 4.2, we describe briefly the system model under consideration. In section 4.3, we derive the pairwise error probability for fast fading and slow fading channels, then we obtain theoretical expressions for probability of error. Section 4.4 presents Monte-Carlo simulations as well as analytical results. Finally, we conclude the chapter in section 4.5.

4.2 Coded System Model

We consider an uplink scenario of a DS-CDMA system. The mobile users transmit their information using the STS scheme presented in [38] for fast fading channels. As the system model for the slow fading channel is easily derived from the fast fading one, we start with the fast fading case. We will only consider communication between the k^{th} user and the base station. As shown in Fig. 4.1, the information stream x_k of user k is first encoded using a convolutional code. The output of the convolutional encoder is then interleaved and split into an odd and an even substreams, $x_{k,1,cod}$ and $x_{k,2,cod}$, respectively, which are both modulated using BPSK modulation to give the two streams $x_{k,1}$ and $x_{k,2}$. The two modulated streams are then spread using two orthogonal codes $s_{k,i}, i = 1, 2$ and combined according to [38].

The encoder of user k produces two codewords

$$x^*_{k,1}s_{k,1} + x^*_{k,2}s_{k,2} \tag{4.1a}$$

$$x_{k,1}s_{k,2} - x_{k,2}s_{k,1} \tag{4.1b}$$

which are transmitted by antenna 1 and 2, respectively, at time t and switched with respect to the transmit antennas at time $t + T$. The information transmitted from user k is subject to channel fading. Given the transmitted code symbols in (4.1a) and

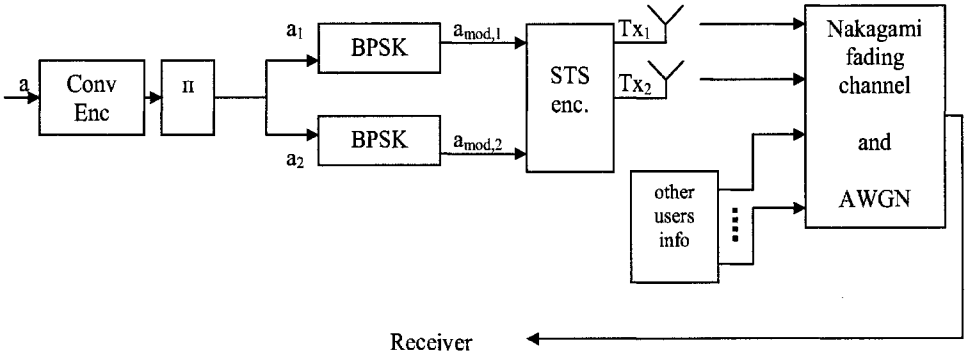

a) Transmission scheme for user k

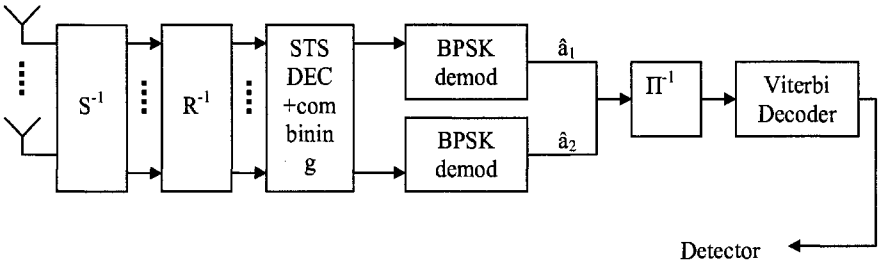

b) Reception scheme at base station

Figure 4.1: Coded ST-CDMA system operating in a Nakagami-m fading environment (a)Transmission scheme for user k (b) Base Station Receiver.

(4.1b), the received signal at the l^{th} receive antenna can be written as

$$r_o^l = \sum_{k=1}^{K} \left[h_{1l,0,k} \cdot (x_{k,1}^* s_{k,1} + x_{k,2}^* s_{k,2}) + h_{2l,0,k} \cdot (x_{k,1} s_{k,2} - x_{k,2} s_{k,1}) + n_{k,0}^l \right] \quad (4.2a)$$

$$r_1^l = \sum_{k=1}^{K} \left[h_{1l,1,k} \cdot (x_{k,1} s_{k,2} - x_{k,2} s_{k,1}) + h_{2l,1,k} \cdot (x_{k,1}^* s_{k,1} + x_{k,2}^* s_{k,2}) + n_{k,1}^l \right] \quad (4.2b)$$

at time t and $t+T$ respectively. The composite signal (4.2) from all K users go through a bank of $2K$ matched filters (MFs), matched to the $2K$ spreading codes of the K users. The output of the $2K$ matched filters at the l^{th} receive antenna can be

expressed as

$$\mathbf{Y}_0^l = \mathbf{R}\mathbf{H}_0^l\mathbf{x} + \mathbf{N}_0^l \tag{4.3a}$$

$$\mathbf{Y}_1^l = \mathbf{R}\mathbf{H}_1^l\mathbf{x} + \mathbf{N}_1^l \tag{4.3b}$$

at times t and $t+T$, respectively. Here $\mathbf{Y}_j^l = \left[y_{j,11}^l, y_{j,12}^l, ..., y_{j,k1}^l, y_{j,k2}^l, ..., y_{j,K1}^l, y_{j,K2}^l\right]^{\mathrm{T}}$, where $y_{j,ki}^l$, $i = 1, 2$, represents the ith matched filter output of user k at times t and $t+T$. The encoded data vector is $\mathbf{x} = [x_{1,1}, x_{1,2}, ..., x_{k,1}, x_{k,2}, ..., x_{K,1}, x_{K,2}]^T$ where $x_{k,i}$, $i = 1, 2$ represents the even and odd coded data symbols for user k. The $(2K \times 1)$ noise vector $\mathbf{N}_j^l$, $j = 0, 1$, consists of N_{kj}^l, $k = 1, ..., K$, $j = 0, 1$ complex Gaussian RVs, each with variance $N_o/2$ per dimension. The $(2K \times 2K)$ channel coefficients matrix $\mathbf{H}_j^l$, $j = 0, 1$, at times t and $t + T$, respectively, and the cross-correlation matrix $\mathbf{R}$ are defined respectively in (3.27) and (3.26).

Here the 2×2 channel coefficient sub-matrices $\mathbf{h}_{0,k}^l$ and $\mathbf{h}_{1,k}^l$ contain the channel fading coefficients $h_{il,j,k}$, and are defined as in (3.28) and (3.29).

In the fast fading channel, fading coefficients are assumed to vary independently from one codeword to the next. Given the matched filter outputs in (4.3a) and (4.3b), the signals at times t and $t + T$ are combined to give the estimates [38]

$$\hat{x}_{k,1} = \sum_{l=1}^{N_r} h_{1l,0,k} y_{0,k1}^{l*} + h_{2l,0,k}^* y_{0,k2}^l + h_{1l,1,k}^* y_{1,k2}^l + h_{2l,1,k} y_{1,k1}^{l*} \tag{4.4a}$$

$$\hat{x}_{k,2} = \sum_{l=1}^{N_r} h_{1l,0,k} y_{0,k2}^{l*} - h_{2l,0,k}^* y_{0,k1}^l - h_{1l,1,k}^* y_{1,k1}^l + h_{2l,1,k} y_{1,k2}^{l*}. \tag{4.4b}$$

As in the uncoded case discussed in Chapter 3, a decorrelator detector is introduced between the MF stage and the space-time combining stage to combat MUI. After space-time combining, the odd and even substreams of user k are demodulated, deinterleaved, merged and passed through a Viterbi decoder. Then an estimate of the original message is obtained.

4.3 Performance Analysis

In this section, we arbitrarily consider user 1 as the desired user for simplicity purpose, and drop the corresponding user index k. We derive error bounds for the performance of the convolutionally coded ST-CDMA system. In what follows, we derive a closed-form expression for the pairwise probability of error (PPE), $P(d)$, of the convolutionally-coded system by first determining the PDF of the SINR at the input of the soft-Viterbi decoder. This average PPE will enable us to evaluate the probability of bit-error bound.

Considering that a codeword ξ is transmitted and the decoded codeword $\hat{\xi}$ differs from ξ at d bit positions then the PPE conditioned on the fading coefficients is given by [53]

$$P(d \mid \bar{\mathbf{h}}) = P\left\{\sum_{v=1}^{d} \hat{x}_v \geq 0\right\} \tag{4.5}$$

where $\bar{\mathbf{h}}$ consists of the corresponding fading coefficients.

4.3.1 Fast Fading

Considering that the channel is fast fading and that a decorrelator detector is used at the receiver side, the SINR of the v^{th} bit at the output of the Viterbi decoder can be given from (4.3a), (4.3b), (4.4a) and (4.4b) as [18, 35]

$$SINR_v = \frac{R_c \cdot \nu^2}{\sigma^2_{\hat{x}_v}} \tag{4.6a}$$

$$\nu = \sum_{l=1}^{N_r} |h_{1l,0,v}|^2 + |h_{2l,0,v}|^2 + |h_{1l,1,v}|^2 + |h_{2l,1,v}|^2 \tag{4.6b}$$

where R_c is the code rate, and $h_{il,j,v}$ is the fading coefficient between transmit antenna $i, i = 1, 2$, and receive antenna $l, l = 1 \ldots N_r$, at time $j = 0, 1$. $h_{il,j,v}$ is modeled as having a Nakagami-m envelope and uniformly distributed phase. Since we employ

the decorrelator detector, $\sigma^2_{\hat{x}_v}$ in (4.6a) is defined as [38],

$$\sigma^2_{\hat{x}_v} = \sigma^2_n \left[R_{11}^{-1} \left(\sum_{l=1}^{N_r} |h_{1l,0,v}|^2 + |h_{2l,1,v}|^2 \right) + R_{22}^{-1} \left(\sum_{l=1}^{N_r} |h_{2l,0,v}|^2 + |h_{1l,1,v}|^2 \right) \right] \quad (4.7)$$

where R_{11}^{-1}, R_{22}^{-1} are the first and second elements of the diagonal of the inverse of the cross-correlation matrix $\mathbf{R} = \mathbf{S}^H \cdot \mathbf{S}$, and $\sigma_n^2 = \frac{N_o}{2}$ is the variance of the independent complex AWGN samples. Let us define now the RVs $\alpha_{1,v}$ and $\alpha_{2,v}$ as

$$\alpha_{1,v} = \sum_{l=1}^{N_r} \left(|h_{1l,0,v}|^2 + |h_{2l,1,v}|^2 \right)$$

$$\alpha_{2,v} = \sum_{l=1}^{N_r} \left(|h_{2l,0,v}|^2 + |h_{1l,1,v}|^2 \right).$$

The RVs $\alpha_{1,v}$ and $\alpha_{2,v}$ are Gamma random variables with PDF

$$f(\alpha_{i,v}) = \frac{1}{\Gamma(2mN_r)} \frac{\alpha_{i,v}^{2mN_r-1}}{\eta^{2mN_r}} \exp^{-\frac{\alpha_{i,v}}{\eta}},$$
$$\alpha_{i,v} \geq 0, \quad i = 1, 2; \quad v = 1 \ldots d; \quad m \geq \frac{1}{2} \quad (4.8)$$

where m is the fading figure, $\eta = \frac{\Omega}{m}$, and $\Omega = E\left[|h^2_{il,j,v}|\right]$ is the power of the Nakagami-m fading coefficient. Let us define $C_1 = R_{11}^{-1}$ and $C_2 = R_{22}^{-1}$, then the $SINR_v$ can be rewritten in terms of a new parameter $\beta_{1,v}$ as:

$$SINR_v = R_c \left(\frac{\alpha_{1,v} + \alpha_{2,v}}{\sqrt{C_1\alpha_{1,v} + C_2\alpha_{2,v}}} \right)^2 = R_c \beta^2_{1,v}. \quad (4.9)$$

Using (4.6a) and (4.9), one can write the pairwise error probability in (4.5) as

$$P(d) = E_{\beta^2_{1,v}} \left[Q\left(\sqrt{\frac{2}{N_o} R_c \sum_{v=1}^{d} \beta^2_{1,v}} \right) \right]. \quad (4.10)$$

In order to simplify our derivation, we use the preferred form of the Gaussian Q-function [21]

$$Q(x) = \frac{1}{\pi} \int_0^{\frac{\pi}{2}} e^{-\frac{x^2}{2\sin^2\theta}} d\theta. \tag{4.11}$$

Assuming an ideal interleaver/deinterleaver pair, $\beta_{1,1}, \ldots, \beta_{1,d}$, are independent and (4.10) can be expanded as:

$$\begin{aligned} P(d) &= \int_0^{\infty} \cdots \int_0^{\infty} Q\left(\sqrt{\frac{2}{N_o} R_c \sum_{v=1}^{d} \beta_{1,v}^2}\right) f(\beta_{1,2}) \cdots \\ &\qquad f(\beta_{1,d})\, d\beta_{i,1} \cdots d\beta_{i,d} \\ &= \int_0^{\infty} \cdots \int_0^{\infty} \frac{1}{\pi} \int_0^{\frac{\pi}{2}} e^{-\frac{R_c \sum_{v=1}^{d} \beta_{1,v}^2}{N_o \sin^2\theta}} f(\beta_{1,2}) \cdots \\ &\qquad f(\beta_{1,d})\, d\theta d\beta_{i,1} \cdots d\beta_{i,d} \\ &= \frac{1}{\pi} \int_0^{\frac{\pi}{2}} \left[\int_0^{\infty} e^{-\frac{R_c \beta_{1,1}^2}{N_o \sin^2\theta}} f(\beta_{1,1})\, d\beta_{1,1}\right] \cdots \\ &\qquad \left[\int_0^{\infty} e^{-\frac{R_c \beta_{1,d}^2}{N_o \sin^2\theta}} f(\beta_{1,d})\, d\beta_{1,d}\right] d\theta. \end{aligned} \tag{4.12}$$

Let us define the Moment Generating Function (MGF) of (4.9) as

$$M_{\beta_{1,v}^2}(s) = \int_0^{\infty} e^{-s \cdot \beta_{1,v}^2} f(\beta_{1,v}) d\beta_{1,v}. \tag{4.13}$$

A closed-from expression of (4.13) is derived in Appendix A. The pairwise error probability $P(d)$ is then given by

$$P(d) = \frac{1}{\pi} \int_0^{\frac{\pi}{2}} \left[M_{\beta_{1,v}^2}\left(\frac{R_c}{N_o \sin^2\theta}\right)\right]^d d\theta. \tag{4.14}$$

Substituting (s) by $\left(\frac{R_c}{N_o \sin^2\theta}\right)$ in (A.16), we get

$$M_{\beta_{1,v}^2}\left(\frac{R_c}{N_o \sin^2\theta}\right) = \lambda \sum_{k=0}^{2mN_r-1} \sum_{j=0}^{2mN_r-1} \frac{(-1)^{k+j}}{4mN_r+k+j+1} \cdot$$
$$\binom{2mN_r-1}{k}\binom{2mN_r-1}{j} \cdot C_2^{2mN_r-k-1} C_1^{2mN_r-j-1} \cdot$$
$$\Gamma(4mN_r)\left(\frac{R_c}{N_o \sin^2\theta}\right)^{-4mN_r} \cdot \Bigg[C_2^{4mN_r+k+j+1} \cdot$$
$${}_2F_1\left(4mN_r+k+j+1, 4mN_r; 4mN_r+k+j+2; \frac{-C_2 N_o \sin^2\theta}{R_c \eta}\right)$$
$$- C_1^{4mN_r+k+j+1} \cdot$$
$${}_2F_1\left(4mN_r+k+j+1, 4mN_r; 4mN_r+k+j+2; \frac{-C_1 N_o \sin^2\theta}{R_c \eta}\right)\Bigg] \qquad (4.15)$$

where

$$\lambda = \frac{1}{\left(\eta^{2mN_r}\right)^2 \left[\Gamma(2mN_r)\right]^2 \left(|C_2 - C_1|\right)^{4mN_r-1}}. \qquad (4.16)$$

If we define the average SNR per channel by $\overline{\gamma} = R_c \frac{E\left[|h_{1l,1,v}|^2\right]}{mN_o} = R_c \frac{\eta}{N_o}$, then we have

$$M_{\beta_{1,v}^2}(\overline{\gamma}, \theta) = \lambda \sum_{k=0}^{2mN_r-1} \sum_{j=0}^{2mN_r-1} \frac{(-1)^{k+j}}{4mN_r+k+j+1} \cdot$$
$$\binom{2mN_r-1}{k}\binom{2mN_r-1}{j} \cdot C_2^{2mN_r-k-1} C_1^{2mN_r-j-1} \cdot$$
$$\Gamma(4mN_r)\beta^{4mN_r}\left(\frac{\overline{\gamma}}{sin^2\theta}\right)^{-4mN_r} \cdot \Bigg[C_2^{4mN_r+k+j+1} \cdot$$
$${}_2F_1\left(4mN_r+k+j+1, 4mN_r; 4mN_r+k+j+2; \frac{-C_2 \sin^2\theta}{\overline{\gamma}}\right)$$
$$- C_1^{4mN_r+k+j+1} \cdot$$
$${}_2F_1\left(4mN_r+k+j+1, 4mN_r; 4mN_r+k+j+2; \frac{-C_1 \sin^2\theta}{\overline{\gamma}}\right)\Bigg]. \qquad (4.17)$$

Using (4.17), the semi-analytical PPE at a specified SNR is thus given by:

$$P(d,\overline{\gamma}) = \frac{1}{\pi}\int_0^{\frac{\pi}{2}} \left[M_{\beta^2_{1,i}}(\overline{\gamma},\theta)\right]^d d\theta. \tag{4.18}$$

We can proceed to a numerical evaluation of (4.18). The computational cost of the semi-analytical expression in (4.18) when compared to simulation results is still very low.

4.3.2 Slow Fading

By setting $h_{1l,0,k} = h_{1l,1,k}$ in (4.6a) and (4.7), and also by dropping the time subscript, the SINR of the $v^{th}, v = 1 \ldots d$, is given by

$$SINR'_v = \frac{2R_c\left(\sum_{l=1}^{N_r} |h_{1l,v}|^2 + |h_{2l,v}|^2\right)}{C\sigma_n^2} \tag{4.19}$$

where $C = C1 + C2$, and $C1$ and $C2$ are defined as before. The PDF of (4.19) is easily obtained, and is one of a Gamma distribution [7]. Now substituting (4.19) into (4.5) we can easily obtain a closed form expression for the pairwise error probability for integer values of the fading figure m,

$$P'(d,\overline{\gamma}) = \left(\frac{1-\mu}{\mu}\right)^{2dmN_r} \cdot \sum_{k=0}^{2dmN_r-1} \binom{2dmN_r - 1 + k}{2dmN_r} \left(\frac{1+\mu}{mu}\right)^k \tag{4.20}$$

where $\mu = \sqrt{\frac{\overline{\gamma}_{slow}/m}{1+\overline{\gamma}_{slow}/m}}$ and $\overline{\gamma}_{slow} = 2R_c\frac{E\left[|h_{1l,v}|^2\right]}{mC\cdot N_o} = 2R_c\frac{\eta}{CN_o}$.

4.3.3 Probability of Error

Finally, using the expressions for the pairwise error probability in (4.18), (4.20), one can obtain an upper bound for the BER using [4]

$$P_e \leq \sum_{d=d_{free}}^{\infty} \xi_d P(d), \tag{4.21}$$

where ξ_d is the number of paths of distance d from the all-zero path that merge with the all-zero path for the first time, and d_{free} is the minimum free distance of the convolutional code.

To find the diversity order of the underlying system, we examine the asymptotic performance as the SNR gets large. First we can obtain a looser bound for (4.21) by considering that at high SNR, the most dominant error event is the one of $d = d_{free}$. Thus,

$$P_e(\overline{\gamma} \longrightarrow \infty) \leq P(d_{free}). \tag{4.22}$$

In the fast fading case, it is known that in the limit, as $\overline{\gamma}$ gets large, the hypergeometric functions ${}_2F_1$ converges to one, hence:

$$\begin{aligned} P_e(\overline{\gamma} \longrightarrow \infty) &\leq P(d_{free}) \\ &\leq \frac{1}{\pi} \int_0^{\frac{\pi}{2}} \left[K \left(\frac{\overline{\gamma}}{sin^2\theta} \right)^{-4mN_r} \right]^{d_{free}} d\theta \\ &\leq K' \left(\frac{1}{\overline{\gamma}} \right)^{4d_{free}mN_r}. \end{aligned} \tag{4.23}$$

We can clearly see from the upper bound in (4.23) that the coded STS scheme achieves a diversity order of $4d_{free}mN_r$.

Similarly for the slow fading channel, in (4.20), when $\overline{\gamma}_{slow}$ gets large (i.e. $\overline{\gamma}_{slow}/m \gg 1$),

$$(1+\mu)/2 \approx 1, \tag{4.24a}$$

$$(1-\mu)/2 \approx 1/4\overline{\gamma}_{slow}, \tag{4.24b}$$

and

$$\sum_{k=0}^{2d_{free}mN_r-1} \binom{2d_{free}mN_r - 1 + k}{2d_{free}mN_r} = \binom{4d_{free}mN_r - 1}{2d_{free}mN_r}. \tag{4.24c}$$

Therefore when $\overline{\gamma}_{slow}/m$ is sufficiently large, the probability of error in (4.22) can be approximated by

$$P_{e,slow}(\overline{\gamma} \longrightarrow \infty) \approx \left(\frac{1}{4\overline{\gamma}_{slow}}\right)^{2d_{free}mN_r} \binom{4d_{free}mN_r - 1}{2d_{free}m}, \tag{4.25}$$

confirming that the achieved diversity order is $2d_{free}mN_r$.

4.4 Numerical Results

Table 4.1: Convolutional codes used in simulation [4].

Codes	Constraint length	Generators in octal	dfree
code1	3	[5 7]	5
code2	5	[23 35]	7
code3	3	[5 7 7]	8

Simulations are carried out using Gold codes of length 11 chips and considering BPSK modulation. Three convolutional codes [4] are used for the purpose of simulation and their specifications are summarized in Table 4.1. A soft-decision Viterbi decoder with 3-bit quantization is used at the receiver. We assume the different channel coefficients from the N_t transmit antennas to the N_r receive antennas to be Nakagami-m fading distributed and perfectly known at the receiver. An interleaver/deinterleaver pair is used in order to establish independence between the convolutionally coded information bits before they are space-time encoded. CSI is assumed to be perfectly known at the receiver. Simulations are carried out for different system loads and fading figures. We consider in our simulations that the CDMA transmission is totally synchronous and that a decorrelator detector is used at the receiver in order to combat MAI. All the transmission channels are assumed to be mutually independent and to be AWGN channels.

Fig. 4.2 presents simulation results for fading figure $m = 1$, for a system with K=3 and 12 users, N_t=2 transmit antennas and one receive antenna, using the convolutional code1 from Table 4.1 in a fast fading environment. The results show the bound in (4.23) (with PPE in (4.14)) to be tight at high SNRs. Since the quantization is finite, there is a slight difference of less than 0.2dB between simulations and error bound. In the same plot, we included the performance of the MRC with the same number of diversity branches (i.e., $4d_{free}mN_r = 20$). Note that the full system diversity is achieved in this case.

Fig. 4.3 provides a BER comparison of slow and fast fading situations considering three different fading figures $m = 1$, $m = 2$ and $m = 3$. From these results it is clear that the diversity is not a function of the system load, but only the fading figure, the free distance of the code and the number of receive antennas.

Fig. 4.4 shows performance bounds for a fast fading configuration with $m = 1, 2, 3$, K=3,12 users, N_t=2 transmit antennas and N_r=1 receive antenna and code1 from Table 4.1. Fig. 4.4 shows that diversity is preserved for the same combination of transmit and receive antennas, and fading figure. There is a dB loss incurred by the system load.

Finally Fig. 4.5 presents some simulation results versus expected bounds for different system configuration and different convolutional codes. We can see how the convolutional codes affect the diversity of the overall system through the minimum free distance d_{free}.

4.5 Conclusion

In this chapter, we derived error bounds for a convolutionally-coded space-time spreading scheme in multiuser DS-CDMA systems. The fading channel is modeled as a Nakagami-m frequency-flat fading channel. The derived BER bounds are shown to be tight when compared to simulation results, an indicative of the overall system diversity. Our results also show that the diversity order of the space-time system is fixed for a given fading figure and receive/transmit antennas regardless of the system load. The next chapter will summarize the content and contribution of this thesis.

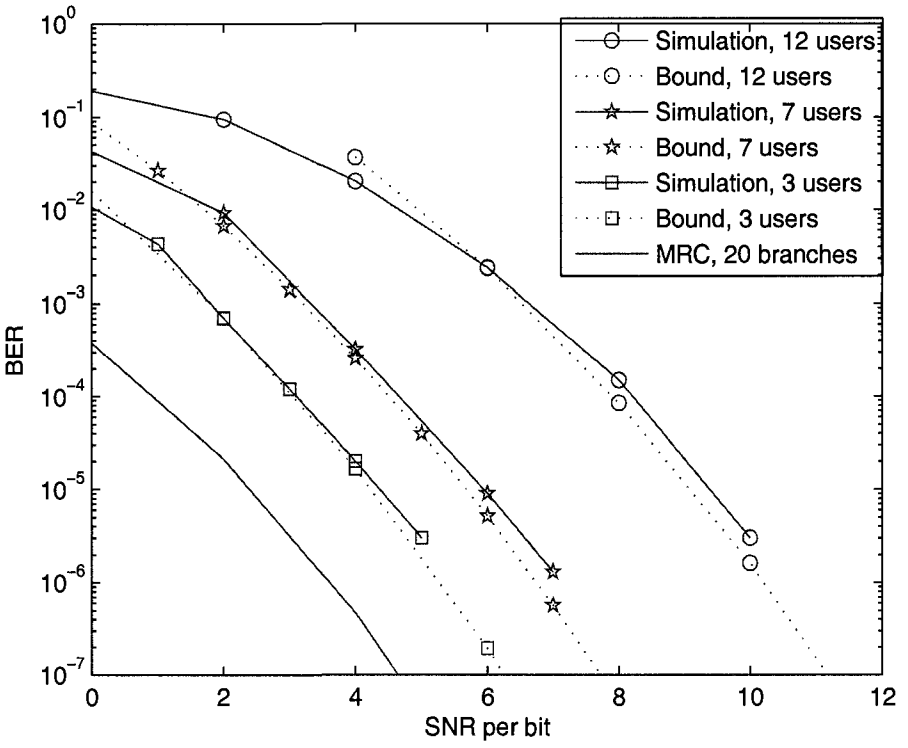

Figure 4.2: Coded STS in fast fading channel, N_t=2, N_r=1, m=1, and K=3, 7 and 12 users.

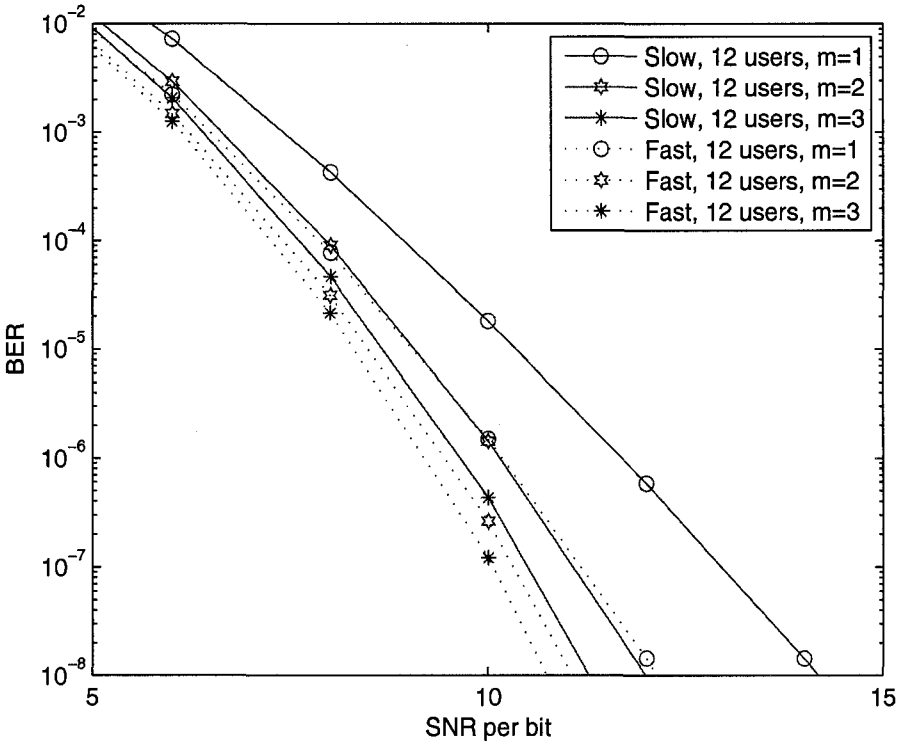

Figure 4.3: Performance bounds for Coded STS schemes in fast and slow fading channel, N_t=2, N_r=1 with different fading figures and a system load of 12 users.

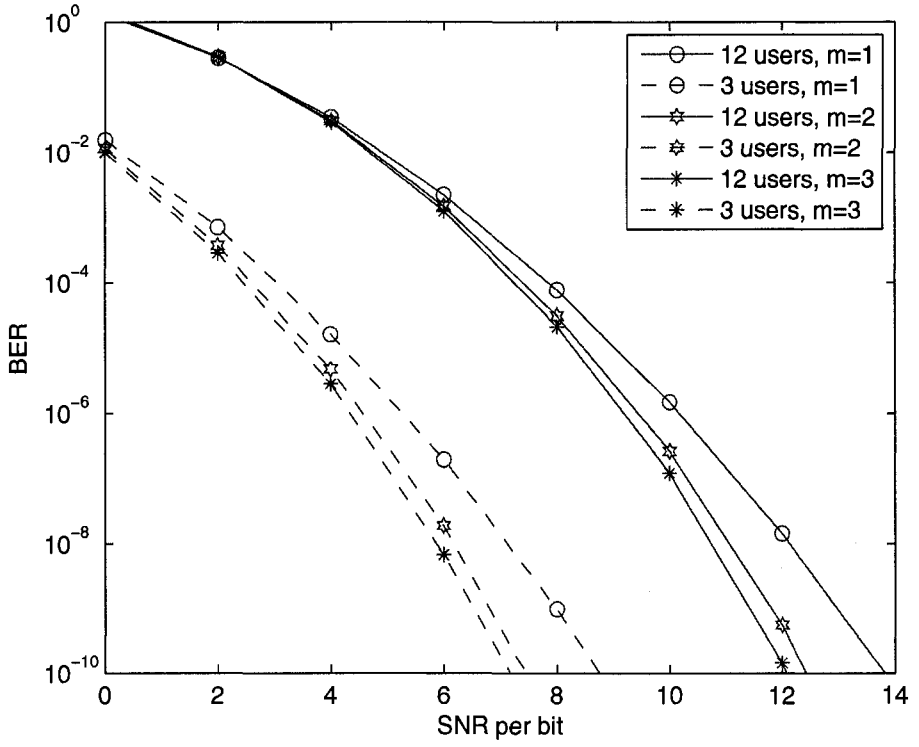

Figure 4.4: Performance bounds for Coded STS in fast fading channel, N_t=2, N_r=1 with different fading figures and system loads.

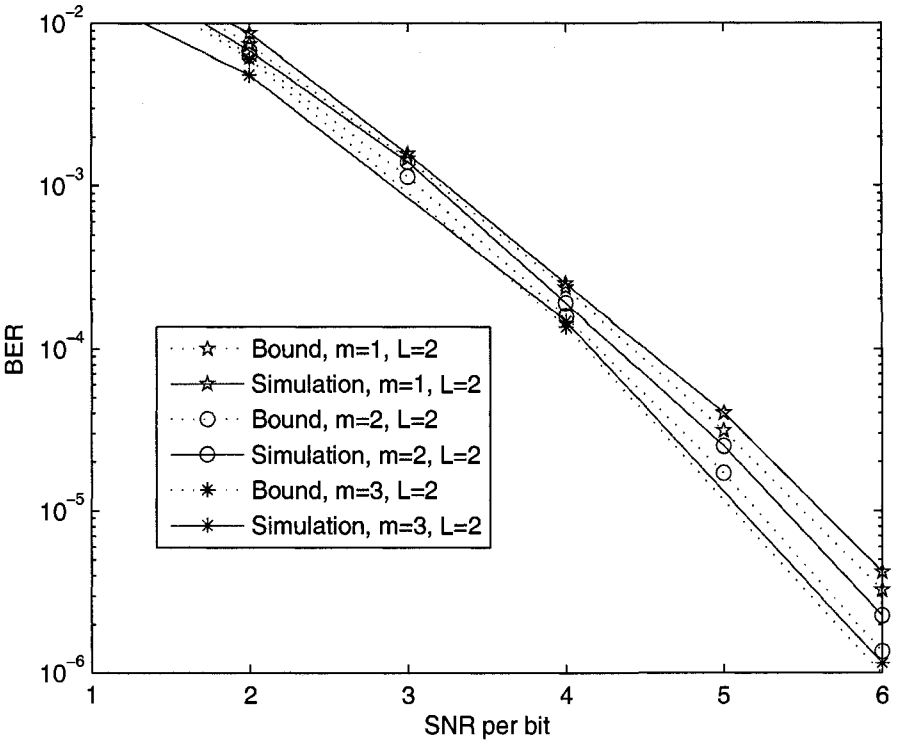

Figure 4.5: Coded STS in fast fading channel for a 12 user system, $N_t = N_r = 2$ and different fading figures.

Chapter 5

Thesis Conclusions and Future Works

5.1 Conclusions

We present in this section a summary of the work accomplished in this thesis.

1. In Chapter 3, we study the performance of the STS scheme presented in [35] in the more general Nakagami-m fading model. BER expressions are obtained for both fast and slow fading channels. In order to support many users, DS-CDMA is considered along with a decorrelator detector at the receiver side. If we assume that CSI is perfectly known at the receiver side, then the system achieves full diversity which is a function only of the number of transmit and receive antennas, and the fading figure m. The accuracy of the derived probability of errors was proven when compared to simulations results. One important thing to point out is that we derived that the diversity is a function of the fading figure m. As m increases to infinity so does diversity, i.e. diversity gets closer to the diversity of the Gaussian channel. The channel is no longer a fading channel, but a simple AWGN channel at really high m.

2. In Chapter 4, we present an integration of space-time coding with convolutional coding. The system is examined over both fast and slow fading channels once

again. We showed that diversity is increased when compared to the uncoded case of Chapter 3, by a factor of d_{free}. Performance bounds are derived and proven accurate when compared to simulation results. The diversity of the system is shown not to be a function of the system load.

5.2 Future Works

We will present here a few paths to consider in order to extend the research summarized in this thesis.

1. We have considered all through this thesis a frequency flat channel. This assumption is realistic for narrowband signals. But to be more realistic we have to extend the scope of this work to wideband signals. The increasing demand for bandwidth, motivated by the widespread of wireless access to multimedia requires that we are able to deal with broadband signal.

2. The closed-form expression of the probability of error derived in Chapter 3 and performance bounds derived in Chapter 4 are results valid only for integer values of the fading figure m. The study of the performance of the space-time system can be extended to non-integer values of the fading figure as well.

3. We have studied the performance of an STS scheme under the assumption that the CDMA transmission is synchronous. Since we are considering the uplink of the communication system, this is an ideal situation. More realistic results can be derived by considering an asynchronous CDMA transmission.

4. Finally, we have considered in this thesis that the CSI is perfectly known at the receiver side and this is a condition for achieving full diversity. Future works can focus on assessing the performance of our coded space-time spreading scheme in a case where CSI is not perfectly known. This can imply the use of adaptive schemes at the receiver side.

Appendix A

Closed Form Expression of Eq. (4.13)

We will derive here a closed form expression for (4.13). The first step will be to determine an expression for the PDF of the RV $\beta_{1,v}$. From (4.9)

$$\beta_{1,v} = \frac{\alpha_{1,v} + \alpha_{2,v}}{\sqrt{C_1\alpha_{1,v} + C_2\alpha_{2,v}}}. \tag{A.1}$$

Let us define a RV $\beta_{2,v}$ as

$$\beta_{2,v} = C_1\alpha_{1,v} + C_2\alpha_{2,v}. \tag{A.2}$$

By applying the rules of transformation of RVs, the joint density function of $\beta_{1,v}$ and $\beta_{2,v}$ is found for integer values of the Nakagami-m fading figure m to be

$$f(\beta_{1,v}, \beta_{2,v}) = \lambda \sum_{k=1}^{2mN_r-1} \sum_{j=1}^{2mN_r-1} I_{j,k,m,N_r} \beta_{1,v}^{2(2mN_r-1)-k-j} \cdot \beta_{2,v}^{2mN_r+\frac{1}{2}(k+j-1)} \exp\left(-\frac{\beta_{1,v}\sqrt{\beta_{2,v}}}{\eta}\right) \tag{A.3}$$

where

$$I_{j,k,m,N_r} = (-1)^{k+j} \begin{pmatrix} 2mN_r \\ k \end{pmatrix} \begin{pmatrix} 2mN_r \\ j \end{pmatrix} \cdot C_1^{2mN_r-k-1} C_2^{2mN_r-j-1} \tag{A.4}$$

and

$$\lambda = \frac{1}{(\eta^{2mN_r})^2 \left[\Gamma(2mN_r)\right]^2 \left(|C_2 - C_1|\right)^{4mN_r-1}}. \tag{A.5}$$

η in (A.3) and (A.5) is defined as previously in (4.8). In order to obtain the PDF of $\beta_{1,v}$ we have to integrate (A.3) over all possible values of $\beta_{2,v}$ with the following requirement

$$min(C_1^2, C_2^2)\beta_{1,v}^2 \leq \beta_{2,v} \leq max(C_1^2, C_2^2)\beta_{1,v}^2, \quad 0 \leq \beta_{1,v} \leq \infty.$$

To perform the integration of (A.3) over $\beta_{2,v}$ let us introduce the following formulae obtained from [9]

$$\int_{C_1}^{C_2} x^n e^{-ax} dx = \frac{1}{a(n+1)} \cdot \left[C_2^n (aC_2)^{-\frac{n}{2}} e^{-\frac{aC_2}{2}} \mathbb{M}\left(\frac{n}{2}, \frac{n+1}{2}, aC_2\right) - C_1^n (aC_1)^{-\frac{n}{2}} e^{-\frac{aC_1}{2}} \mathbb{M}\left(\frac{n}{2}, \frac{n+1}{2}, aC_1\right) \right] \tag{A.6}$$

and

$$\mathbb{M}(k, m, z) = z^{\frac{1}{2}+m} e^{-\frac{z}{2}} {}_1F_1(m - k + \frac{1}{2}; 1 + 2m; z). \tag{A.7}$$

$\mathbb{M}(k,m,z)$ represents the WhittakerM function defined in [9] as

$$\begin{aligned}\mathbb{M}(k,m,z) =& z^{\frac{1}{2}+m}e^{-\frac{z}{2}}\Bigg[1+\frac{\frac{1}{2}+m-k}{1!(2m+1)}z \\ &+\frac{(\frac{1}{2}+m-k)(\frac{3}{2}+m-k)}{2!(2m+1)(2m+2)}z^2+\ldots\Bigg]\end{aligned} \tag{A.8}$$

and ${}_1F_1(a;b;z) = \sum_{n=0}^{\infty}\frac{(a)_n}{(b)_n}\frac{z^n}{n!}$ is the confluent hypergeometric function and $(a)_n$, $(b)_n$ are Pochhammer symbols [9].

Using (A.6) and (A.7) and proceeding to the proper changes of variables in (A.3), and after some involved calculations the PDF of $\beta_{1,v}$ is found to be

$$f(\beta_{1,v}) = 2\lambda\sum_{k=1}^{2mN_r-1}\sum_{j=1}^{2mN_r-1} I_{j,k,m,N_r}(I_{2,\beta_{1,v}} - I_{1,\beta_{1,v}}) \tag{A.9}$$

where

$$\begin{aligned}I_{2,\beta_{1,v}} =& \beta_{1,v}^{8mN_r-1}C_2^{4mN_r+k+j+1} \\ & e^{-\frac{C_2\beta_{1,v}^2}{\eta}}{}_1F_1(1;4mN_r+k+j+2;\frac{C_2\beta_{1,v}^2}{\eta})\end{aligned} \tag{A.10}$$

$$\begin{aligned}I_{1,\beta_{1,v}} =& \beta_{1,v}^{8mN_r-1}C_1^{4mN_r+k+j+1} \\ & e^{-\frac{C_1\beta_{1,v}^2}{\eta}}{}_1F_1(1;4mN_r+k+j+2;\frac{C_1\beta_{1,v}^2}{\eta}).\end{aligned} \tag{A.11}$$

Given the PDF in (A.9), the MGF in (4.13) can now be evaluated. Let us rewrite

(4.13) as

$$M_{\beta_{1,v}^2}(s) = \int_0^\infty e^{-s\cdot\beta_{1,v}^2} f(\beta_{1,v}) d\beta_{1,v},$$
$$= 2\lambda \sum_{k=1}^{2mN_r-1} \sum_{j=1}^{2mN_r-1} I_{j,k,m,N_r} \cdot$$
$$\int_0^\infty e^{-s\cdot\beta_{1,v}^2} (I_{2,\beta_{1,v}} - I_{1,\beta_{1,v}}) d\beta_{1,v}. \tag{A.12}$$

Let us introduce the following formulas [40, eq. (7.621.4)]

$$\int_0^\infty e^{-st} t^{b-1} {}_1F_1(a; c; kt) dt =$$
$$\Gamma(b)(s-k)^{-b} {}_2F_1(c-a, b; c; \frac{k}{k-s}) \tag{A.13}$$

and [40, eq. (7.512.12)]

$$\int_0^1 x^{v-1}(1-x)^{\mu-1} {}_pF_q(a_1, \ldots, a_p; b_1, \ldots, b_q; ax) dx$$
$$= \frac{\Gamma(\mu)\Gamma(v)}{\Gamma(\mu+v)} {}_{p+1}F_{q+1}(v, a_1, \ldots, a_p; \mu+v, b_1, \ldots, b_q; a). \tag{A.14}$$

Using (A.13), and the change of variable $r = \beta_{1,v}^2$, we get

$$
\begin{aligned}
I_{1,\theta} &= \int_0^\infty e^{-s\cdot\beta_{1,v}^2} I_{1,\beta_{1,v}} d\beta_{1,v} \\
&= \int_0^\infty \beta_{1,v}^{8mN_r-1} C_1^{4mN_r+k+j+1} \exp(-\frac{C_1\beta_{1,v}^2}{\eta} - s\cdot\beta_{1,v}^2)\cdot \\
&\quad {}_1F_1(1; 4mN_r+k+j+2; \frac{C_1\beta_{1,v}^2}{\eta}) d\beta_{1,v} \\
&= \frac{1}{2} C_1^{4mN_r+k+j+1} \Gamma(4mN_r) \left(\frac{1}{s}\right)^{4mN_r} \cdot \\
&\quad {}_2F_1\Bigg(4mN_r+k+j+1, 4mN_r; 4mN_r + \\
&\quad k+j+2; -\frac{C_1}{\eta\cdot s}\Bigg).
\end{aligned} \tag{A.15}
$$

A similar expression for $I_{2,\theta}$ can be found. We thus have a closed form expression for (4.13) as

$$
\begin{aligned}
M_{\beta_{1,v}^2}(s) &= \lambda \sum_{k=0}^{2mN_r-1} \sum_{j=0}^{2mN_r-1} \frac{(-1)^{k+j}}{4mN_r+k+j+1} \cdot \\
&\quad \binom{2mN_r-1}{k} \binom{2mN_r-1}{j} \cdot C_2^{2mN_r-k-1} C_1^{2mN_r-j-1} \cdot \\
&\quad \Gamma(4mN_r)(s)^{-4mN_r} \cdot \Bigg[C_2^{4mN_r+k+j+1} \cdot \\
&\quad {}_2F_1\Bigg(4mN_r+k+j+1, 4mN_r; 4mN_r+k+j+2; \\
&\quad -\frac{C_2}{\eta\cdot s}\Bigg) - C_1^{4mN_r+k+j+1} \cdot \\
&\quad {}_2F_1\Bigg(4mN_r+k+j+1, 4mN_r; 4mN_r+k+j+2; \\
&\quad -\frac{C_1}{\eta\cdot s}\Bigg)\Bigg].
\end{aligned} \tag{A.16}
$$

Bibliography

[1] N. C. Beaulieu and C. Cheng, "Efficient Nakagami-m fading channel simulation," *IEEE Trans. on Veh. Techn.*, vol. 54, no. 2, pp. 413–424, Mar. 2005.

[2] V. Tarokh, N. Seshadri, and A. R. Calderbank, "Space-time codes for high data rate wireless communication: performance criterion and code construction," *IEEE Trans. Inform. Theory*, vol. 44, no. 2, pp. 744–765, Mar. 1998.

[3] B. Hochwald, T. Marzetta, and C. Papadias, "A transmitter diversity scheme for wideband CDMA systems based on space-time spreading," *IEEE J. Select. Areas Commun.*, vol. 19, no. 1, pp. 1451–1458, Jan. 2001.

[4] J. G. Proakis, *Digital Communications.* McGraw Hill, 2000.

[5] M. Nakagami, "The m-distribution, a general formula of intensity distribution of rapid fading," in *Statistical Methods in Radio Wave Propagation: Proceedings of a Symposium held at the University of California*, P. Press, Ed., 1960, pp. 3–36.

[6] C. Cheng, "A Nakagami-m fading channel simulator," Master's thesis, Queen's University, Kingston, Canada, Nov. 2000.

[7] A. Sacramento and W. Hamouda, "Performance of decorrelator detector in space-time CDMA systems over quasi-static and frequency non-selective nakagami-m fading channels," in *IEEE International Symposium on Signal Processing and its Applications*, Feb. 2007.

[8] ——, "Space-time CDMA systems over Nakagami-m fast fading channels," in *The 18th Annual International Symposium on Personal, Indoor and Mobile Radio Communications*, Sep. 2007.

[9] M. Abramowitz and I. A. Stegun, *Handbook of Mathematical Functions with Formulas, Graphs and Mathematical Tables.* New York:Dover, 1964.

[10] T. Aulin, "Characteristics of a digital mobile radio channel," *Vehicular Technology, IEEE Transactions on*, vol. 30, no. 2, pp. 45–53, May 1981.

[11] U. Charash, "Reception through Nakagami fading multipath channels with random delays," *Communications, IEEE Transactions on*, vol. 27, no. 4, pp. 657–670, Apr. 1979.

[12] H. Suzuki, "A statistical model for urban multipath," *Communications, IEEE Transactions on*, vol. 25, no. 7, pp. 673–680, Jul. 1977.

[13] M. D. Yacoub, J. E. V. Bautistu, and L. G. de Rezende Guedes, "On higher order statistics of the Nakagami-m distribution," *Vehicular Technology, IEEE Transactions on*, vol. 48, no. 3, pp. 790–794, May 1999.

[14] K.-W. Yip and T.-S. Ng, "A simulation model for Nakagami-m fading channels, $m<1$," *Communications, IEEE Transactions on*, vol. 48, no. 2, pp. 214–221, Feb. 2000.

[15] U. Dersch and R. J. Ruegg, "Simulations of the time and frequency selective outdoor mobile radio channel," *Vehicular Technology, IEEE Transactions on*, vol. 42, no. 3, pp. 338–344, Aug. 1993.

[16] W. R. Braun and U. Dersch, "A physical mobile radio channel model," *Vehicular Technology, IEEE Transactions on*, vol. 40, no. 2, pp. 472–482, May 1991.

[17] C. Hastings, *Approximations for digital computers.* NJ: Princeton Univ. Press, 1955.

[18] S. Verdu, *Multiuser Detection.* Cambridge University Press, 2001.

[19] S. W. Golomb, *Shift Register Sequences*, revised edition ed. Aegean Park Pr, Jun. 1981.

[20] S. Verdu, "Minimum probability of error for asynchronous multiple-access communication systems," in *Proc. of 1983 IEEE Military communications Conf.*, vol. 1, Nov. 1983, pp. 213 – 219.

[21] M. K. Simon and M. Alouini, "A unified approach to the performance analysis of digital communication over generalized fading channels," *Proc. of the IEEE*, vol. 86, pp. 1860–1877, Sep. 1998.

[22] T. S. Rappaport, *Wireless Communications: Principles and Practice.* Prentice Hall, 1996.

[23] S. Lin and D. J. Costello, *Error Control Coding*, 2nd ed. Pearson Prentice Hall, 2004.

[24] S. M. Alamouti, "A simple transmit diversity technique for wireless communications," *IEEE J. Select. Areas Commun.*, vol. 16, no. 8, pp. 1451–1458, Oct. 1998.

[25] E. Biglieri, R. Calderbank, A. Constantinides, A. Goldsmith, A. Paulraj, and H. V. Poor, *MIMO wireless communications.* Cambridge: Cambridge University Press, 2007.

[26] H. Bolcskei, D. Gesbert, C. B. Papadias, and A.-J. van der Veen, *Space-time wireless systems : from array processing to MIMO communications.* Cambridge University Press, Jul. 2006.

[27] V. Kuhn, *Wireless Communications over MIMO Channels: Applications to CDMA and Multiple Antenna Systems.* Wiley, Aug. 2006.

[28] L. M. Correia, *Mobile broadband multimedia networks : techniques, models and tools for 4G*, 1st ed. Academic Press, Jun. 2006.

[29] S. G. Glisic, *Advanced wireless communications : 4G technologies*, 1st ed. Wiley, Jun. 2005.

[30] V. Tarokh, H. Jafarkhani, and A. R. Calderbank, "Space-time block codes from orthogonal designs," *IEEE Trans. Inform. Theory*, vol. 45, no. 5, pp. 1456–1467, July 1999.

[31] G. Foschini and M. Gans, "On limits of wireless communication in a fading environment when using multiple antennas," *Wireless Pers. Commun.*, vol. 6, no. 4, pp. 311–335, Mar. 1998.

[32] W. Firmanto, B. Vucetic, and J. Yuan, "Space-time TCM with improved performance on fast fading channels," *IEEE Commun. Letters*, vol. 5, no. 4, pp. 154–156, Apr. 2001.

[33] M. Aljerjawi and W. Hamouda, "Performance analysis of space-time diversity in multiuser CDMA systems over Rayleigh fading channels," in *Proc. IEEE International Conference on Communications(ICC 2006)*, vol. 12, Jun. 2006, pp. 5622–5627.

[34] S. Jayaweera and H. Poor, "Iterative multiuser detection for space-time coded synchronous CDMA," in *Proc. IEEE Veh. Techn. Conf.*, vol. 4, 2001, pp. 2736–2739.

[35] M. Aljerjawi and W. Hamouda, "Performance analysis of multiuser DS-CDMA in MIMO systems over Rayleigh fading channels," *IEEE Transactions on Vehicular Technology : Accepted for future publication*, 2007.

[36] M. Aljerjawi, "Space-time spreading and transmit diversity for DS-CDMA systems over fading channels," Master's thesis, Concordia University, 2006.

[37] E. Al-Hussaini and I. Sayed, "Performance of the decorrelator receiver for DS-CDMA mobile radio system employing RAKE and diversity through nakagami fading channel," *IEEE Trans. on Commun.*, vol. 50, no. 10, pp. 1566–1570, Oct. 2002.

[38] M. Aljerjawi and W. Hamouda, "Performance of space-time spreading in multiuser DS-CDMA systems over fast fading channels," vol. 3, Nov./Dec. 2005, pp. 1525–1529.

[39] A. Papoulis and S. Pillai, *Probability, Random Variables and Stochastic Processes.* McGraw Hill, 2002.

[40] I. S. Gradshteyn and I. M. Ryzhik, *Table of Integrals, Series and Products.* New York:Academic, 1995.

[41] R. T. Derryberry, S. D. Gray, D. M. Ionescu, G. Mandyam, and B. Raghothaman, "Transmit diversity in 3G CDMA systems," *IEEE Communications Magazine*, vol. 40, no. 4, pp. 68–75, Apr. 2002.

[42] R. M. Buehrer, R. A. Soni, and R. D. Benning, "Transmit diversity for combined 2G and 3G CDMA systems," *IEEE Transactions On Communications*, vol. 52, no. 10, pp. 1648–1653, Oct. 2004.

[43] L. Wei and T. A. Gulliver, "A new CDMA/SDMA architecture with transmit diversity," in *IEEE/ACEC International Conference on Wireless Communications and Applied Computational Electromagnetics*, Apr. 2005, pp. 646–649.

[44] W. Sherwin and H. Haim, "Increase of reverse link capacity of the 3G CDMA network by mobile transmit diversity," in *2007 IEEE Radio and Wireless Symposium*, Jan. 2007, pp. 373–375.

[45] L. Yang and L. Hanzo, "Performance of broadband multicarrier DS-CDMA using space-time spreading-assisted transmit diversity," *IEEE Trans. on Wireless Commun.*, vol. 4, no. 3, pp. 885–894, May 2005.

[46] M. Abou-Khousa, A. Ghrayeb, and M. El-Tarhuni, "A multipath detection scheme for CDMA systems with space-time spreading," *IEEE Transactions on Vehicular Technology : Accepted for future publication*, 2007.

[47] G. G. Messier and W. A. Krzymien, "Performance of turbo coding with improved interference estimation on the CDMA space-time transmit diversity forward link," *IEEE Transactions on Vehicular Technology*, vol. 55, no. 3, pp. 1074–1079, May 2006.

[48] Z. Ding, D. Ward, and W. H. Chin, "A general scheme for equalization of space-time block-coded systems with unkown CSI," *IEEE transactions on Sig. Proc.*, vol. 54, no. 7, pp. 2737–2746, Jul. 2006.

[49] J. Luo, J. R. Zeidler, and J. G. Proakis, "Error probability performance for W-CDMA systems with multiple transmit and receive antennas in correlated Nakagami fading channels," *IEEE Transations on Vehicular Technology*, vol. 51, no. 6, pp. 1502–1516, Nov. 2002.

[50] J. Tang and X. Zhang, "Transmit selection diversity with maximal-ratio combining for multicarrier DS-CDMA wireless networks over nakagami-m fading channels," *IEEE Journal On Selected Areas In Communications*, vol. 24, no. 1, pp. 104–112, Jan. 2006.

[51] W. Hamouda and A. Ghrayeb, "Performance of combined channel coding and space-time block coding with antenna selection," in *IEEE 59th Vehicular Technology Conference*, vol. 2, May 2004, pp. 623–627.

[52] G. Bauch and J. Hagenauer, "Analytical evaluation of space-time transmit diversity with FEC-coding," in *IEEE Global Telecommunications Conference*, vol. 1, Nov. 2001, pp. 435–439.

[53] A. Viterbi and J. Omura, *Principles of Digital Communication and Coding.* McGraw-Hill Publishing, 1979.